DCT 197

Instrumented Geogrid Reinforced Mechanically Stabilized Earth Wall Undergoing Large Settlement

by

DOV LESHCHINSKY
S.A. BERKHEIMER
CHRISTOPHER L. MEEHAN

Department of Civil and Environmental Engineering
College of Engineering
University of Delaware

May 2007

Delaware Center for Transportation
University of Delaware
355 DuPont Hall
Newark, Delaware 19716
(302) 831-1446

Instrumented Geogrid Reinforced Mechanically Stabilized Earth Wall Undergoing Large Settlement

By

Dov Leshchinksy
S.A. Berkheimer
Christopher L. Meehan

Department of Civil and Environmental Engineering
College of Engineering
University of Delaware

DELAWARE CENTER FOR TRANSPORTATION
University of Delaware
Newark, Delaware 19716

This work was sponsored by the Delaware Center for Transportation and was prepared in cooperation with the Delaware Department of Transportation. The contents of this report reflect the views of the authors who are responsible for the facts and accuracy of the data presented herein. The contents do not necessarily reflect the official views of the Delaware Center for Transportation or the Delaware Department of Transportation at the time of publication. This report does not constitute a standard, specification, or regulation.

The Delaware Center for Transportation is a university-wide multi-disciplinary research unit reporting to the Chair of the Department of Civil and Environmental Engineering, and is co-sponsored by the University of Delaware and the Delaware Department of Transportation.

DCT Staff

Ardeshir Faghri
Director

Jerome Lewis
Associate Director

Ellen M. Pletz
Assistant to the Director

Lawrence H. Klepner
T^2 Program Coordinator

Matheu J. Carter
T^2 Engineer

Sandra Wolfe
Secretary

DCT Policy Council

Robert Taylor, Co-Chair
Chief Engineer, Delaware Department of Transportation

Michael Chajes, Co-Chair
Dean, College of Engineering

The Honorable Tony DeLuca
Chair, Delaware Senate Transportation Committee

The Honorable Richard Cathcart
Chair, Delaware House of Representatives Transportation Committee

Timothy K. Barnekov
Dean, College of Human Resources, Education and Public Policy

Harry Shenton
Chair, Civil and Environmental Engineering

Ralph A. Reeb
Director of Planning, Delaware Department of Transportation

Stephen Kingsberry
Director, Delaware Transit Corporation

Shannon Marchman
Representative of the Director of the Delaware Development Office

Roger Roy
Representative, Transportation Management Association

Jim Johnson
Executive Director, Delaware River & Bay Authority

Delaware Center for Transportation
University of Delaware
Newark, DE 19716
(302) 831-1446

Instrumented Geogrid Reinforced Mechanically Stabilized Earth Wall Undergoing Large Settlement

by D. Leshchinsky, S. A. Berkheimer, and C. L. Meehan

DEPARTMENT OF
CIVIL & ENVIRONMENTAL ENGINEERING
UNIVERSITY OF DELAWARE

The Center For
INNOVATIVE
BRIDGE ENGINEERING

May 2007

Executive Summary

The goal of this project was to explore the effects of large settlement on the geogrid reinforcement of a mechanically stabilized earth (MSE) wall. Geogrid-reinforced MSE walls have been constructed to support new bridge approach embankments at the Indian River Inlet in Sussex County, Delaware. These embankments, however, have been constructed over poor foundation soil, a layer of soft clay about 60 feet thick. A large magnitude of settlement is expected, and therefore the embankments have been instrumented with settlement plates, piezometers, and inclinometers. Along with this instrumentation, at the south abutment the geogrid reinforcement in a 34.5-foot-high section of MSE wall 1 has been instrumented with strain gages. The use of strain gages is necessary to verify that the geogrid reinforcement is not overstressed, as MSE wall design does not account for large foundation settlement. Attachment of strain gages to the high-density polyethylene geogrid used in this project is challenging and requires a unique technique. Proper calibration of the strain gages allows for resistances read to be converted to strains and forces in the geogrid.

Four months after the completion of construction, the ultimate predicted settlement has already been exceeded, with settlement continuing. High excess pore water pressures are dissipating at a slow rate. Large horizontal movements have been measured. Strain measured in the geogrid has exceeded three percent, a value significantly higher than seen in similar applications. This report presents the effects of the large magnitude of settlement on the MSE wall using measured field data provided from the strain gages, settlement plates, piezometers, and inclinometers. Based on field calibration, the ultimate consolidation settlement is predicted.

The report is organized as follows:

Chapter 1 outlines the problems associated with constructing an MSE wall on a poor-quality foundation. It was anticipated that the construction of the large embankments over this soft clay layer would result in a large amount of settlement, a phenomenon that is largely unexplored because the walls are generally constructed on competent foundations.

Chapter 2 presents, as background, cases involving MSE walls constructed over poor foundation soils where large settlement occurred during and after construction, including an MSE wall along I-15 in Utah.

Chapter 3 describes the instrumentation plan, including both the types and locations of all monitoring devices. The system includes strain gages installed on the geogrid panels and monitored by the UD researchers, as well as settlement plates, piezometers, and inclinometers installed and monitored by the Delaware Department of Transportation (DelDOT). DelDOT collected data, which was shared with the UD team to augment and enhance the significance of the data from the strain gages.

Chapter 4 discusses the data collected in the project. The installed instrumentation was monitored throughout the construction process. Strain gage readings were taken on a regular basis. Data was also collected for all settlement plates, piezometers, and inclinometers throughout construction.

Chapter 5 interprets the data. It was found that data collected from the strain gages, settlement plates, piezometers, and inclinometers appear to be in agreement.

Chapter 6 presents conclusions and recommendations for future research. The data collected from the various instruments proved valuable in determining how the soft foundation soil is responding to the embankment load, as well as how the embankment is behaving. The settlement plates, piezometers, and inclinometers have all provided input to enable assessment of how the foundation soil is responding to the embankment load.

The following summarizes the conclusions of the project:

- The strain gages attached to the geogrid reinforcement give an indication of how the wall and embankment are behaving while settlement is occurring.
- The settlement plate data shows that settlements have far exceeded the original predictions of the designer. Through analysis using the computer program FoSSA®, a model of the embankment was calibrated to produce modified predictions of settlement that more closely match the settlement measured in the field. This was accomplished by adjusting the compression index from the value used by the designer.
- The data from the piezometers is consistent with the observed settlement. The excess pore water pressure was greatest near the end of construction, as is generally expected. However, after the peak pore water pressure value was reached, dissipation of excess pore water pressure is occurring at a slow, but steady rate. This coincides with the fact that settlement is continuing at a constant rate.
- Stability analyses conducted reveal that the factor of safety against deep-seated failure of the embankment at the end of construction was between 1.18 and 1.35 for the condition assuming instantaneous embankment construction and no excess pore water pressure dissipation. The low factor of safety is in agreement with the large horizontal movement measured by the inclinometers. In addition, the depth at which the predicted critical failure planes and surrounding areas with a low factor of safety according to the safety maps are located correspond to the depth at which the largest horizontal movements have been measured by the inclinometers. Stability analyses conducted for the post-consolidation condition show an increase in the factor of safety to an acceptable level.

- The strain gage data is particularly important. There is little known regarding the behavior of an MSE wall that is constructed on poor foundation soil. In general, design for MSE walls assumes a competent foundation. Thus, monitoring the strain in the geogrid reinforcement is important in order to determine the effect of large settlement on the structure.
- Data collected from the strain gages in this research project gives an indication of how the reinforcement is responding to the settlement of the structure. Strains higher than are typical for MSE walls have been observed over the entire length of the reinforcement. It appears that the highest strains in the geogrid are occurring near the back of the reinforcement, away from the face of the wall. This is most likely due to the sand backfill settling at a faster rate than the reinforced soil. As a result, the backfill is exerting a down drag force on the rear boundary of the reinforced soil mass. This down drag force subjects the geogrid reinforcement to stress that is not typically considered in design.

It is recommended that efforts be made to continue collecting and analyzing data from all of the instrumentation installed at station 289+00. At the time of the writing of this report, the embankment was continuing to undergo significant settlement. Excess pore water pressure levels remained high, and were dissipating slowly, indicating that settlement would continue for some time. Even once settlement is nearly complete, it will still prove useful to continue monitoring the strain gages to determine long-term effects such as creep of the geogrid reinforcement. There is little knowledge concerning the behavior of geogrid reinforced MSE walls constructed over poor foundation soils. Hence, this research has the potential to make a significant contribution to the literature in this area.

INSTRUMENTED GEOGRID REINFORCED MECHANICALLY STABILIZED EARTH WALL UNDERGOING LARGE SETTLEMENT

by

Scott A. Berkheimer

A thesis submitted to the Faculty of the University of Delaware in partial fulfillment of the requirements for the degree of Master of Civil Engineering

Spring 2007

INSTRUMENTED GEOGRID REINFORCED

MECHANICALLY STABILIZED EARTH WALL

UNDERGOING LARGE SETTLEMENT

by

Scott A. Berkheimer

Approved: _____

Dov Leshchinsky, Ph.D.
Professor in charge of thesis on behalf of the Advisory Committee

Approved: _____

Michael J. Chajes, Ph.D.
Chair of the Department of Civil and Environmental Engineering

Approved: _____

Eric W. Kaler, Ph.D.
Dean of the College of Engineering

Approved: _____

Carolyn A. Thoroughgood, Ph.D.
Vice Provost for Research and Graduate Studies

ACKNOWLEDGMENTS

I would like to express my most sincere appreciation to my advisor, Dr. Dov Leshchinsky, for providing me with this research opportunity, as well as his wisdom and guidance throughout my graduate studies at the University of Delaware. I would like to thank Dr. Leshchinsky in particular for his continual support during the writing of this thesis.

I also wish to extend my gratitude to the Delaware Department of Transportation for providing the funding that made this research, thesis, and my graduate studies possible.

I would also like to thank Danny Richardson and Gary Wenczel for their assistance in the laboratory and in the field.

Finally, I would like to thank my brother for his encouragement and my parents for their support.

TABLE OF CONTENTS

LIST OF TABLES

LIST OF FIGURES

ABSTRACT

Geogrid reinforced mechanically stabilized earth (MSE) walls have been constructed to support new bridge approach embankments at the Indian River Inlet in Sussex County, Delaware. These embankments, however, have been constructed over poor foundation soil, a layer of soft clay about 60 feet thick. A large magnitude of settlement is expected, and therefore, the embankments have been instrumented with settlement plates, piezometers, and inclinometers. Along with this instrumentation, at the south abutment the geogrid reinforcement in a 34.5 foot high section of MSE wall 1 has been instrumented with strain gages. The use of strain gages is necessary to verify that the geogrid reinforcement is not overstressed, as MSE wall design does not account for large foundation settlement. Attachment of strain gages to the high density polyethylene geogrid used in this project is challenging and requires a unique technique. Proper calibration of the strain gages allows for resistances read to be converted to strains and forces in the geogrid.

Four months after the completion of construction, the ultimate predicted settlement has already been exceeded, with settlement continuing. High excess pore water pressures are dissipating at a slow rate. Large horizontal movements have been measured. Strain measured in the geogrid has exceeded three percent, a value significantly higher than seen in similar applications. Presented are the effects of the large magnitude of settlement on the MSE wall using measured field data provided from the strain gages, settlement plates, piezometers, and inclinometers. Based on field calibration, the ultimate consolidation settlement is predicted.

Chapter 1

INTRODUCTION

The construction of two new approach embankments is necessary for a new bridge that will replace the existing bridge that carries Delaware Route 1 over the Indian River Inlet in Sussex County, Delaware. The embankment fill is supported on each side by geogrid reinforced mechanically stabilized earth (MSE) walls. The embankments, however, are being constructed on poor foundation soil. A 60 foot thick normally consolidated clay layer is located approximately 30 feet below the ground surface. It is anticipated that the construction of the large embankments over this soft clay layer will result in a large amount of settlement.

The effect of a large magnitude of settlement on geogrid reinforced MSE walls is relatively unknown. This is because MSE walls are generally constructed on a competent foundation. In fact, design methodologies such as AASHTO assume that the foundation is competent and are silent about the potential impact of large settlement on the reinforcement stress or required length. Hence, in order to monitor the effects of the large settlement on the geogrid reinforcement, geogrid layers have been instrumented with strain gages at station 289+00 in MSE wall 1, which supports the south abutment. Other instrumentation located at this station includes settlement plates, piezometers, and inclinometers.

At station 289+00, the height of the MSE wall is 34.5 feet. There are 23 geogrid layers spaced vertically every 1.5 feet, with 13 of these layers instrumented with strain gages. The strain gages are necessary for this application to ensure that the

geogrid reinforcement does not become overstressed from the large predicted settlement of 45 inches. Overstressing may occur because the MSE wall was designed using the AASHTO approach, in which the design assumes a competent foundation. This assumption is questionable in this case, and therefore, monitoring of the wall during and after construction is of critical importance. This thesis analyzes and discusses the measured field data provided from the strain gages, settlement plates, piezometers, and inclinometers.

The settlement measured exceeded the designer's predicted ultimate settlement about nine months after construction began. Significant settlement continues to occur 13 months after construction started. Predictions developed in this study suggest the ultimate settlement will be around 80 inches. Strain measured in the geogrid has exceeded three percent, a value that is significantly higher than seen in similar applications. In addition, the highest strains have been measured near the rear of the geogrid, away from the wall face. This is unexpected, as higher strains generally develop in the reinforcement near the face of the wall.

Chapter 2

BACKGROUND

2.1 Instrumented Mechanically Stabilized Earth Walls

The following cases involve mechanically stabilized earth walls that have been constructed over poor foundation soils where large settlement occurred during and after construction. The reinforcement has been instrumented with strain gages in order to monitor these structures.

2.1.1 MSE Wall along I-15 in Utah

A large MSE wall with metallic reinforcement has been constructed over soft soils as part of the I-15 reconstruction project in Salt Lake City, Utah. The wall was instrumented with over 500 strain gages on the welded wire bar mats and fascia panels, three vertical and two horizontal inclinometers, 60 horizontal extensometers, five pressure cells, and three Sondex settlement systems. The instrumented section of the wall is about 30 feet high, with the foundation soils consisting of multiple clay layers, as summarized in Table 2.1 (Bay, Anderson, Budge, & Goodsell, 2003).

Table 2.1 Site Soil Strata (Bay et al., 2003)

Stratum	Material Description	Approximate Depth, ft
I	Fill: Course Sand and Concrete Rubble	Surface to 8
II	Soft Clay	8 to 19
III	Soft Silty Clay	19 to 30
IV	Stiff to Hard Sandy Clay	30 to 85
V	Very Stiff to Hard Clay	85 to 90

Due to the existing soil strata and the relatively tall wall being constructed, settlements around three feet were anticipated near the face of the wall. As a result, the wall was susceptible to deformations near its foundation, potentially including bulging, sagging, and negative batter. To counteract this, the reinforcement design used was modified. The original design included welded-wire reinforcing bar mats connected by pins to galvanized steel mesh fascia panels. The bar mats consisted of between four and six 24 feet long wires spaced every six inches and welded to transverse bars spaced every 12 to 24 inches, depending on the location of the mat in the wall. These mats were spaced vertically every 30 inches. To modify this design, shorter welded wire bar mats were included between the primary reinforcement bar mats in the lower portion of the wall, from the base up to a height of 15 feet below the top of the wall. The intermediate sections of reinforcement were 10 feet long, with longitudinal wires spaced every six inches and welded to transverse bars spaced every

12 inches. The number of longitudinal bars depended on the location of the mat in the wall. The intermediate bar mats were spaced evenly between the primary reinforcement mats. The fascia panels were made up of a grid-like pattern with longitudinal and transverse wires spaced every six inches. Concrete fascia panels were added in the second stage of construction (Bay et al., 2003).

The modified design, however, was not used continuously through the wall. Some portions used the older design, which utilized only the 30 inch vertically spaced primary reinforcement mats. Thus, two sections were instrumented; one section using the old design and one section using the modified design. Strain gages were installed on every other layer of primary reinforcement in each section. In the modified section, gages were also placed on the intermediate layer directly above each instrumented primary layer of reinforcement (Bay et al., 2003). Figures 2.1 and 2.2 show the instrumented reinforcement layers in each wall section.

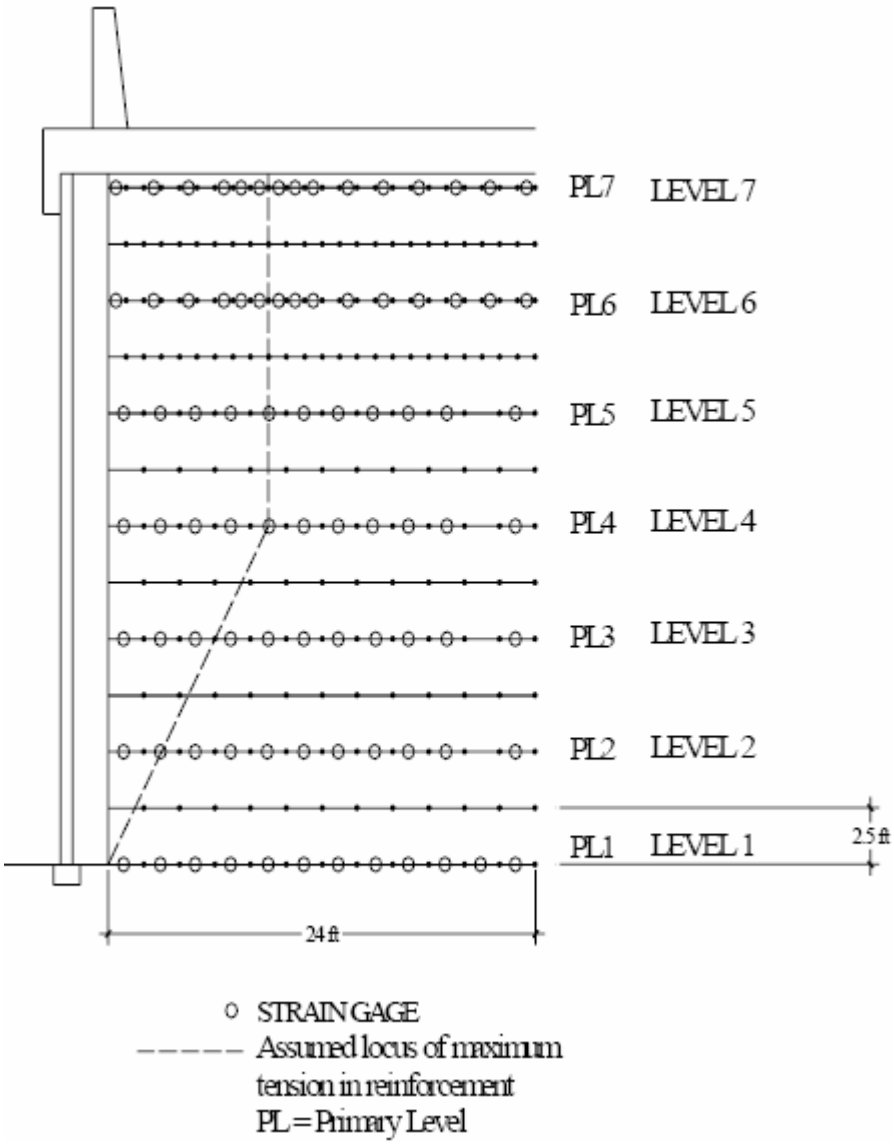

Figure 2.1 Elevation View of Wall Section with Instrumented Primary Reinforcement (Bay et al., 2003)

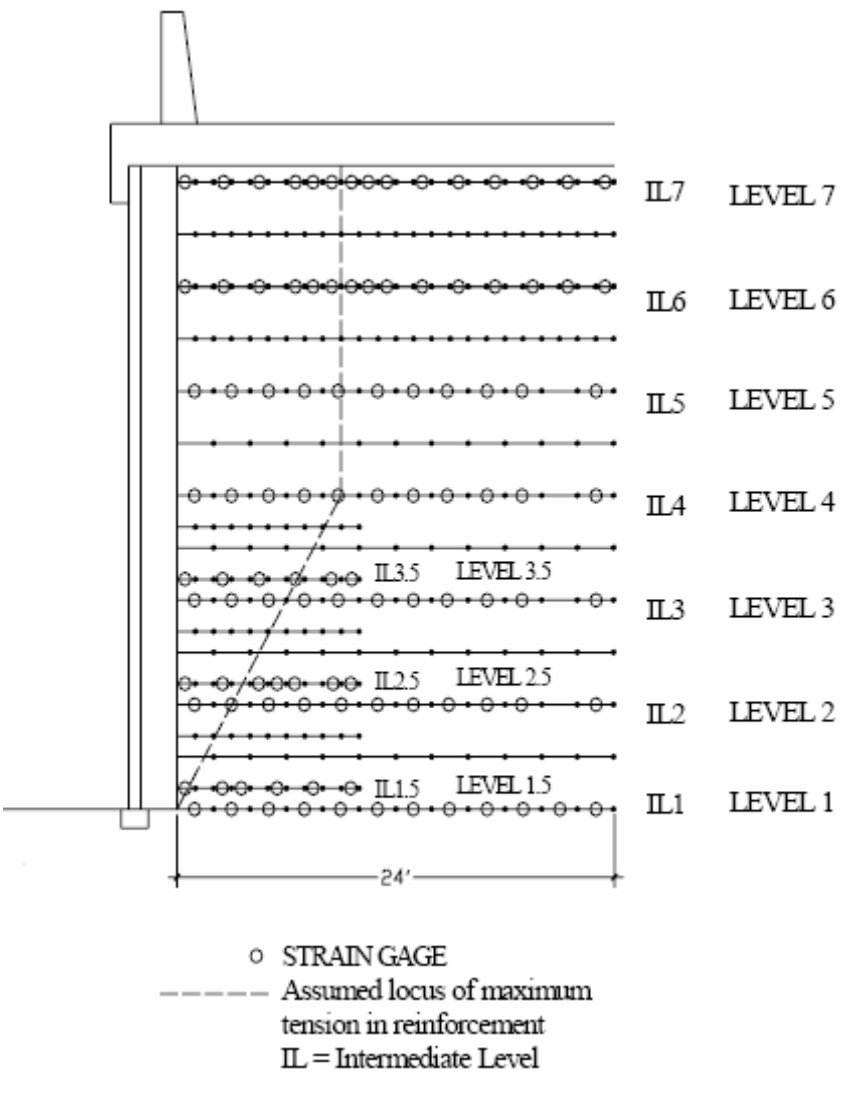

Figure 2.2 Elevation View of Wall Section with Instrumented Primary and Intermediate Reinforcement (Bay et al., 2003)

The strain gages measured the tensile stress distributions along the reinforcement layers within the wall, and the bar forces were determined for various

fill heights above the mat level. An example of the measured bar forces is shown in Figure 2.3.

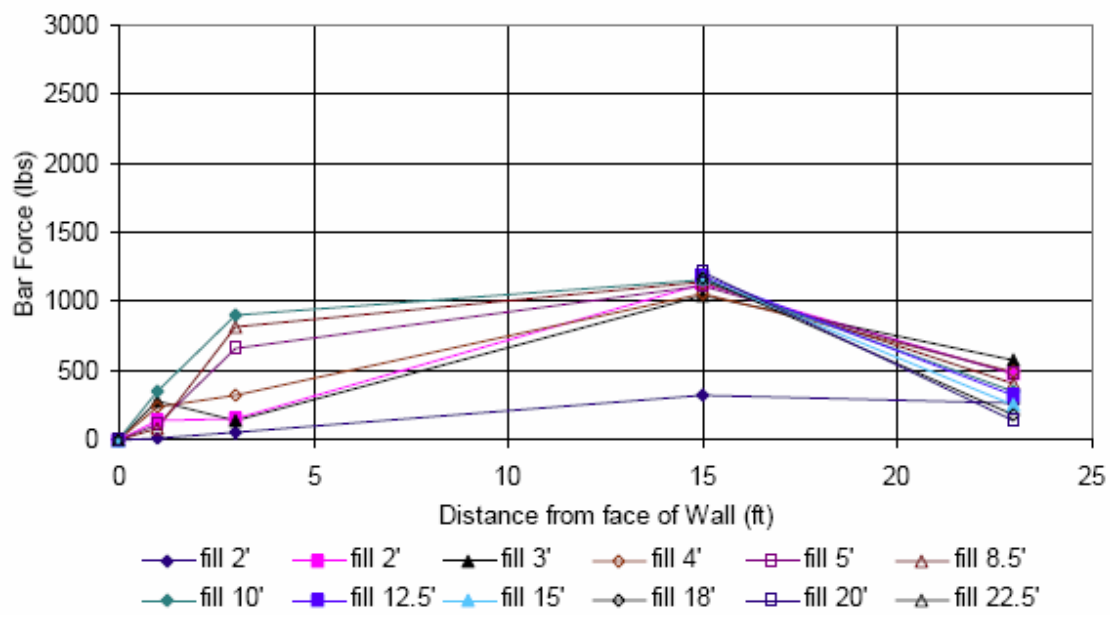

Figure 2.3 Measured Bar Forces for Primary Reinforcement Only Layer 2 (Bay et al., 2003)

The strain gages were also used to determine the loci of maximum tension in the bar mats. Figure 2.4 illustrates an example of the tension distribution measured before the completion of construction in the section of wall containing both primary and intermediate reinforcement.

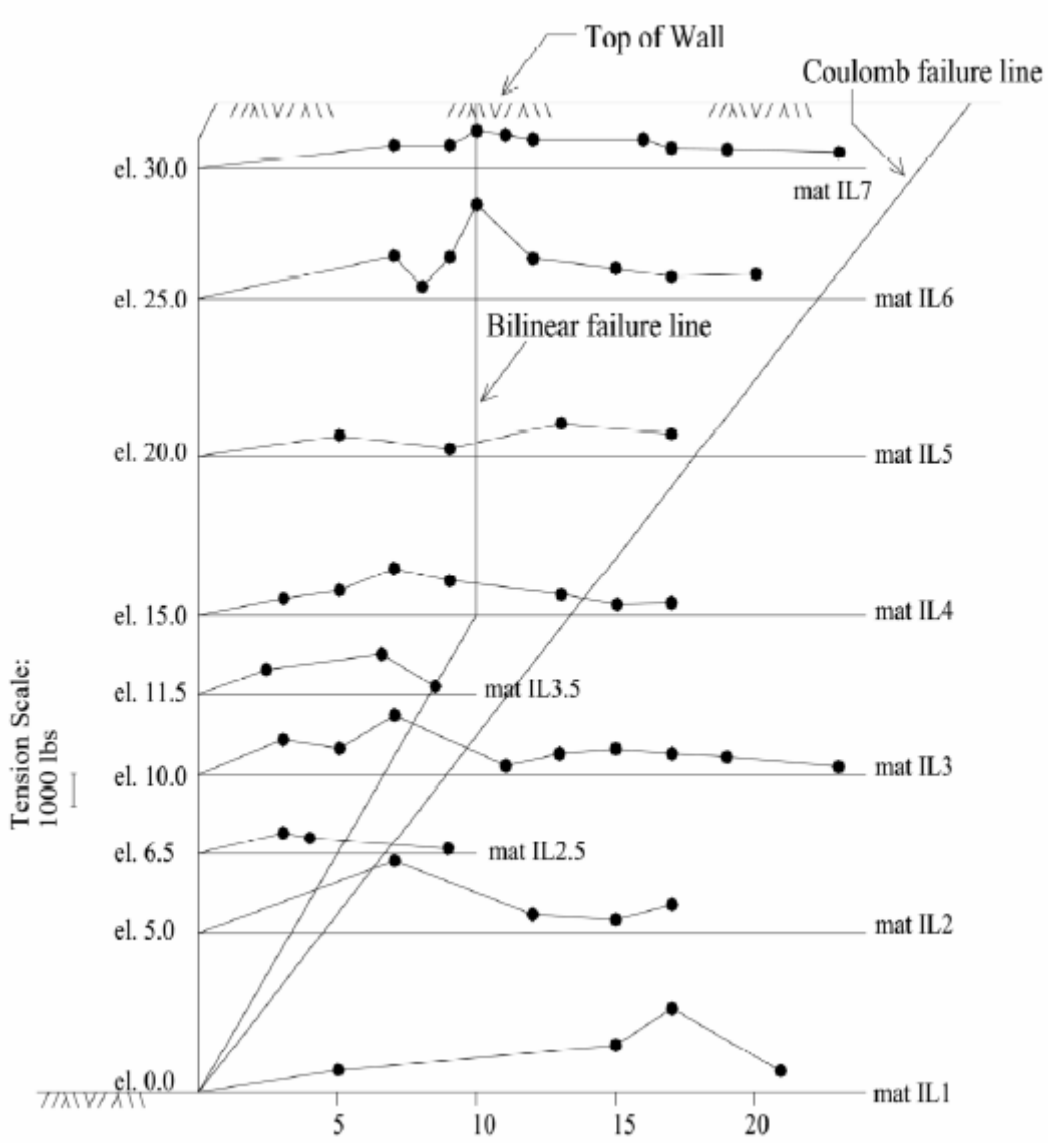

Figure 2.4 Tension Distribution in Bar Mats in the Primary and Intermediate Reinforced Wall Section (Bay et al., 2003)

Through the measurements, it was concluded that the maximum tension occurring in the bar mats was less than the allowable tension of the mats in design.

The minimum ratio of allowable yield stress to existing tensile stress in the longitudinal reinforcing bars was 2.5. This ratio only occurred for one gage position out of 90 functioning positions. The next lowest ratio was 5.0, which only occurred at four gage positions. Thus, most of the bar mats are under a tension of less than 20 percent of the yield strength of the material (Bay et al., 2003). These ratios, however, were calculated without accounting for long-term material cross-section loss due to corrosion.

In inspecting the vertical stress distribution along all layers defined by the strain gage measurements, it was concluded that the distribution followed a similar pattern to other MSE walls with inextensible reinforcement. The vertical stresses near the face of the wall were low. Stress increased to a maximum value approximately six feet from the face of the wall. After this point, the stress decreased to the value anticipated from the overburden pressure some distance from the face of the wall (Bay et al., 2003).

The Sondex settlement tubes indicated that the wall settled about 1.5 feet vertically during construction. A majority of this settlement occurred in the two layers of soft clay, in the upper 22 feet of the foundation soil, beneath the concrete rubble backfill. Survey monuments indicated that no measurable settlement occurred outside the wick drain zone. Readings taken after the end of primary consolidation indicate that only 0.3 inches of settlement has occurred, a result of secondary consolidation (Bay et al., 2003).

Overall, the results of the instrumentation plan indicate that the behavior of the wall through construction and afterwards has been quite good. The results also verify that the reinforcement within the wall is sufficient, with the existing stresses

being comfortably below allowable stresses. The wall is both internally and externally stable, despite the large primary settlement (Bay et al., 2003).

2.1.2 Instrumented Geosynthetics Reinforced Soil Walls

Won and Kim (2006) present a case where two five meter high geosynthetics reinforced soil (GRS) walls were constructed on a shallow-layered weak foundation, installed with an arrangement of non-woven and woven geosynthetics. The walls were backfilled with a low plasticity clayey soil. The deformations of the geosynthetics were measured with 124 strain gages that were attached to non-woven and woven geotextiles, as well as geogrids. Data was collected for approximately a year and a half.

The results show that for up to 25 days after the construction of the walls, deformation of the geosynthetics increases. The maximum deformation measured in the geogrid during construction up to 10 days after construction completion was 1.067%. The maximum deformation in the geogrid after 16 months was 2.326%. These values are similar to the corresponding values for the woven geosynthetic of 0.650% and 2.915%, but smaller than the corresponding deformations in the non-woven geosynthetic of 2.938% and 9.054%. The latter value may have been erroneous due to effects of outside elements, thus making the maximum 6.052% for 16 months (Won & Kim, 2006). Figure 2.5 shows the geosynthetics deformation for a section containing non-woven and geogrid reinforcements.

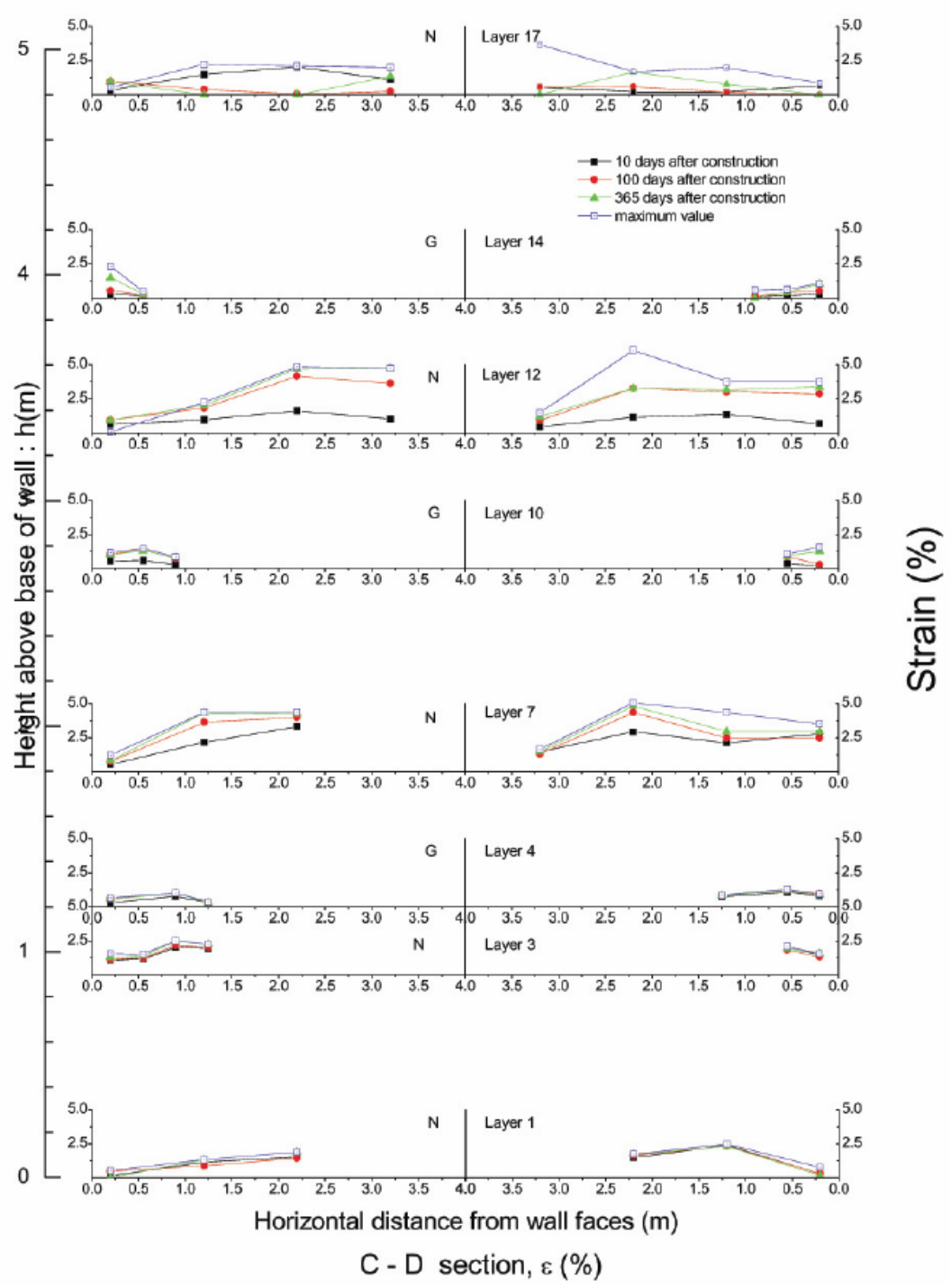

Figure 2.5 Geosynthetics Deformation in C-D Section (Won & Kim, 2006)

2.2 Attachment of Strain Gages to Geosynthetics

Bonding strain gages to geosynthetics, including high density polyethylene (HDPE) geogrids, presents a challenge. This is due to the waxy coating on the geogrid, a result of the manufacturing process. A method must be used that creates a lasting bond between the gage and the geogrid, but still allows the gage to deform with the geogrid. It is for this reason that the preparation of the geogrid surface is critical in the procedure.

A strain gage attachment procedure has been suggested by Soong and Koerner (1998). It is recommended to first use a degreaser or solvent to degrease the surface. Next, the surface should be abraded using a dry powdered cleaner that lightly scratches the surface, creating more surface area for bonding. The surface should next be cleaned using a cotton swab and rubbing alcohol. A strain gage should be placed bonding side down on a clean glass plate. A piece of cellophane tape is placed over the gage, and then lifted to act as a carrier for the gage. At this point, a thin layer of adhesive is placed on the prepared area of the geogrid, and the tape with the gage is placed over the glued surface. A piece of gauze should be used to wipe over the area, pressing the gage into the glue. Now, a glass slide and a Neoprene backup pad are placed over the installed gage, followed by deadweight for curing. The weight, rubber, and glass should be removed after the adhesive is cured. The tape is then removed by slowly pulling it back over itself. Wires are soldered to the terminal points of the gage, with slack left in the leads to prevent tensile force from being transferred to the terminal. Finally, the entire gage assembly should be coated with RTV silicone (Soong & Koerner, 1998).

Chapter 3

INSTRUMENTATION

The test section where instrumentation was installed and used for this research is located at the Indian River Inlet site south abutment, mechanically stabilized earth (MSE) wall 1, at station 289+00. Figure 3.1 shows the stationing for the south abutment, as well as the MSE walls that will support the approach and abutment.

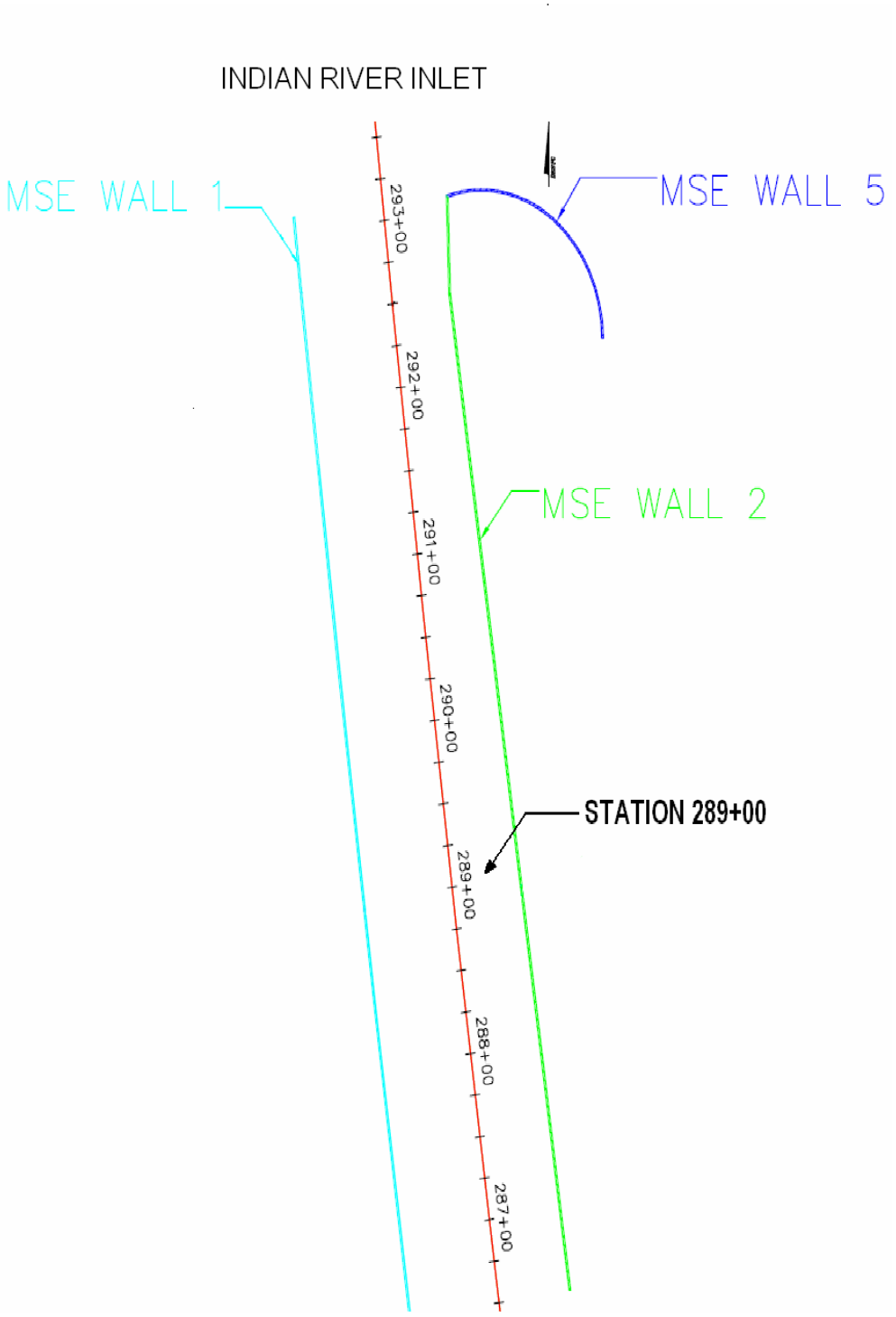

Figure 3.1 Stationing and Wall Layout for South Abutment

Strain gages were installed on geogrid panels and monitored by the writer. The Delaware Department of Transportation (DelDOT) monitored settlement plates, piezometers, and inclinometers installed at this location. DelDOT collected data, which was shared with the writer to augment and enhance the significance of the data from the strain gages.

3.1 Strain Gages

All strain gages installed are Vishay Micro-Measurements general purpose foil strain gages. Two types of gages were used. The strain gages installed on the Tensar UX1700HS and UX1600HS HDPE geogrids have a gage length of 0.124 inches, with a maximum strain of ± 5%. They have the following properties: a resistance in ohms of 120.0±0.3%, a gage factor at 24ºC of 2.085±0.5% with the t.c. of gage factor being (+1.2±0.2) %/100 ºC, and a transverse sensitivity of (+0.7±0.2)%. The strain gages installed on the Tensar UX1500HS and UX1400HS HDPE geogrids are high elongation gages, having a gage length of 0.124 inches and a maximum strain of ± 10%. They have the following properties: a resistance in ohms of 120.0±0.15%, a gage factor at 24ºC of 2.065±0.5% with the t.c. of gage factor being (+0.7±0.2) %/100 ºC, and a transverse sensitivity of (+1.3±0.2)%.

3.1.1 Strain Gage Installation

The installation of strain gages on high density polyethylene (HDPE) geogrid for long-term, in-situ performance is not well established. This case was especially challenging, as the bottom layers of geogrid are submerged in sea water. The overall challenge is to create a sufficient bond between the strain gage and the geogrid such that the gage will strain with the geosynthetic, but not stiffen the bonding

area. Stiffening of the bonding area will render local stress concentration, a disturbance that does not reflect reality. The gage must also be made waterproof. The procedure suggested by Soong and Koerner (1998) that was discussed in Section 2.2 was slightly modified for this application.

The first step in the strain gage installation procedure is to lay out the appropriate length of geogrid on a flat surface and mark the locations where the strain gages are to be attached. For the geogrid used, the strain gages were attached within less than an inch of a transverse rib, which is the weakest and softest point. The reason for selecting this location and not the middle of the longitudinal rib is that by virtue of being nearly the softest area, and therefore having nearly the lowest stiffness, the strain response for a given load will be the largest. This performance enhances the sensitivity, and therefore effectiveness, of the strain gage reading.

Five gages were installed on each twenty-two foot long geogrid panel rendering one gage approximately every four and a half feet. A gage was installed in front of the second longitudinal rib from the front end of the panel. The remaining four gages were installed in front of every third rib along the panel. All five gages were installed in the center of the geogrid panel, each panel being approximately four and a half feet wide.

The surface of the geogrid where the gage will be attached must be prepared. This is accomplished by lightly abrading the geogrid surface using 220 grit silicon carbide sand paper. The surface is abraded in two perpendicular directions, along the length of the reinforcement, as well as in the direction parallel with the rib of the geogrid. This texture helps create more surface area for improved glue adhesion. Next, the area is cleaned using Micro-Measurements M-Prep Neutralizer 5A, which is

an ammonia and water based surface cleaner. The solution should be applied to a clean gauze pad, which is then used to wipe the sanded area. This is then repeated until a wipe across the surface yields a clean gauze pad. The surface should be level, clean, and dry. Each location on the geogrid should be prepared before moving to the next step.

The next step is to prepare the strain gage. The gage should be removed from the packaging by grasping its edge with tweezers. The gage is then placed onto a clean glass plate, with the side to be bonded facing the plate. Now, a piece of cellophane tape, approximately one inch long, is placed over the gage. The tape is pulled at a 45 degree angle until the tape comes off the glass with the gage. It is important to pull the tape carefully without exceeding a 45 degree angle so the tape is not peeled back over itself. This could cause the strain gage to be damaged. The strain gage is placed on the edge of the glass plate, and this procedure is repeated for each strain gage to be applied.

At this point the epoxy must be mixed. In this project, Micro-Measurements M-Bond AE-10 adhesive was used. The epoxy must be mixed for five minutes to ensure consistent and uniform mixing of the two ingredients. Once the epoxy glue is ready, a heat burnishing method must be used. This step is critical in the procedure, as it produces a much better bond between the adhesive and geogrid. A heat gun is used to heat the gage application area of the geogrid. The heat gun should be passed back and forth over geogrid, at a height of six to twelve inches above the surface. The geogrid should be heated until the finish has a slight sheen, or until it cannot be touched for longer than two or three seconds. Heating longer than this may damage the geogrid. As soon as the surface is heated adequately, a drop of the epoxy

should be placed on the heated area of the geogrid using an applicator. Figure 3.2 shows the epoxy drop size and the location of the gage attachment. Now, a taped strain gage should be placed on the epoxy and lightly pressed directly with a finger into place. This procedure must be quickly repeated for each gage to be installed, as the epoxy will set in approximately ten minutes.

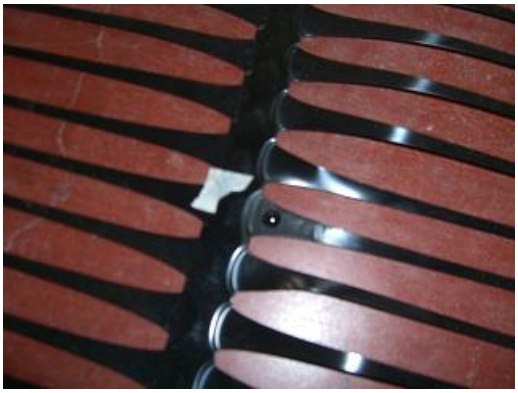

Figure 3.2 Epoxy Drop to Bond Strain Gage onto Longitudinal Rib

The epoxy was allowed to cure for twenty-four hours. After this, the tape was pulled off the gage by pulling it back over itself. At this stage, the gage leads are soldered to the gage. Following this, the gage is coated with polyurethane. After the polyurethane is dry, a coating of Dow Corning 3145 RTV is applied to the gage and exposed portions of the leads. This provides moisture protection. Once the RTV is cured, a "pigtail" should be made with each wire an inch or two in front of the gage,

as shown in Figure 3.3. This technique prevents the wires leading to the measurement device from exerting tension onto the strain gage. Each wire extending from each strain gage is then joined together with the other wires to be run down the center of the geogrid. A piece of one-half inch outside diameter PVC tubing should be cut long enough to encase and protect the wires. Then, the tubing is split along its length. Now the wires can be run inside the tubing, which should be wrapped around the longitudinal ribs of the geogrid. The tubing should be secured in place using cable ties. The geogrid panel can then be loosely rolled up to be transported to the construction site.

Figure 3.3 Lead Pigtail

3.1.2 Field Installation of Instrumented Geogrid

The instrumented panels of geogrid were transported from the University of Delaware in Newark, to the Indian River Inlet construction site to be installed. Geogrid layers are vertically spaced every eighteen inches in the mechanically stabilized earth wall, starting at the base of the wall, elevation 0. Instrumented panels were installed in every other layer, or every three feet, starting at the base layer. An instrumented panel was also installed in consecutive layers when a change in the strength of geogrid used along the height occurred. This occurred between layers 5 and 6, and layers 10 and 11. The installation opportunity for layer 21 was missed, so the instrumented layer was installed as layer 22 instead. Figure 3.4 shows the cross-section of the reinforced wall at Station 289+00. As can be seen, there are four types of HDPE geogrid. The instrumented layers are labeled on the figure.

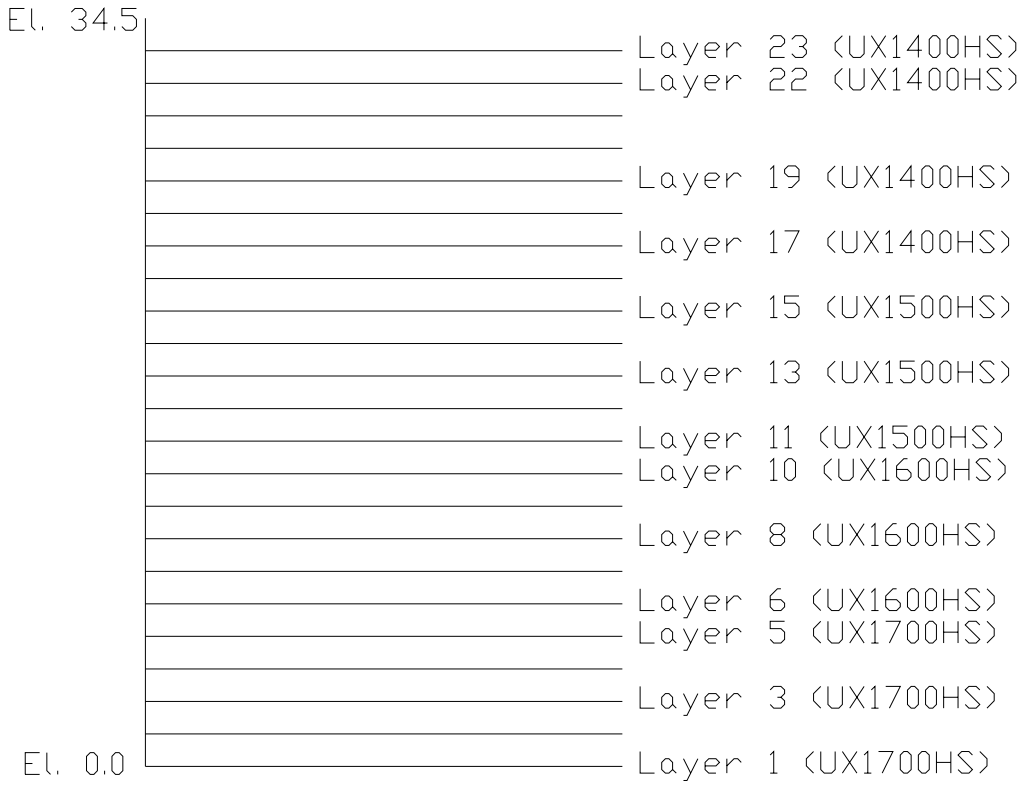

Figure 3.4 Instrumented Geogrid Layers at Station 289+00

The installation of the instrumented geogrid panel was completed by the contractor in the same manner as the non-instrumented geogrid was installed elsewhere in the wall. The only difference is that small sand-filled bags were placed over the gage locations to protect the gages from being damaged by placement of the backfill. This is shown in Figure 3.5. Care was taken during backfilling to avoid damaging the strain gages.

Figure 3.5 Installed Instrumented Geogrid Panel: PVC pipe protects the wires and sandbags protect each strain gage

3.1.3 Strain Gage Calibration

The resistance of the field-installed strain gages was periodically measured with an ohmmeter, having an accuracy of 0.01 ohms. As the geogrid deforms under stress due to soil overburden, the tightly bonded strain gage deforms as well. Hence, by measuring the resistance of each strain gage periodically, one can obtain the change in its resistance due to loading. However, the change in resistance is of little interest; what is needed is the corresponding tensile strain and tensile load. These values are related to the long term strength of the geogrid as used in design.

In order to accurately determine the strain and the respective stress in the instrumented geogrid panels installed in the field, the strain gages must be calibrated. Calibration is necessary so that an increase in resistance measured (in ohms) with the ohmmeter can be transformed back into a measurement of strain and stress. Calibration of the strain gages was accomplished through laboratory testing at the University of Delaware.

For calibration testing, strain gages were installed on geogrid test specimens following the same procedure as for the field geogrid panels, including the location of strain gages on the longitudinal rib. The only difference is that two gages were attached to each sample, on opposite sides of the longitudinal rib. The locations of these gages are shown in Figure 3.6. Five samples were tested of each of the four different geogrids. Three of these samples were tested by straining them at a rate of half a percent per minute, one sample was tested at a strain rate of one percent per minute, and the final sample was tested at a rate of ten percent strain per minute. The half percent per minute strain rate was chosen to represent a slow strain rate, assumed to represent field conditions. The one percent per minute test was conducted to investigate the material response to loading speed, and thus see if the rate of half a

percent strain per minute is realistic to represent field conditions. The last rate corresponds to the rate at which the standard wide-width tensile strength test is conducted. The three test speeds should provide a perspective of rate effects, especially at low strain.

The testing was performed using a 200-kip Tinius Olson machine. The sample was secured in the machine using standard machine grips, which were tested for slippage before running the tests so that no slippage during testing will occur. Each specimen initially was comprised of three longitudinal ribs – see Figure 3.6. After secured in the testing machine, the two outside strands of the geogrid were cut, leaving the central rib, to which the gages are attached, as the load barrier. An ohmmeter was attached to the leads of each strain gage. Figure 3.7 shows the sample setup. The test data was recorded by a computer linked to the testing machine. The test was also recorded using a camcorder, which was focused on the output display of the testing machine and the ohmmeters. Having a video recording of each test allowed for the video to be watched and stopped at any point in the test to record the load, displacement, and elapsed time from the testing machine, along with the corresponding resistance reading from the ohmmeters. The described test setup is shown in Figure 3.8.

Figure 3.6 Location of Strain Gages on Geogrid Calibration Test Sample

Figure 3.7 Calibration Testing Sample Setup

Figure 3.8 Calibration Testing Data Recording Setup

The testing apparatus measured and recorded the displacement between the jaws continuously during each test. Using a displacement from any point in the test, the strain in the sample for that time was determined by dividing the recorded displacement at that time by the original distance between the jaws, which was measured before the test commenced. The testing apparatus also continuously measured and recorded the applied load during the test. Therefore, the force per unit width that corresponds with any strain can be determined. Force per unit width was calculated by multiplying the measured force by the number of longitudinal ribs in one foot of geogrid width. The two ohmmeters continuously measured the resistance in each strain gage during each test.

The data from the tests was compiled and analyzed. The output file from the data collection system provided the force applied and the displacement of the

specimen for a large number of time increments throughout the test. Watching the video recording of the test allowed playback of the test to be paused at any desired increment to record the corresponding resistance readings displayed on the ohmmeters. For each increment, a resistance reading was determined by averaging the two readings from the ohmmeters. Once this was completed for a number of increments throughout the test, a graph was constructed showing the percent strain in the geogrid versus the resistance change of the strain gage. Since three tests were run at a rate of half a percent strain per minute, the average of these three tests was determined. An example of the strain versus resistance change graph, as well as the average half percent strain rate plot is shown in Figure 3.9.

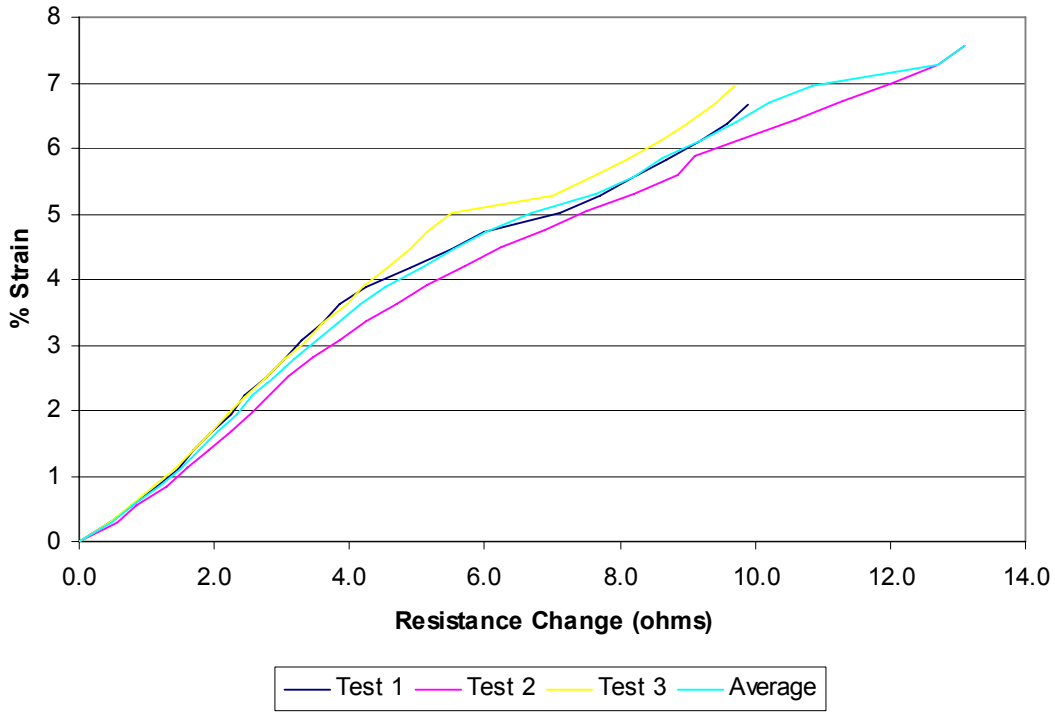

Figure 3.9 Calibration Test Results for Half Percent Strain Rate Tests on UX1700HS HDPE Geogrid

Two graphs were constructed for each geogrid tested. The first graph shows the relationship between the change in resistance and percent strain in the geogrid; the second shows the applied force and resulting percentage of strain. Each graph includes the curve for the one percent per minute and ten percent per minute strain rate tests, as well as the average curve for the half percent strain per minute tests. The test results are shown in Figures 3.10 through 3.17.

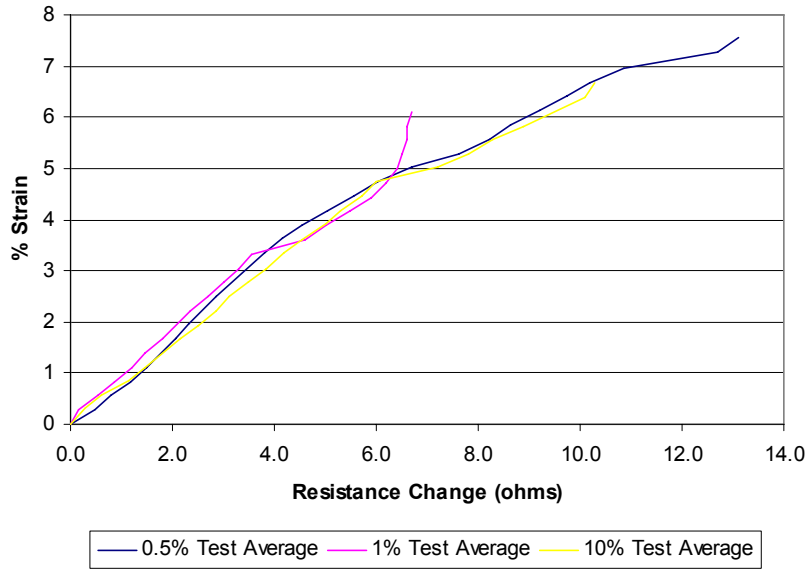

Figure 3.10 UX1700HS % Strain vs. Change in Resistance Curves

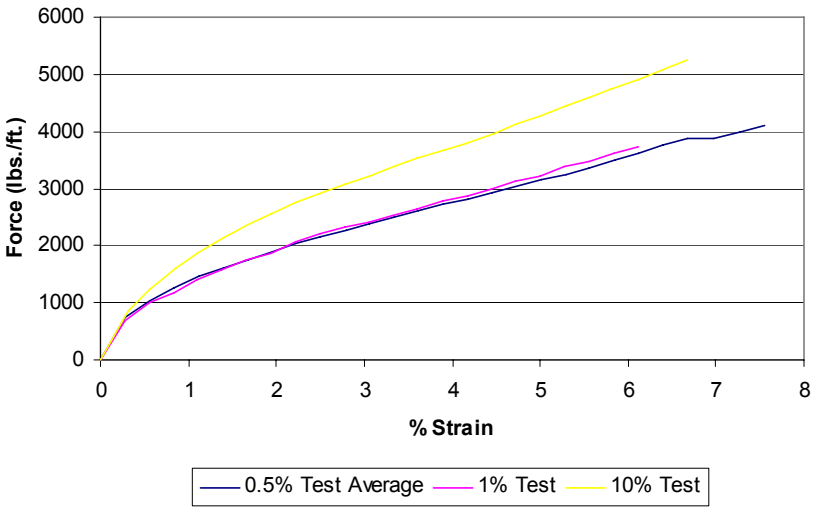

Figure 3.11 UX1700HS Force vs. % Strain Curves

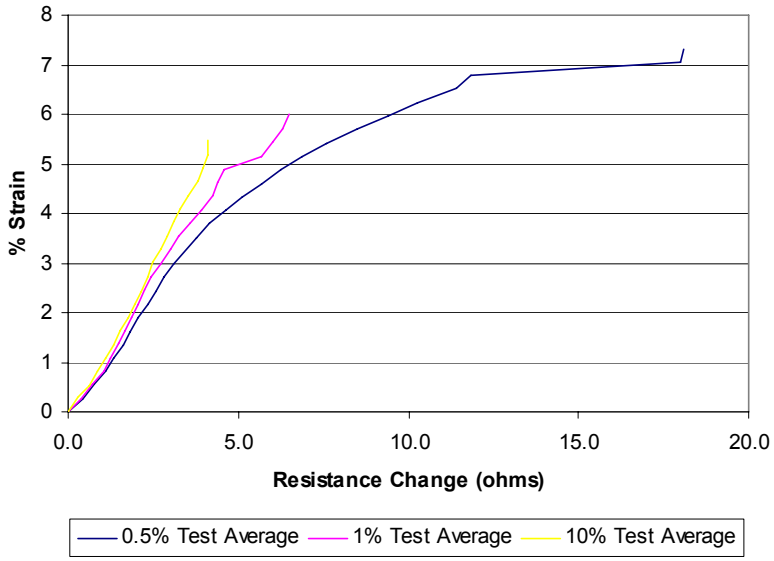

Figure 3.12 UX1600HS % Strain vs. Change in Resistance Curves

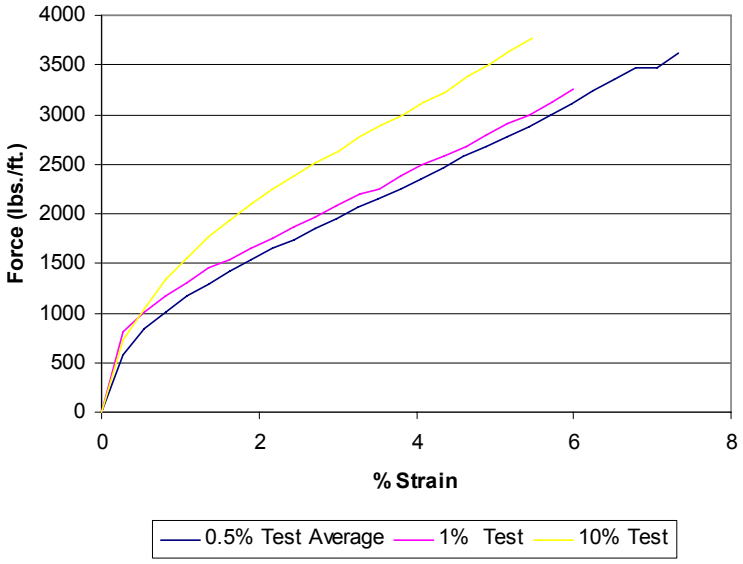

Figure 3.13 UX1600HS Force vs. % Strain Curves

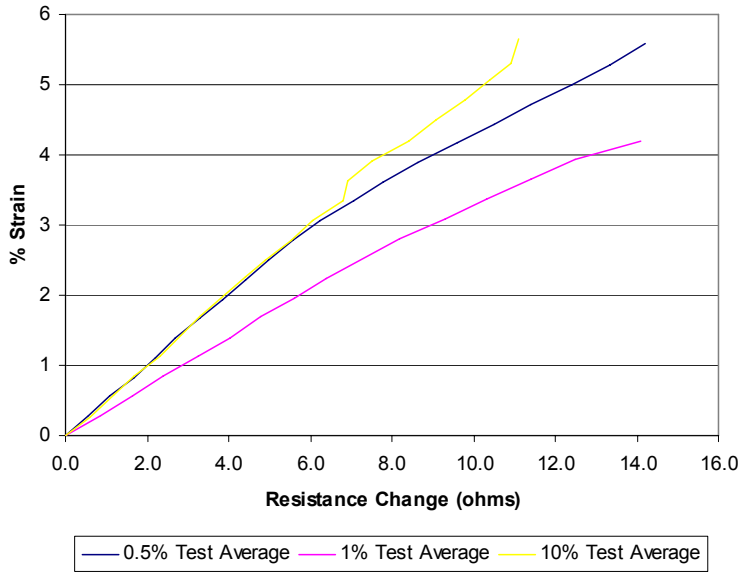

Figure 3.14 UX1500HS % Strain vs. Change in Resistance Curves

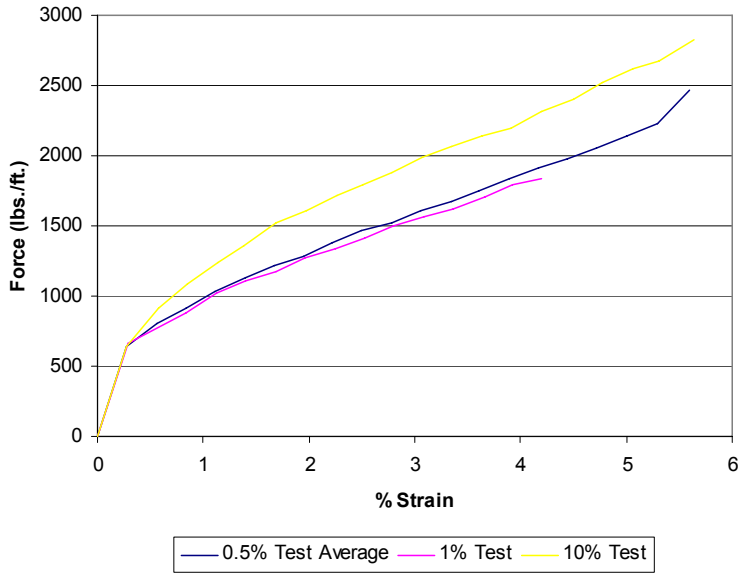

Figure 3.15 UX1500HS Force vs. Resistance Curves

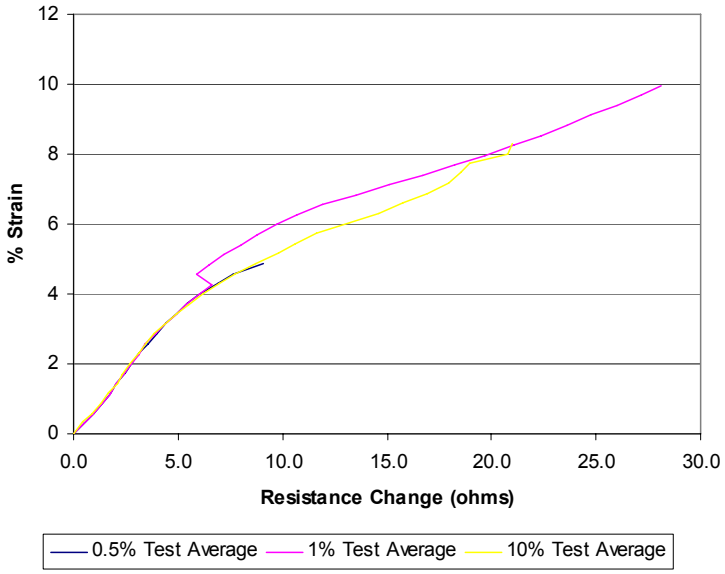

Figure 3.16 UX1400HS % Strain vs. Change in Resistance Curves

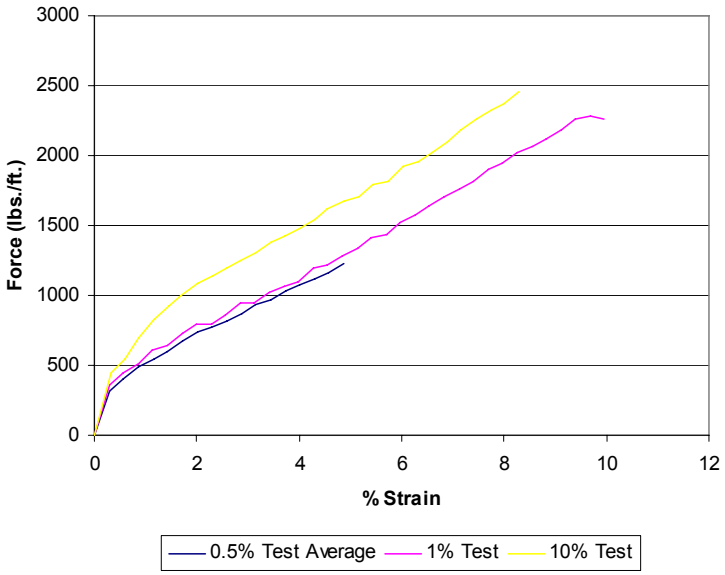

Figure 3.17 UX1400HS Force vs. % Strain Curves

In general, the results are very consistent. The strain results from the three tests performed at half a percent strain per minute were extremely close between tests for each different geogrid strength. Figure 3.9 demonstrates an example of the similarity. Clearly, each geogrid tested has very uniform properties. It can also be seen in the results that the resistance readings from the strain gages were relatively consistent at each different strain rate. There is, however, one obvious deviation in the behavior of the geogrid under different strain rates. As can be seen in the force versus strain curves, during the ten percent per minute strain rate tests, strains similar to the slower rate tests are produced with much higher loads. A conclusion that may be drawn is that the material is much stiffer at high strain rates. This increase in apparent strength and stiffness has to do with creep. At a high rate of loading, there is only a small component of creep, and as a result the material exhibits higher strength. However, this effect does not appear to take place at low strains, less than about half a percent strain in these tests. This indicates that at low strains, the strain rate has minimal influence.

After each instrumented geogrid layer was installed in the field, the resistance, in ohms, of each strain gage was measured. This reading serves as an initial, or zero reading. The initial reading is subtracted from each consecutive reading, yielding the change in resistance in the strain gage due to the loading condition at the time the reading was taken. Using the curves derived from the calibration testing, the measured resistance change can be transformed into the percent strain of the geogrid. A polynomial equation was developed for each curve. To determine the strain corresponding to a given resistance, the measured resistance difference served as the independent variable, x, in the polynomial equation developed

from the strain versus resistance curve. Solving this equation yielded the strain in percent, ε. Strains were obtained from Equation 1 for the UX1700HS geogrid, Equation 2 for the UX1600HS geogrid, Equation 3 for the UX1500HS geogrid, and Equation 4 for the UX1400HS geogrid.

$$\varepsilon = 2E\text{-}05x^6 - 0.0009x^5 + 0.0167x^4 - 0.1426x^3 + 0.5183x^2 + 0.2119x + 0.0478 \quad (1)$$

$$\varepsilon = -1E\text{-}05x^4 + 0.002x^3 - 0.077x^2 + 1.2373x - 0.2851 \quad (2)$$

$$\varepsilon = -1E\text{-}06x^6 + 4E\text{-}05x^5 - 0.0003x^4 - 0.0016x^3 + 0.0155x^2 + 0.4842x - 0.0008 \quad (3)$$

$$\varepsilon = -7E\text{-}06x^6 - 1E\text{-}05x^5 + 0.0038x^4 - 0.0511x^3 + 0.2216x^2 + 0.4196x + 0.0027 \quad (4)$$

The same process was used to determine the corresponding force. A polynomial equation was developed from the appropriate force versus strain curve. The previously determined strain served as the independent variable, x, to solve for force. The dependent variable, T, is the tensile load in the geogrid in pounds per foot. Forces were obtained from Equation 5 for the UX1700HS geogrid, Equation 6 for the UX1600HS geogrid, Equation 7 for the UX1500HS geogrid, and Equation 8 for the UX1400HS geogrid.

$$T = -0.4276x^6 + 10.698x^5 - 106.01x^4 + 529.73x^3 - 1407.3x^2 + 2309.9x + 77.08 \quad (5)$$

$$T = -0.4866x^6 + 11.68x^5 - 110.56x^4 + 524.53x^3 - 1304.7x^2 + 1984.3x + 49.021 \quad (6)$$

$$T = -1.7755x^6 + 36.446x^5 - 288.22x^4 + 1111.8x^3 - 2176.5x^2 + 2304.1x + 45.295 \quad (7)$$

$$T = -2.4271x^6 + 40.059x^5 - 257.91x^4 + 818.79x^3 - 1338.5x^2 + 1252.5x + 12.792 \quad (8)$$

This process was repeated for each gage, for every date a reading of the strain gages was taken.

3.2 Settlement Plates

Settlement plates used in this project were fabricated by the contractor. Each consisted of a two feet by two feet square steel plate. Two pipes were installed onto each plate, one encased inside the other. The outer pipe is held in place by the soil. The plate was placed at the original ground surface location. As settlement occurs due to the embankment being constructed, the plate moves downward, along with the inner pipe. Since the outer pipe is held in place, the relative movement, or settlement, can be measured. This is accomplished by the surveyor. Using a level, the surveyor places his rod on top of the pipe and reads the elevation. The change in elevation is the result of the settlement that occurred. As the embankment was constructed, three to four feet long sections of pipe were added to both of the pipes so that they rose with the embankment, allowing for continued readings.

Four settlement plates were installed at different offsets at station 289+00. The initial reading for three of these settlement plates was taken on March 1, 2006. For settlement plate 289-53R, the initial reading was not taken until May 16, 2006. The locations of the settlement plates can be seen in Figure 3.18, denoted by circles. Table 3.1 shows the offsets and elevations of the settlement plates.

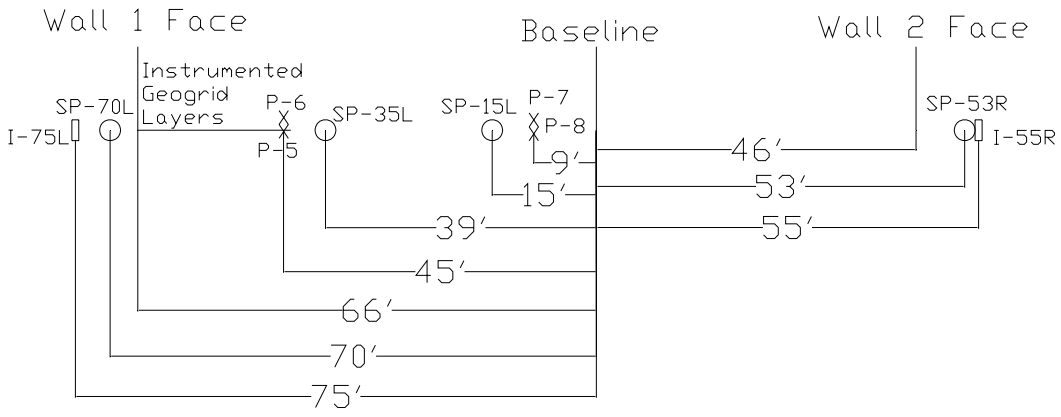

Figure 3.18 Instrumentation Locations at Station 289+00

Table 3.1 Settlement Plate Locations and Elevations

Plate Number	Location	Distance from Wall Face (ft)	Original Ground Elevation (ft)	Original Plate Elevation (ft)
289-15L	In Embankment	51	4.00	1.71
289-35L	In Embankment	31	3.50	1.47
289-53R	Outside Embankment	119	10.25	8.06
289-70L	Outside Embankment	4	1.50	-0.21

3.3 Piezometers

Prior to the start of construction, piezometers were installed by the contractor in order to monitor the level of excess pore water pressure as construction of the embankment proceeded. The piezometers used in this project are general purpose Slope Indicator 100 pounds per square inch vibrating wire piezometers. When a change in water pressure occurs on the diaphragm of the instrument, a change in tension of wire inside occurs. An electro-magnetic coil is used to excite the wire, which then vibrates. A frequency signal is then transmitted to the readout device. Calibration factors are applied to the frequency to determine the corresponding pressure (Slope Indicator 2006b).

The piezometers were installed by lowering the device into a borehole to the specified depth, then filling the borehole with a bentonite-cement grout. Four piezometers were installed at station 289+00. The locations of these piezometers are as shown in Figure 3.18, each marked by an "X." Details concerning the installation of these piezometers are shown in Table 3.2.

Table 3.2 Piezometer Installation Data

				Installation						
Piez. #	Sta.	Offset (ft)	GS El. (ft ±)	Depth (ft ±)	Tip El. (ft ±)	Drilled (ft ±)	Dist. to Wall (ft ±)	Cable Length (ft)	Serial #	Install Date
5	289 +00	45	2.7	73	-70.3	77	20	130	85011	01/05/ 06
6	289 +00	45	2.7	53	-50.3	57	20	100	85003	01/10/ 06
7	289 +00	10	2.9	73	-70.1	77	65	180	85021	01/09/ 06
8	289 +00	10	2.9	53	-50.1	57	65	160	85016	01/10/ 06

3.4 Inclinometers

Vertical inclinometers were installed for this project to monitor the deformations of the embankment. To install a vertical inclinometer, 3.34" QC casing made from high-grade ABS plastic was installed in a vertical borehole. This casing was then surveyed using a Digitilt inclinometer probe manufactured by Slope Indicator, control cable, pullout assembly, and readout device. To make a survey, the probe is pulled upward from the bottom of the casing and stopped at intervals of two feet for a reading. The inclination of the probe is measured with two force-balanced servo-accelerometers. One of these accelerometers measures tilt in the plane of the inclinometer wheels, while the other measures the tilt perpendicular to this direction (Slope Indicator 2006a). The first survey was completed at the time of installation and serves as the initial case. Subsequent surveys are compared to the initial case to reveal any movement of the ground.

Two inclinometers were originally installed at station 289+00. In October, the inclinometer offset -75 feet was replaced, as it became inoperable. The probe could not be lowered to the bottom of the casing. Most likely, the casing was shifted too far from its original vertical orientation due to large movements in the soil. In January, the inclinometer offset 55 feet began to give unreliable readings, and it was replaced. The locations of the two original inclinometers, as well as the replacement, are shown in Figure 3.18. The installation details for the inclinometers are shown in Table 3.3.

Table 3.3 Vertical Inclinometer Installation Details

Design Station	Design O/S	Ground El.	Top Pipe El.	Approx. Tip El.	AB Station	AB Offset	Status
289+00	-75	3.00	5.62	-105	289+00.98	-75.94	Abandoned
289+10	-75	1.29	4.09	-108	289+08.81	-74.87	Replacement
289+00	55	10.28	12.56	-105	288+99.62	54.57	Abandoned
289+00	55	9.75	12.17	-105	289+09.00	53.45	Replacement

Chapter 4

MEASURED DATA

The installed instrumentation was monitored throughout the construction process. Strain gage readings were taken on a regular basis. Data was also collected for all settlement plates, piezometers, and inclinometers throughout construction.

4.1 Strain Gages

Strain gage resistance readings were performed by the University of Delaware. Data was collected from all of the installed strain gages every time a new instrumented layer was placed. After all layers were placed, readings were taken every two to four weeks. Resistance readings were taken on site and then converted to strains and forces as described in Section 3.1.3.

The following figures provide a visual representation of the strains measured in each layer of geogrid along the height of the wall. Each figure represents a different date that readings were taken, thus showing the progression of strain. The current location of the toe of the wall resulting from settling of the wall is shown. The elevation of the top of the wall at the time the readings were taken is also indicated. In the case that an instrumented layer was installed, but only the initial reading was taken, then values of strain were not yet available since strains were attained by determining the difference between a reading and the initial reading. This situation is depicted in the figures by a layer being labeled "data not available." In the case of a

malfunctioning gage, a dotted line represents interpolation between two adjacent working gages.

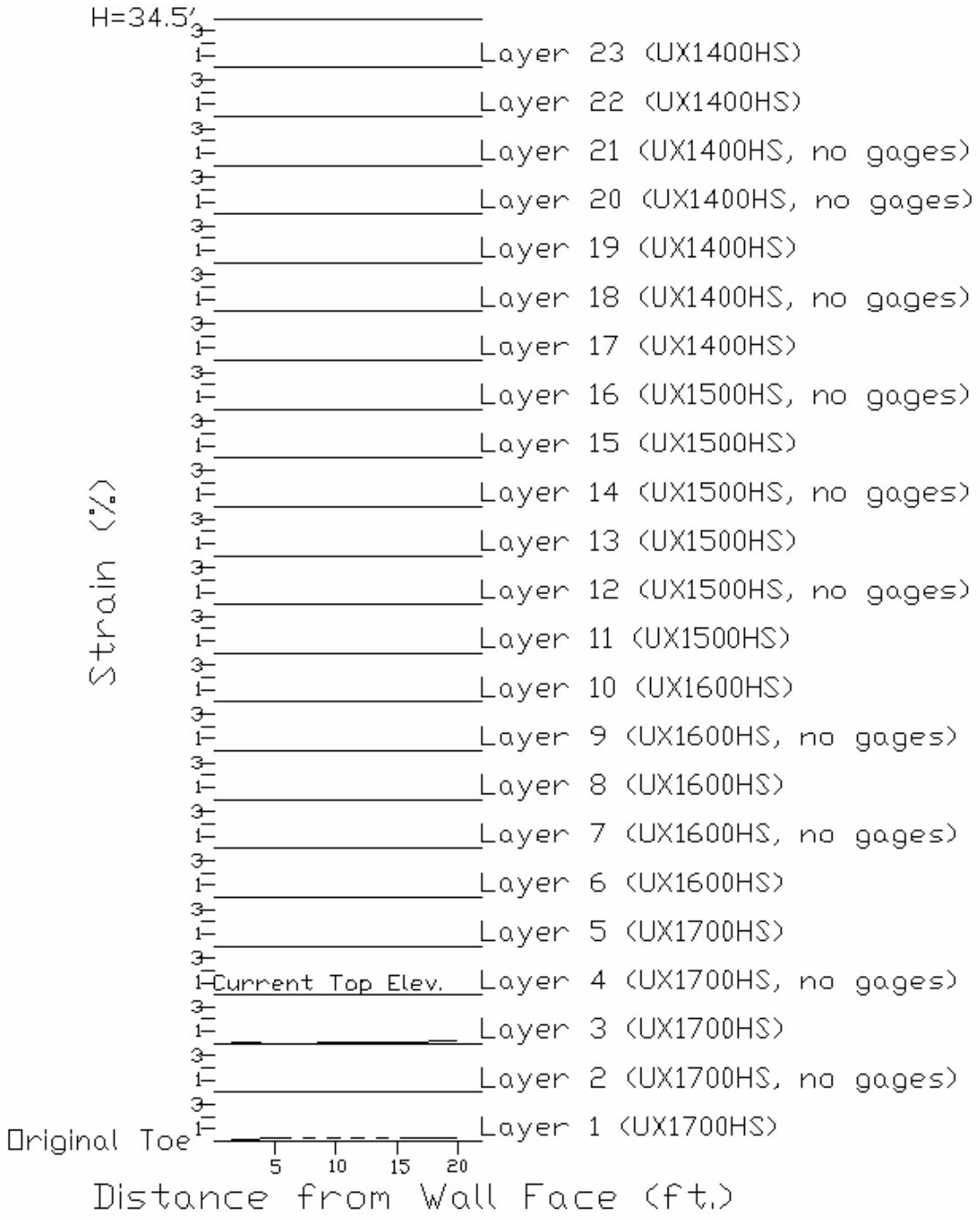

Figure 4.1 Strains Measured 3/1/06

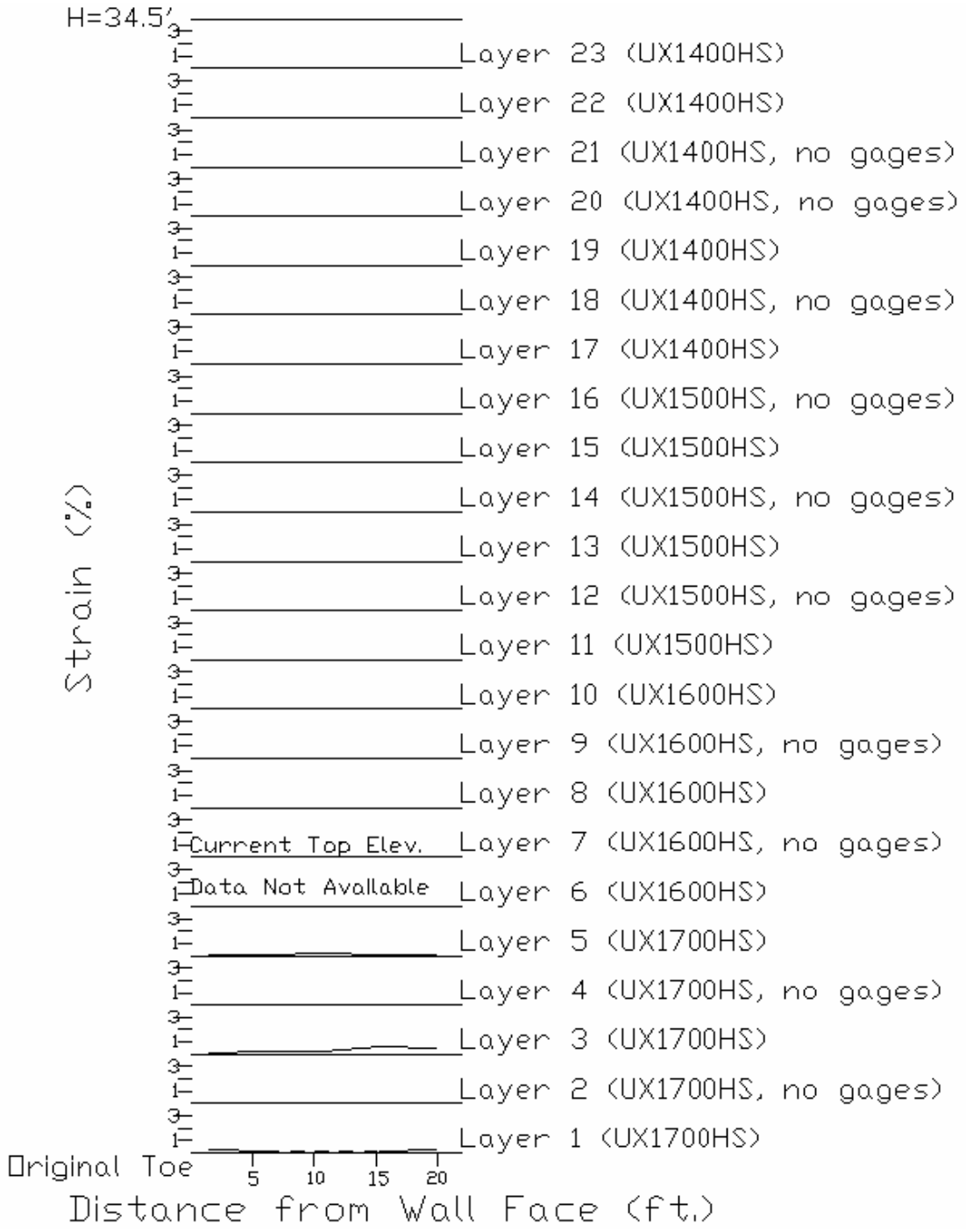

Figure 4.2 Strains Measured 3/23/06

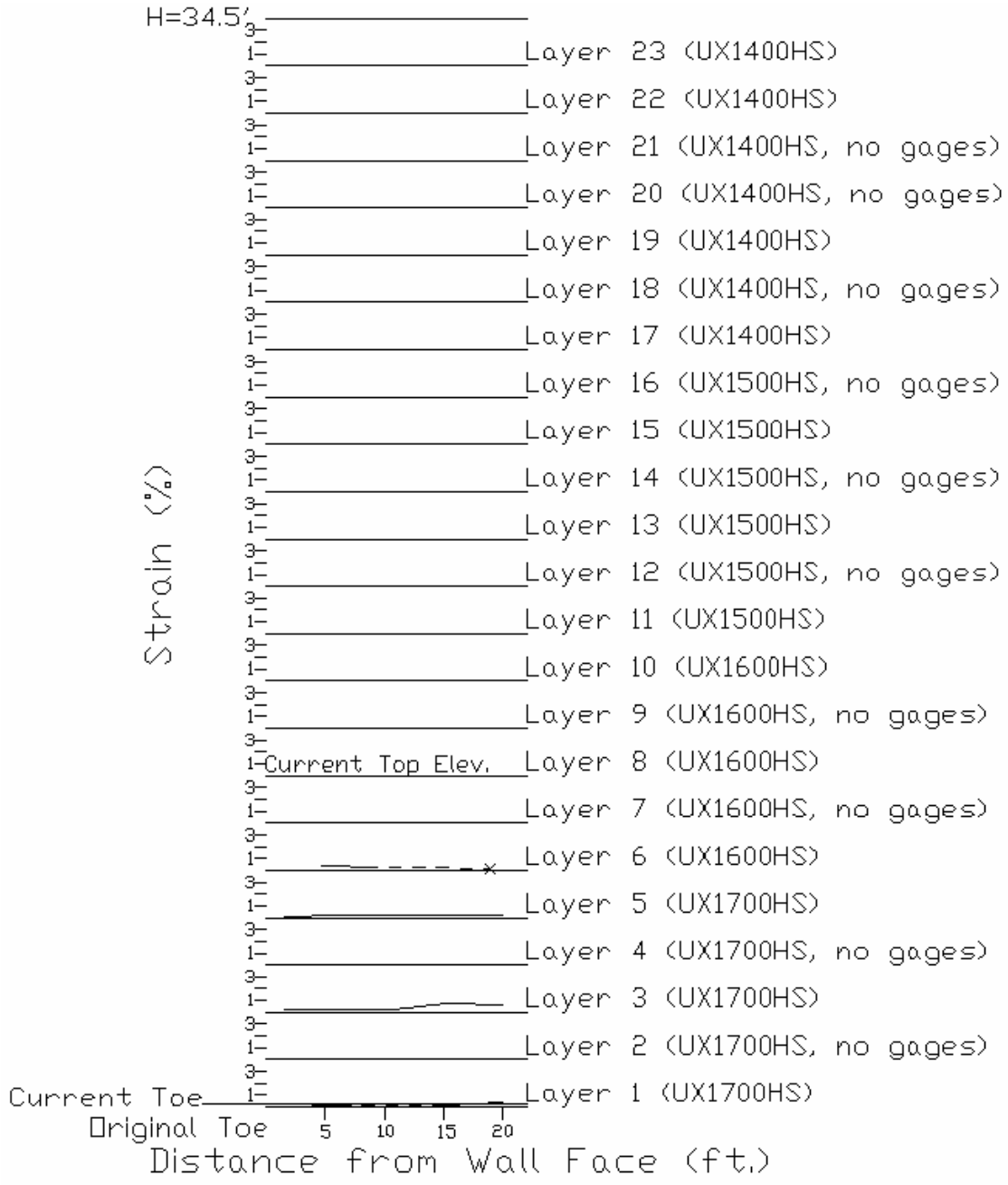

Figure 4.3 Strains Measured 4/11/06

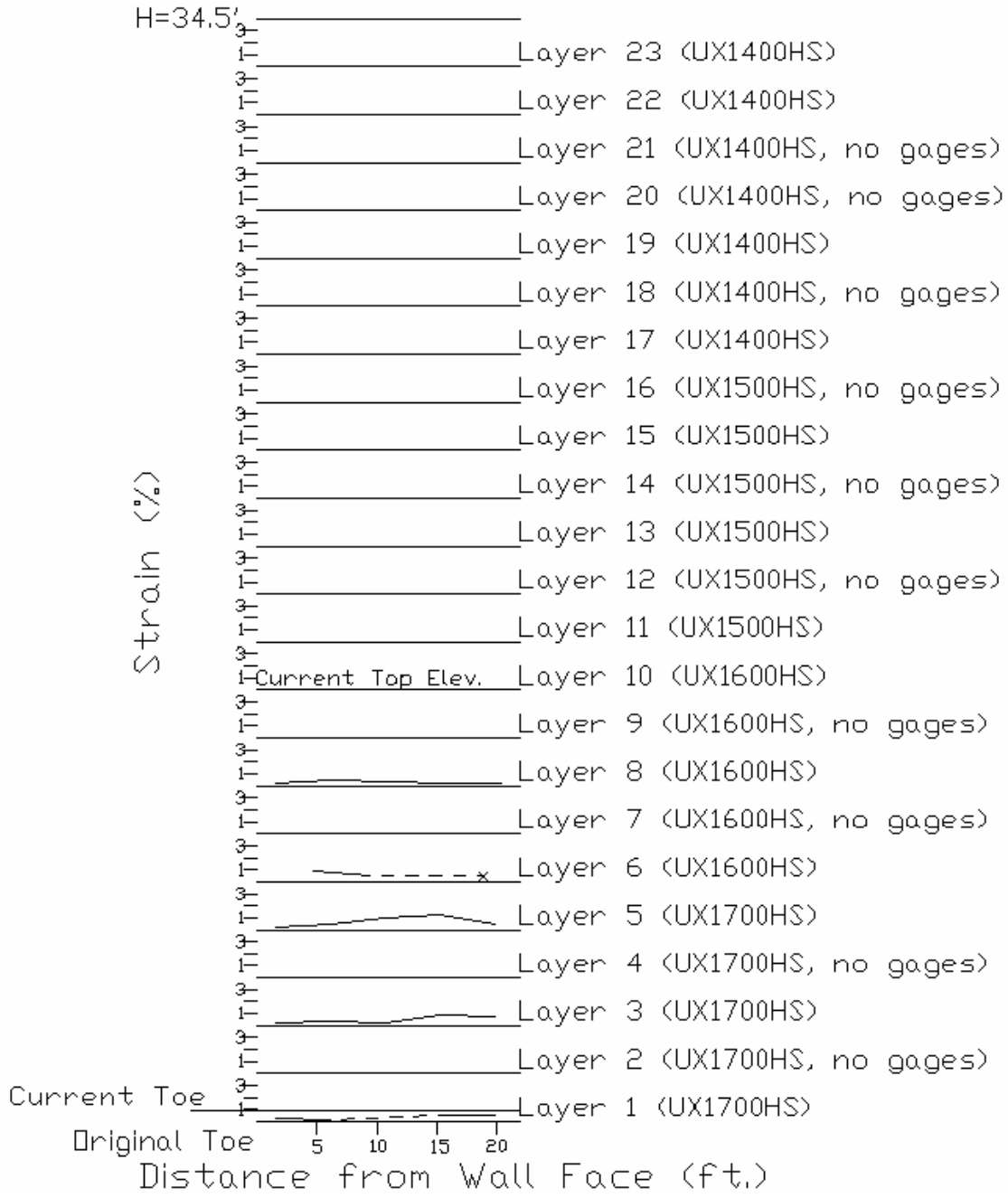

Figure 4.4 Strains Measured 5/16/06

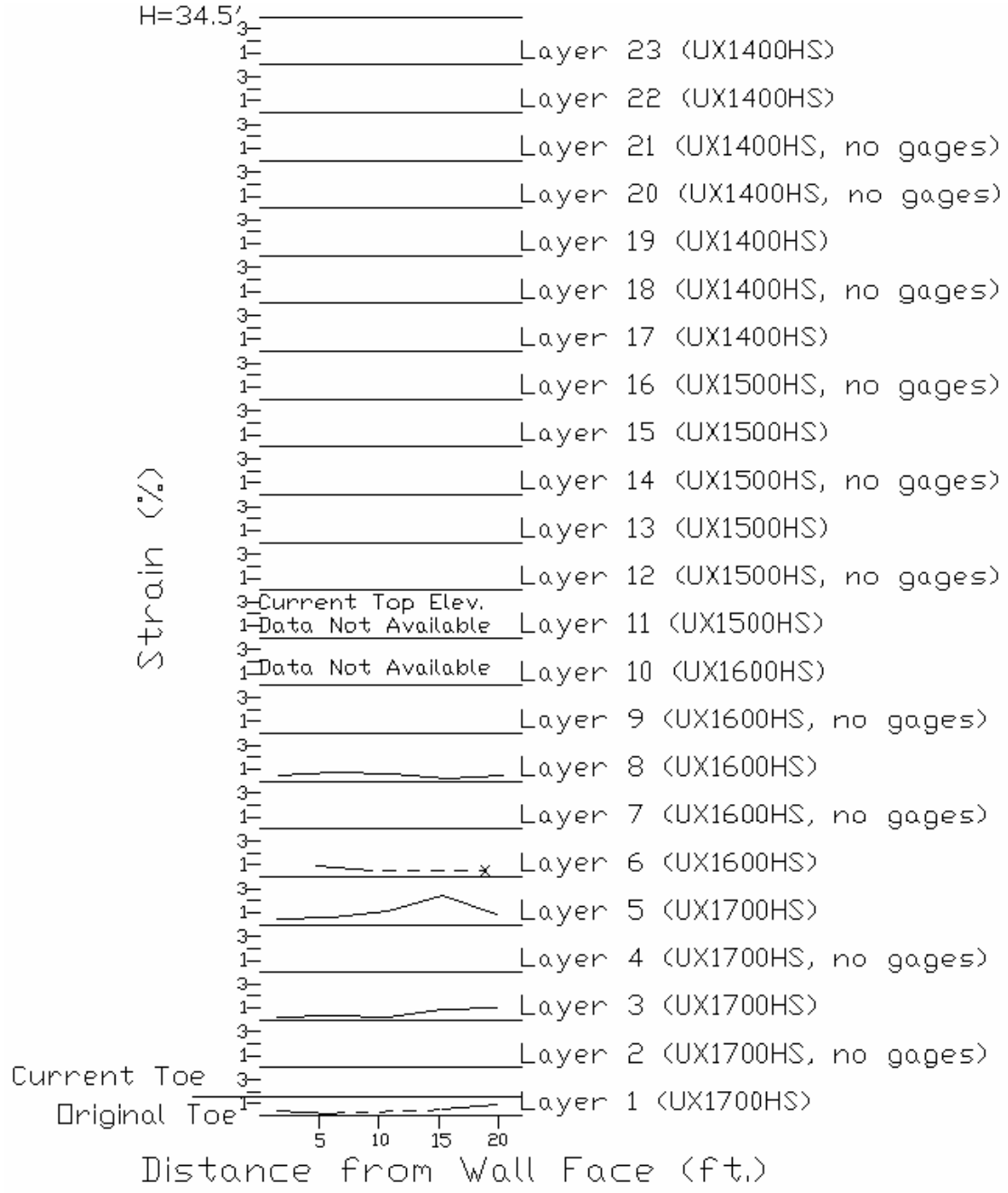

Figure 4.5 Strains Measured 6/27/06

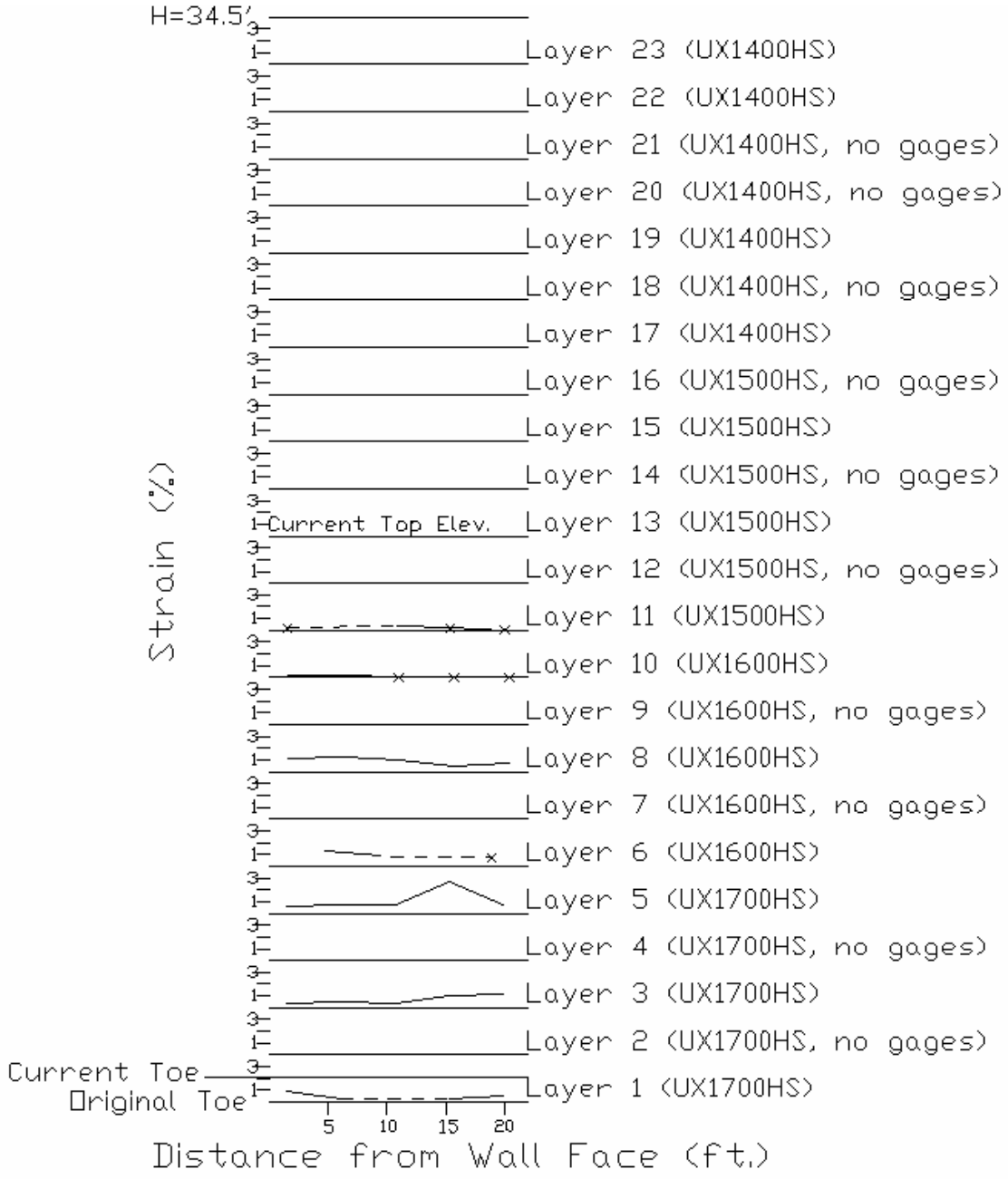

Figure 4.6 Strains Measured 7/24/06

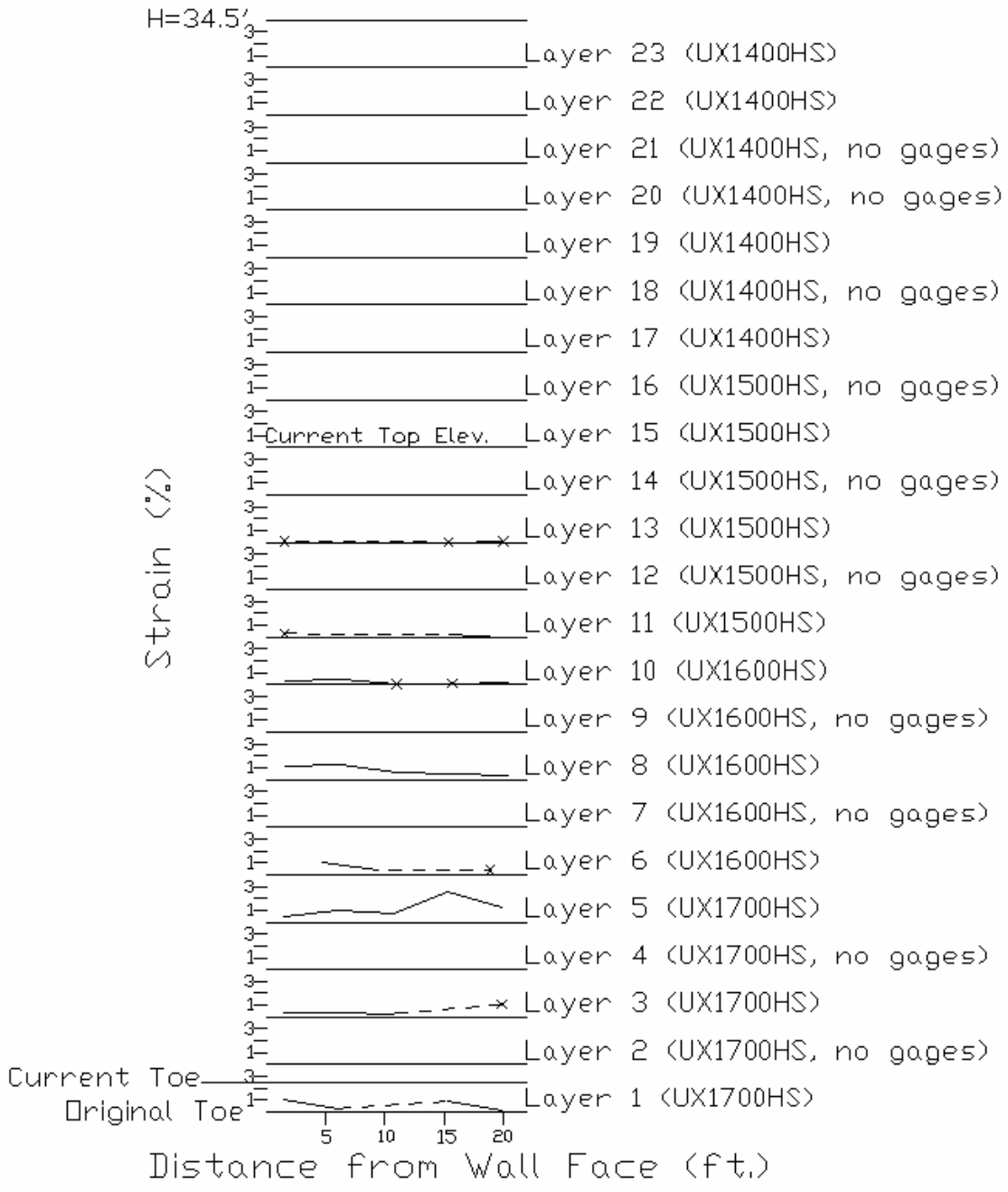

Figure 4.7 Strains Measured 8/11/06

After this reading, it became necessary to extend the leads coming from the layers installed thus far. Additional lengths of wire were spliced with the existing leads so that all of the leads could be run to a temporary box serving to protect the wire ends from corrosion. When this task was completed, however, the additional resistance of the added length of wire was not accounted for. As a result, the next readings taken from the strain gages were significantly higher. In order to account for the added resistance resulting from the additional length of wire, the added wires were removed, and the gage resistances were measured again. The wires were then reattached, and the resistances were again measured as a check to ensure this reading was the same as the reading before the additional lengths of wire were removed. By subtracting the resistance values taken without the additional lengths of wires attached from the readings with the lead extensions attached, the additional resistance from the extra lengths of wire was calculated. For every strain gage reading thereafter, the additional resistance value from the lead extensions was subtracted, resulting in a measurement consistent with previous readings.

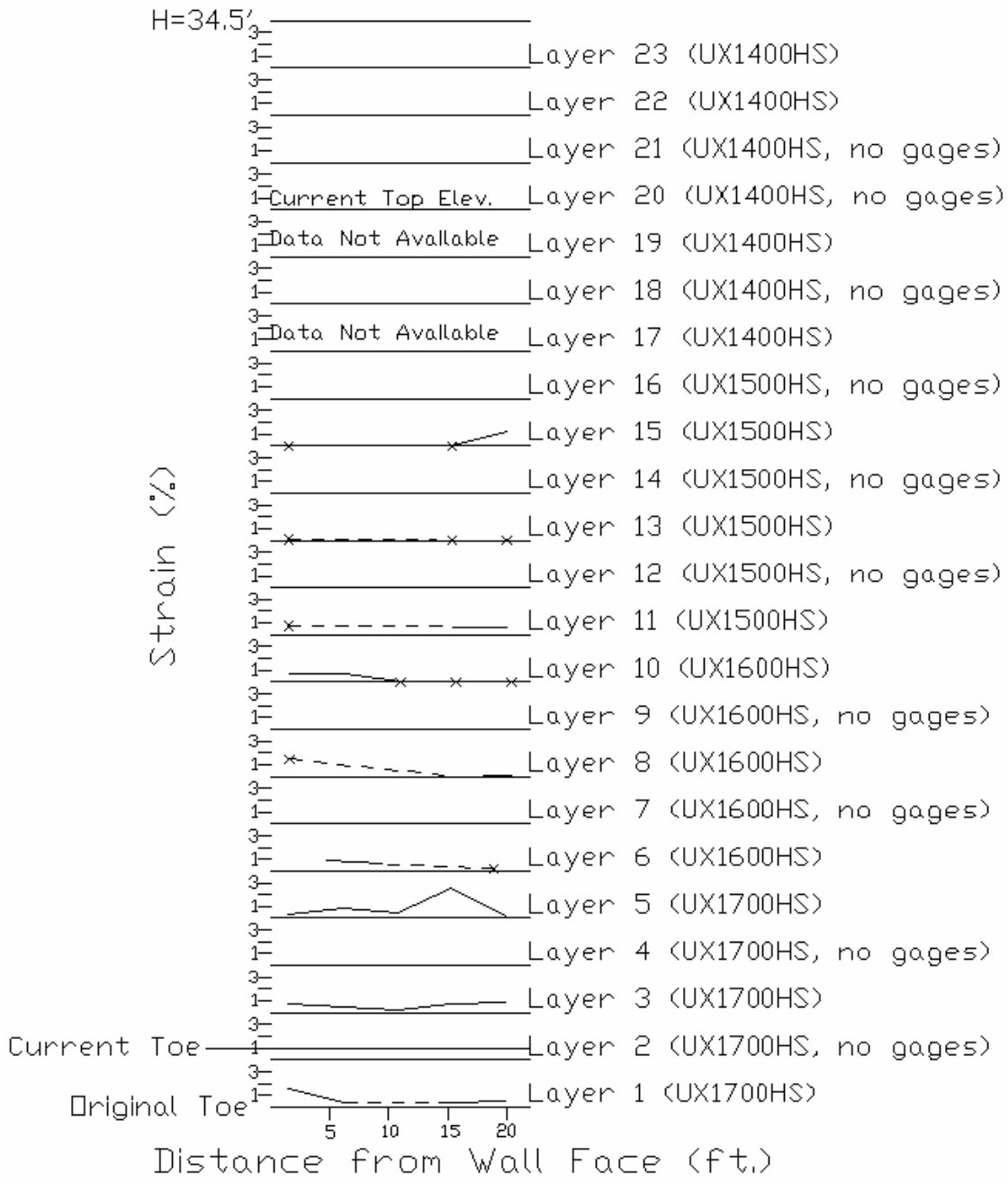

Figure 4.8 Strains Measured 10/5/06

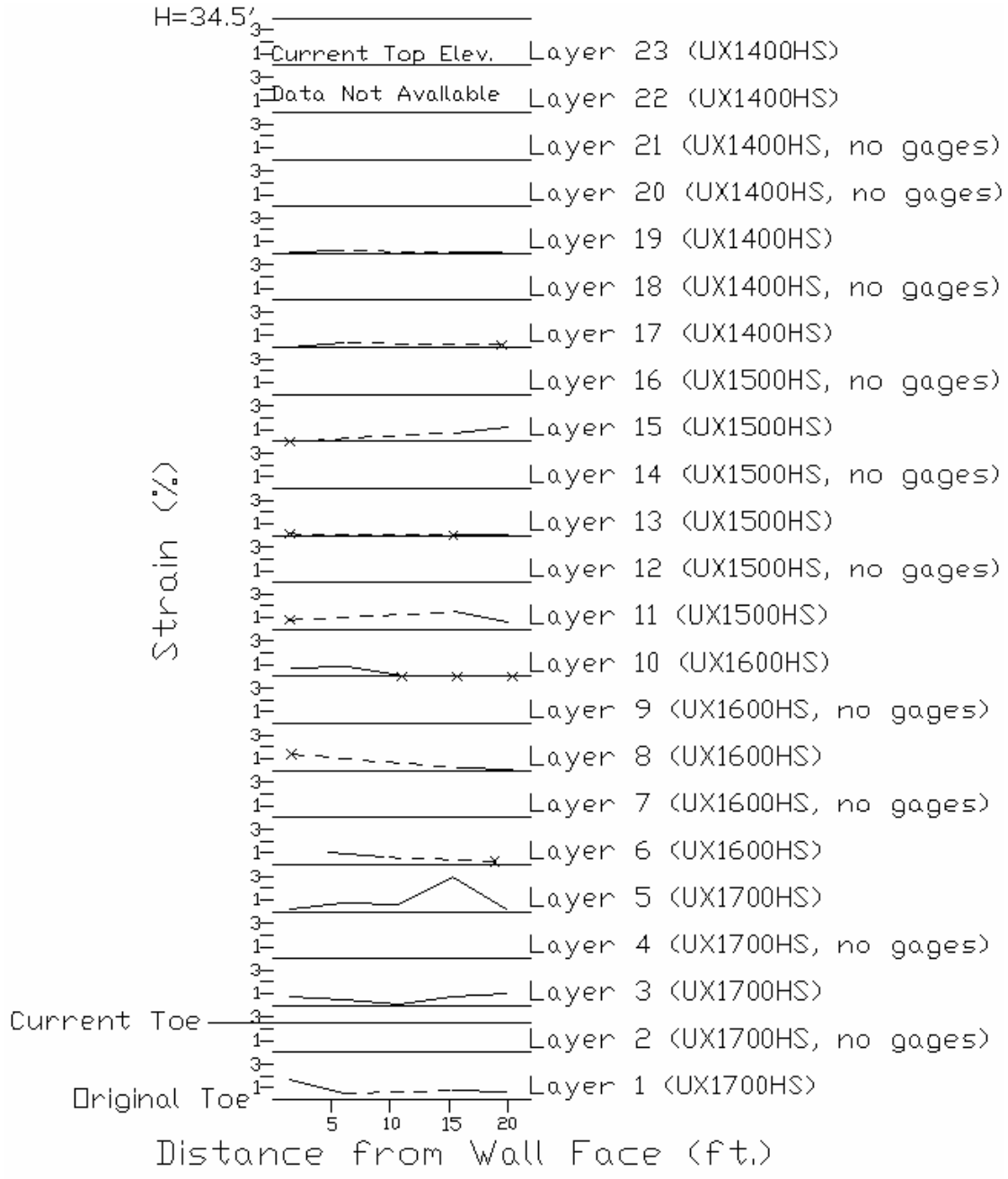

Figure 4.9 Strains Measured 11/9/06

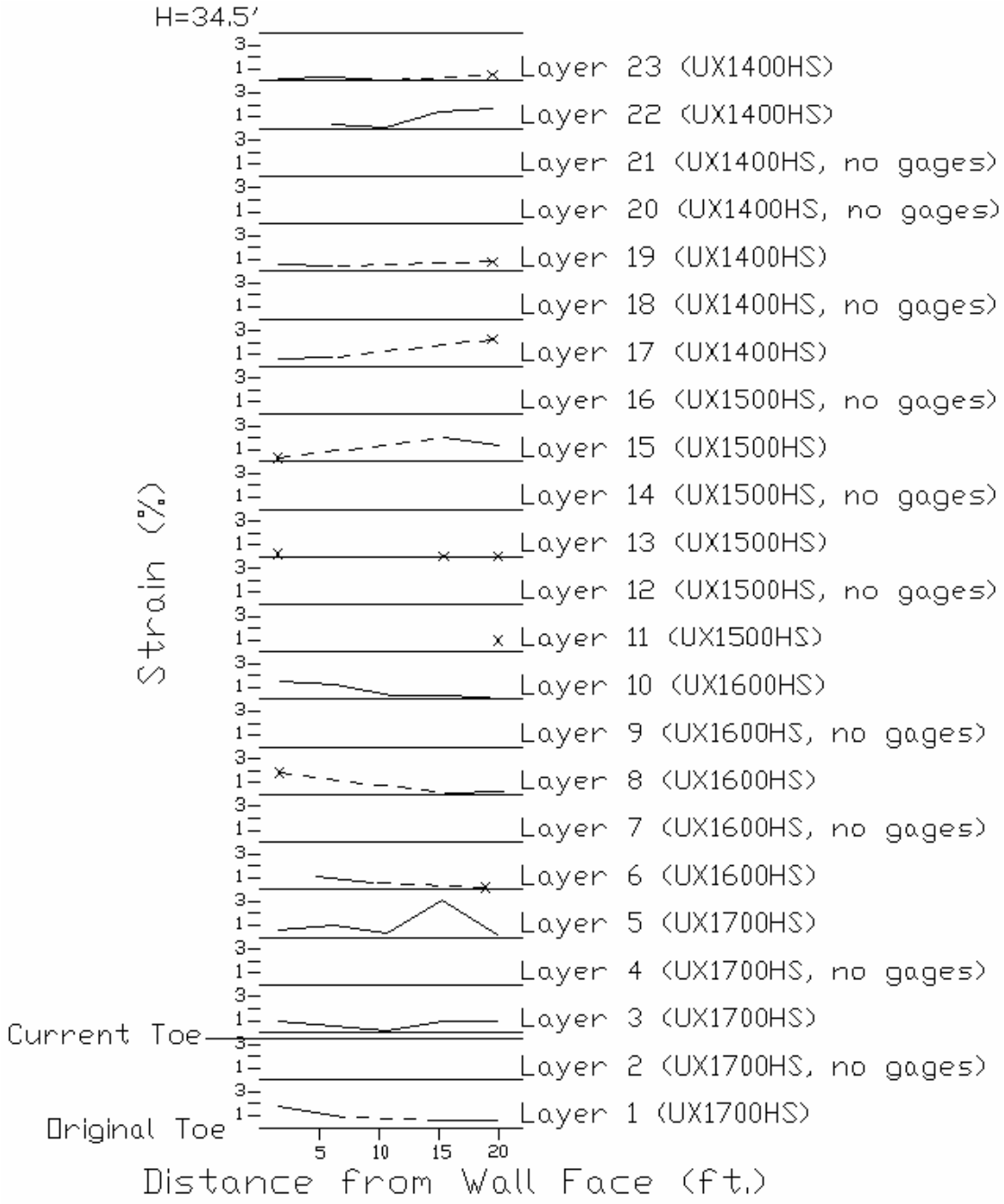

Figure 4.10 Strains Measured 12/5/06

As can be seen in Figure 4.10, the highest value of strain measured up to this point occurs in geogrid layer 5, about 15 feet from the wall face. This value is 3.18 percent strain. It is interesting to note that at the next time gage readings were taken, this gage was no longer functioning. This is seen in Figure 4.11. It is most likely that the large amount of strain caused the gage to malfunction.

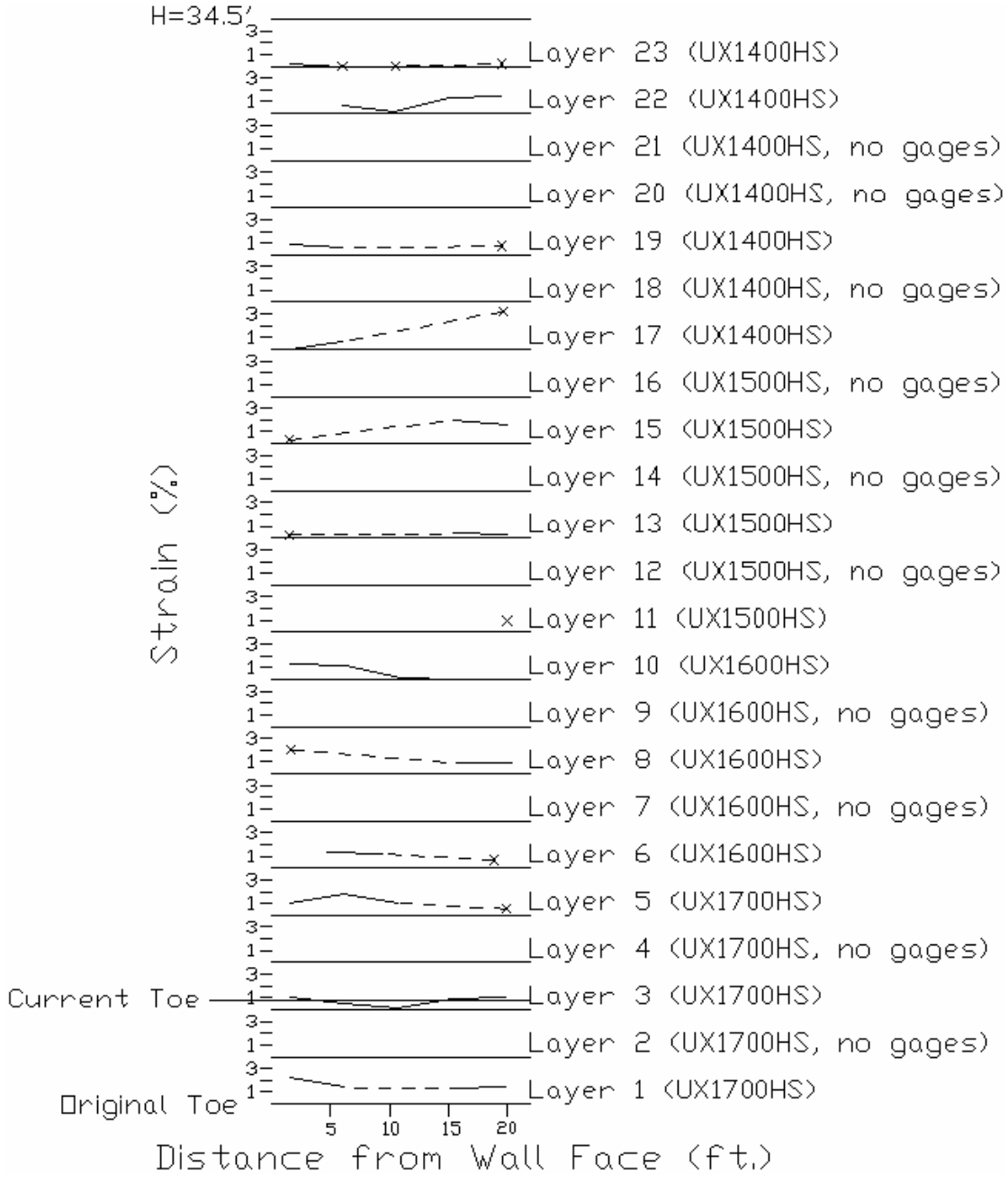

Figure 4.11 Strains Measured 1/12/07

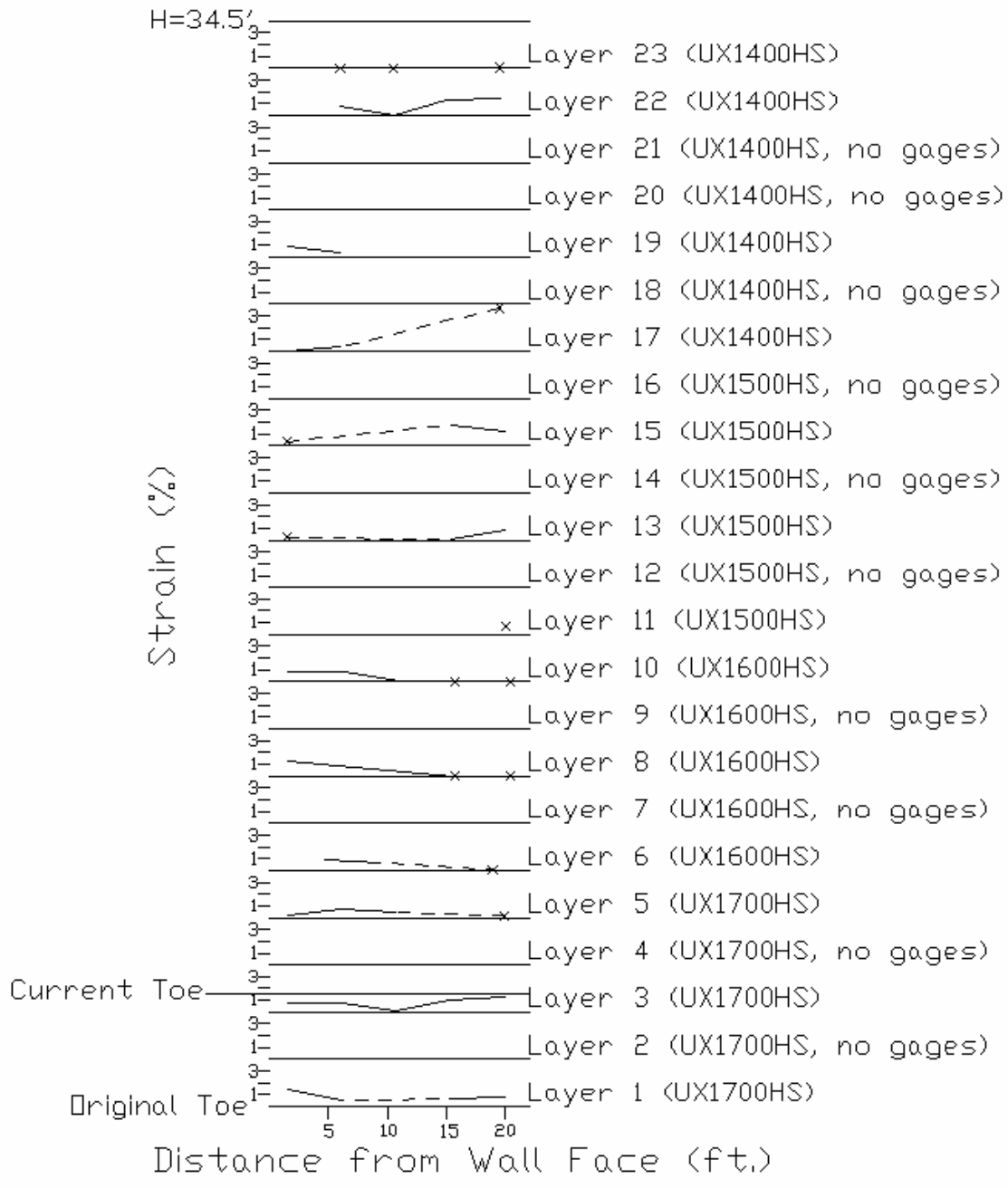

Figure 4.12 Strains Measured 2/12/07

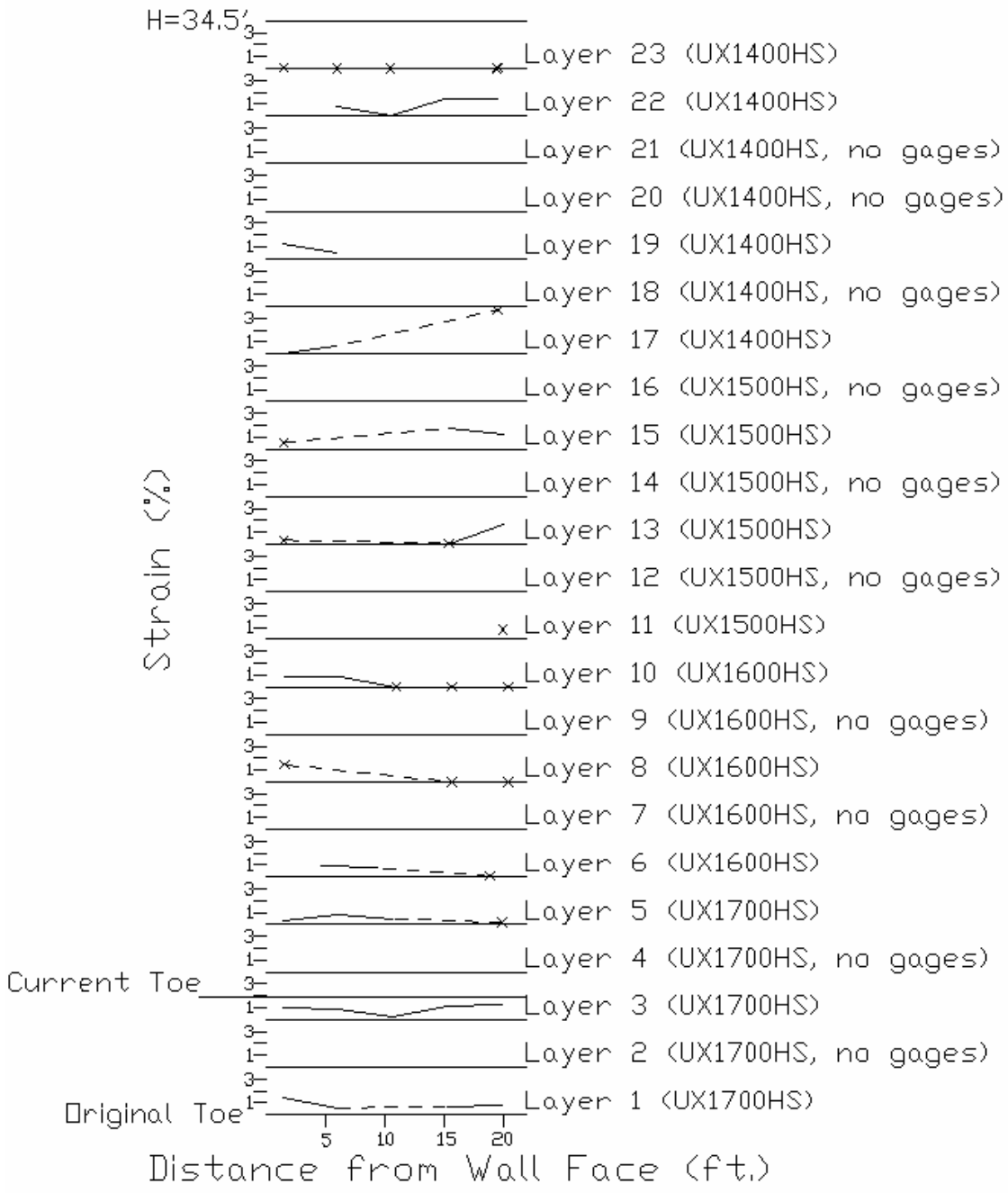

Figure 4.13 Strains Measured 3/12/07

As shown in Figures 4.11 through 4.13, measured strains have remained fairly constant since construction completion, with a couple exceptions. The February 12 data shows a decrease in almost all of the strains measured. The March 12 data is nearly identical to the February data, except that a few of the gages located farthest away from the wall face show an increase in strain. Possible causes of these measurements will be discussed in Chapter 5.

The next set of figures shows the forces in the instrumented geogrid layers that correspond to the strains shown in the previous set of figures.

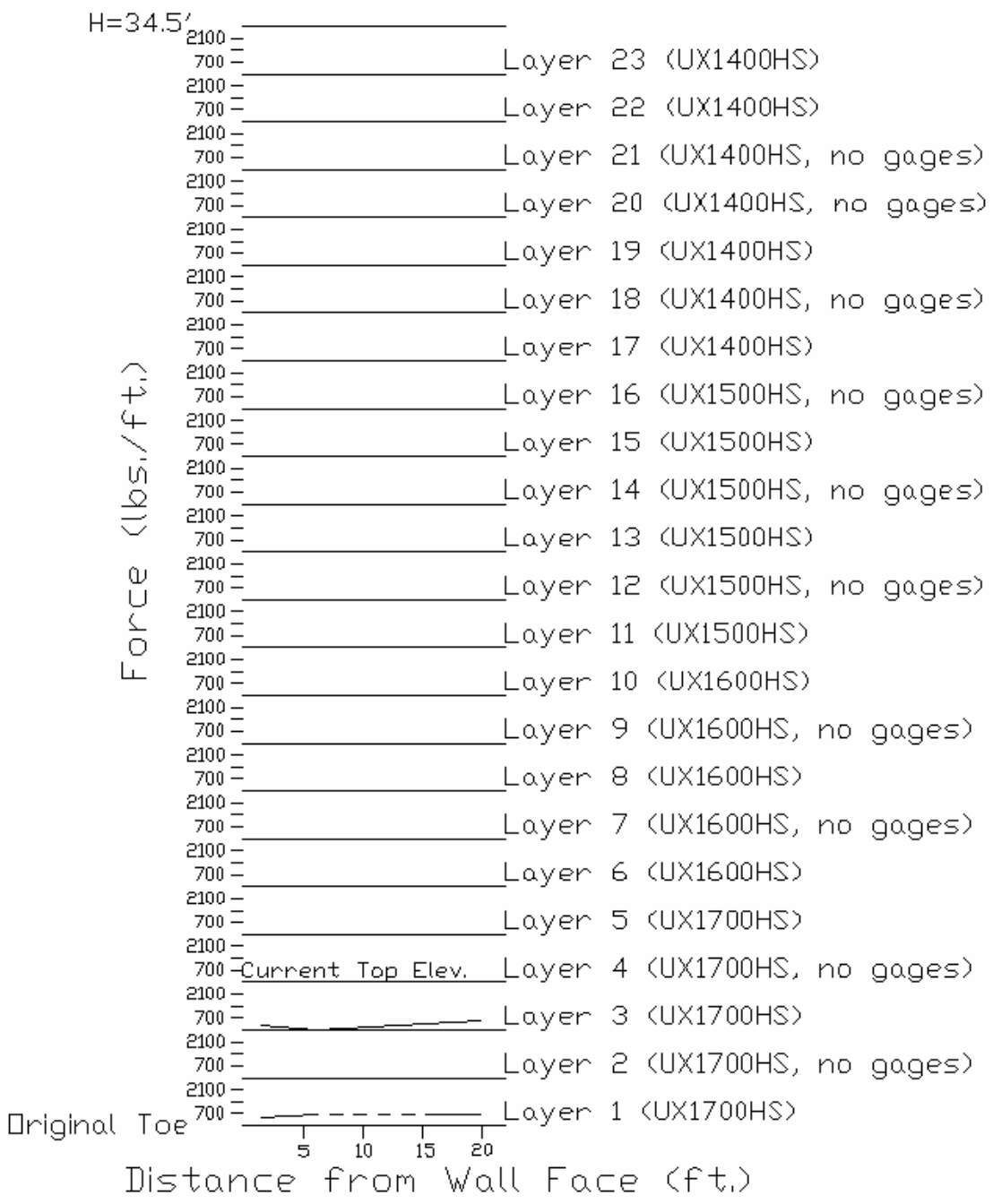

Figure 4.14 Forces Measured 3/1/06

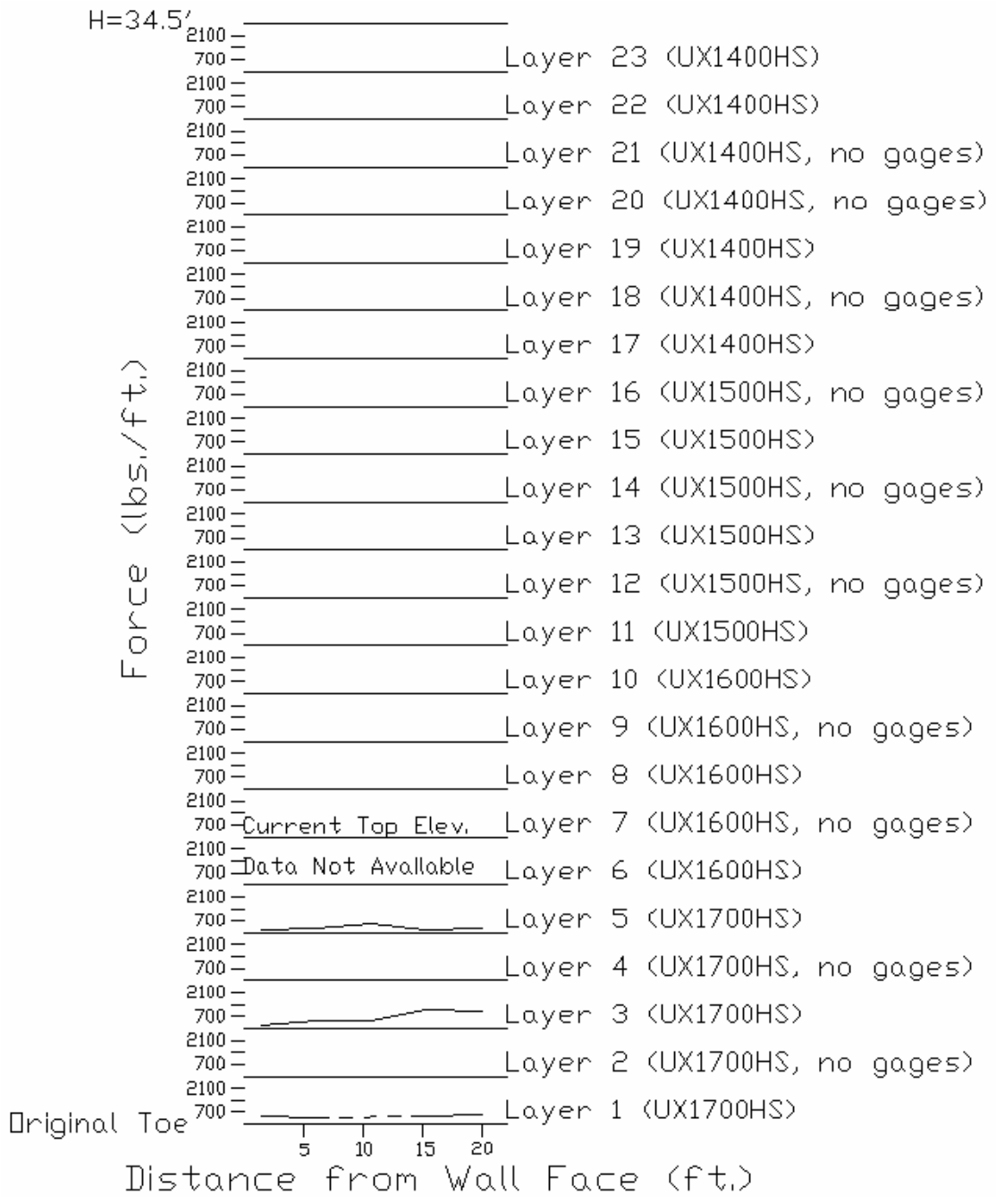

Figure 4.15 Forces Measured 3/23/06

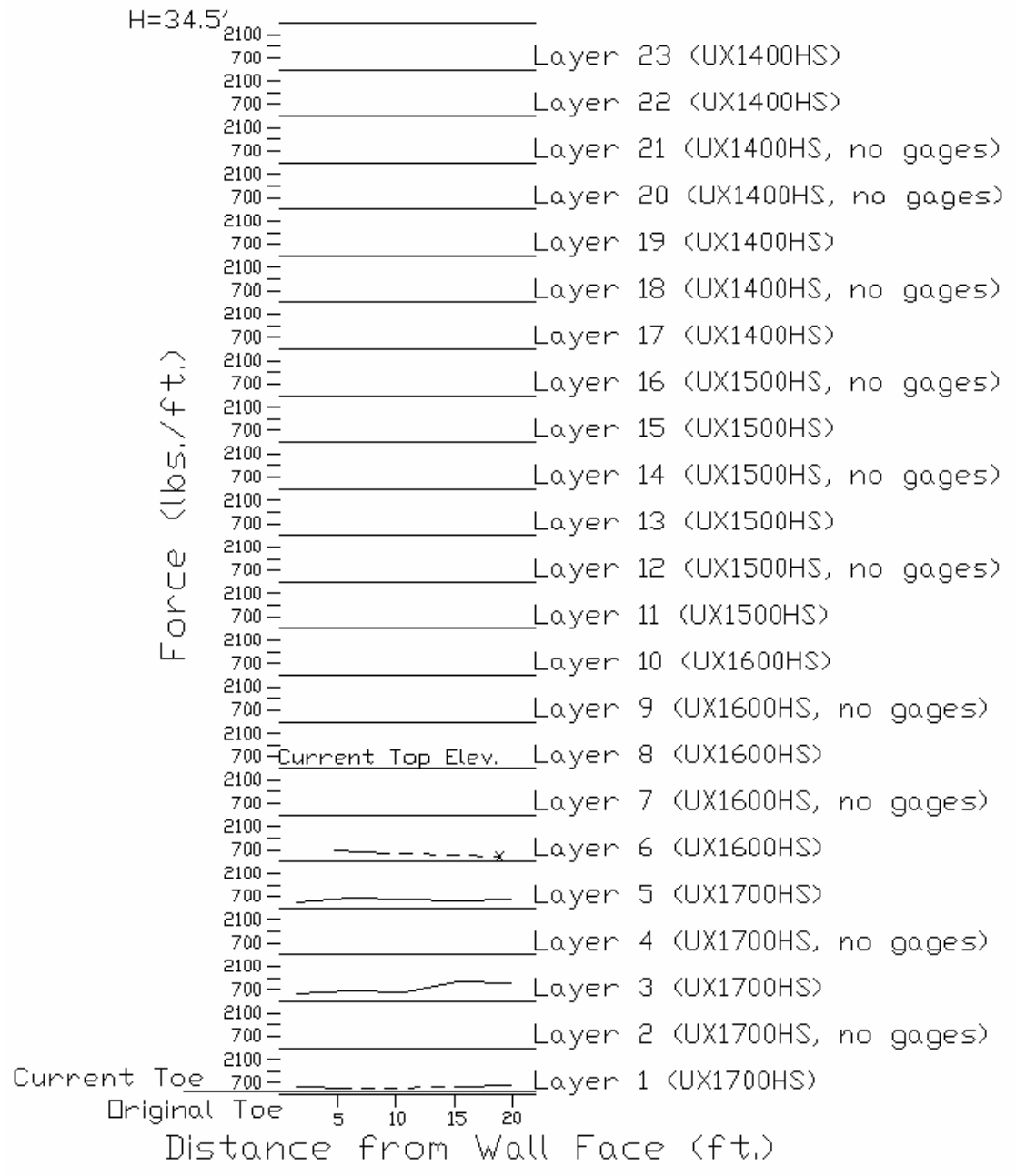

Figure 4.16 Forces Measured 4/11/06

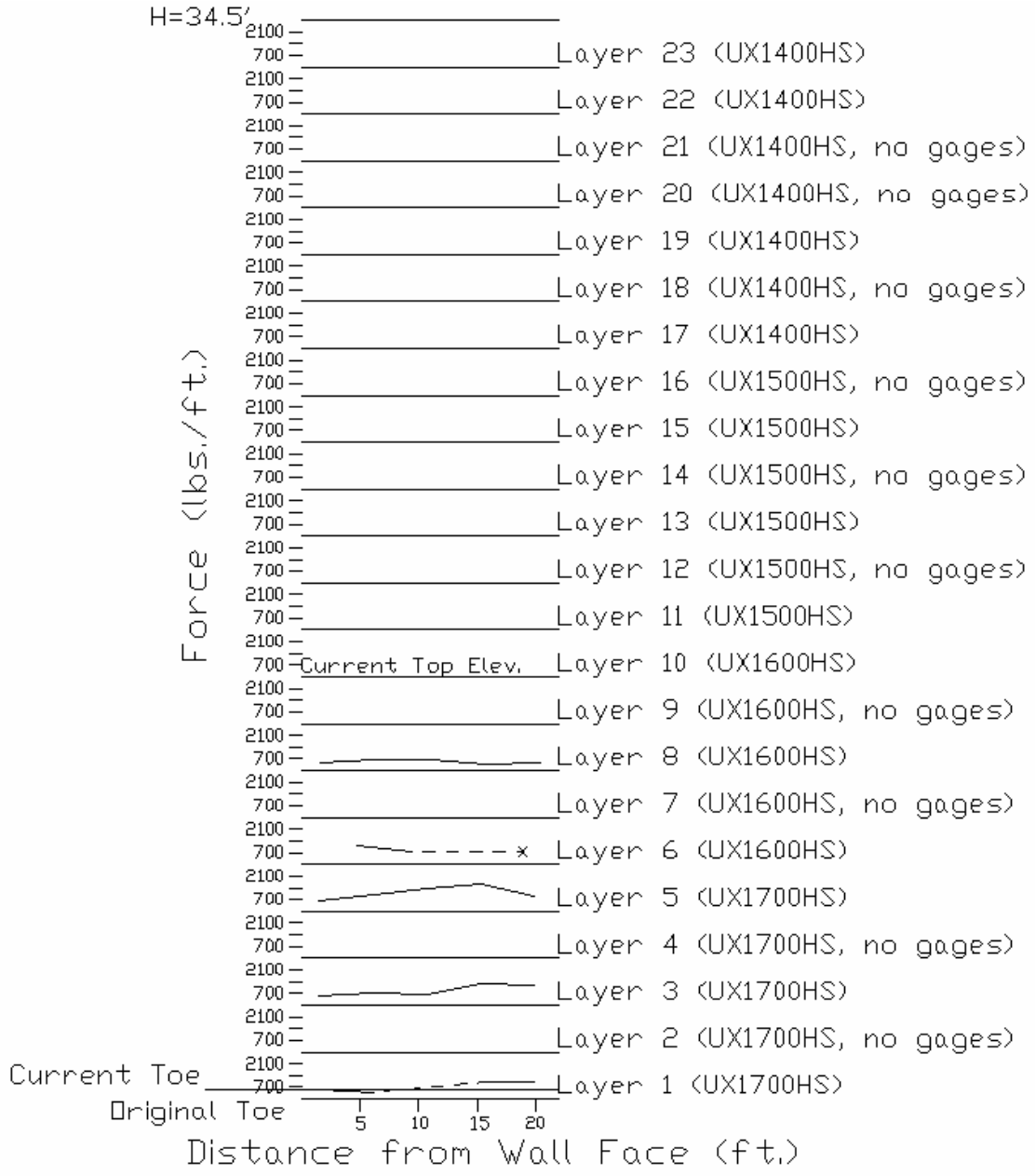

Figure 4.17 Forces Measured 5/16/06

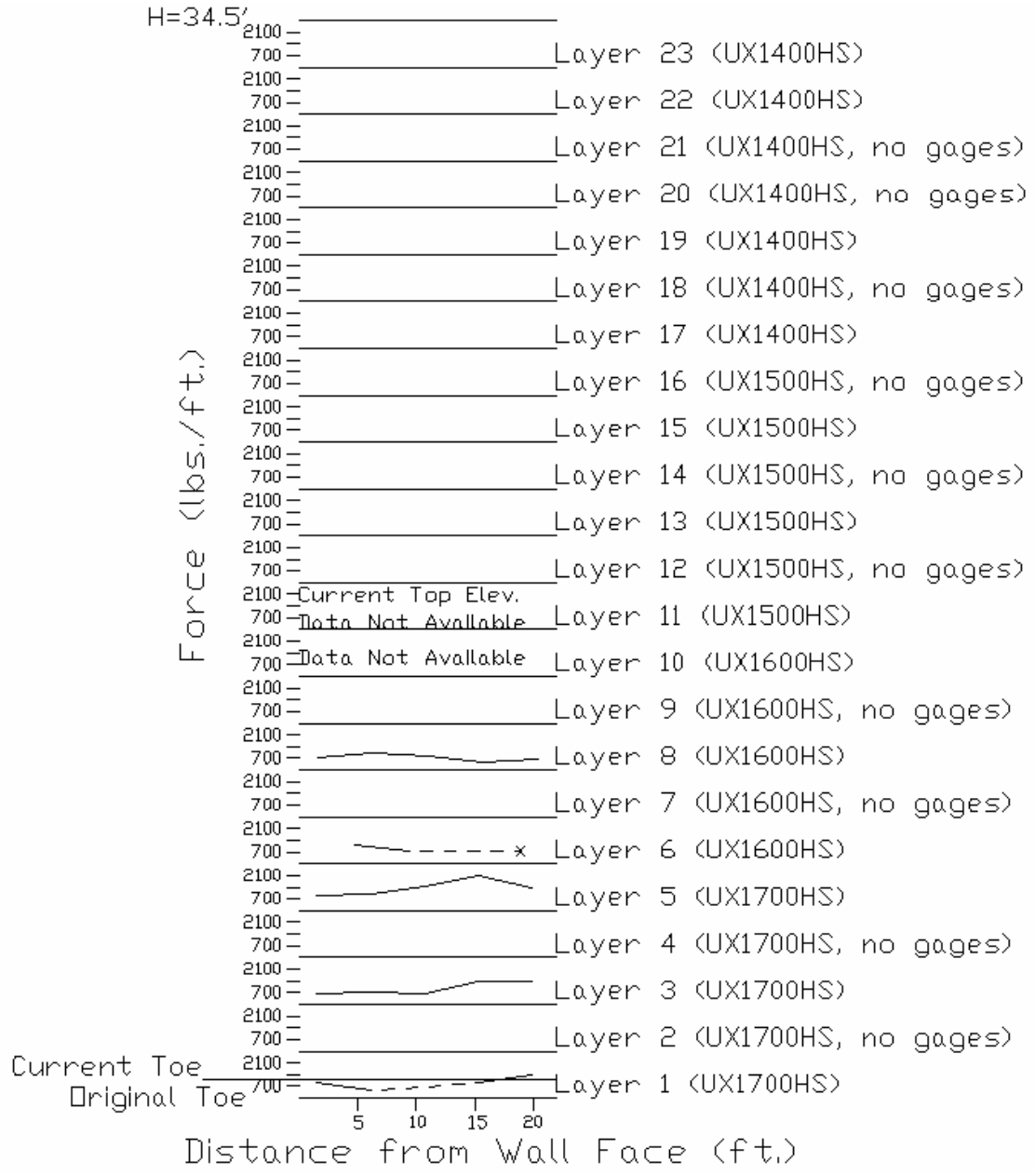

Figure 4.18 Forces Measured 6/27/06

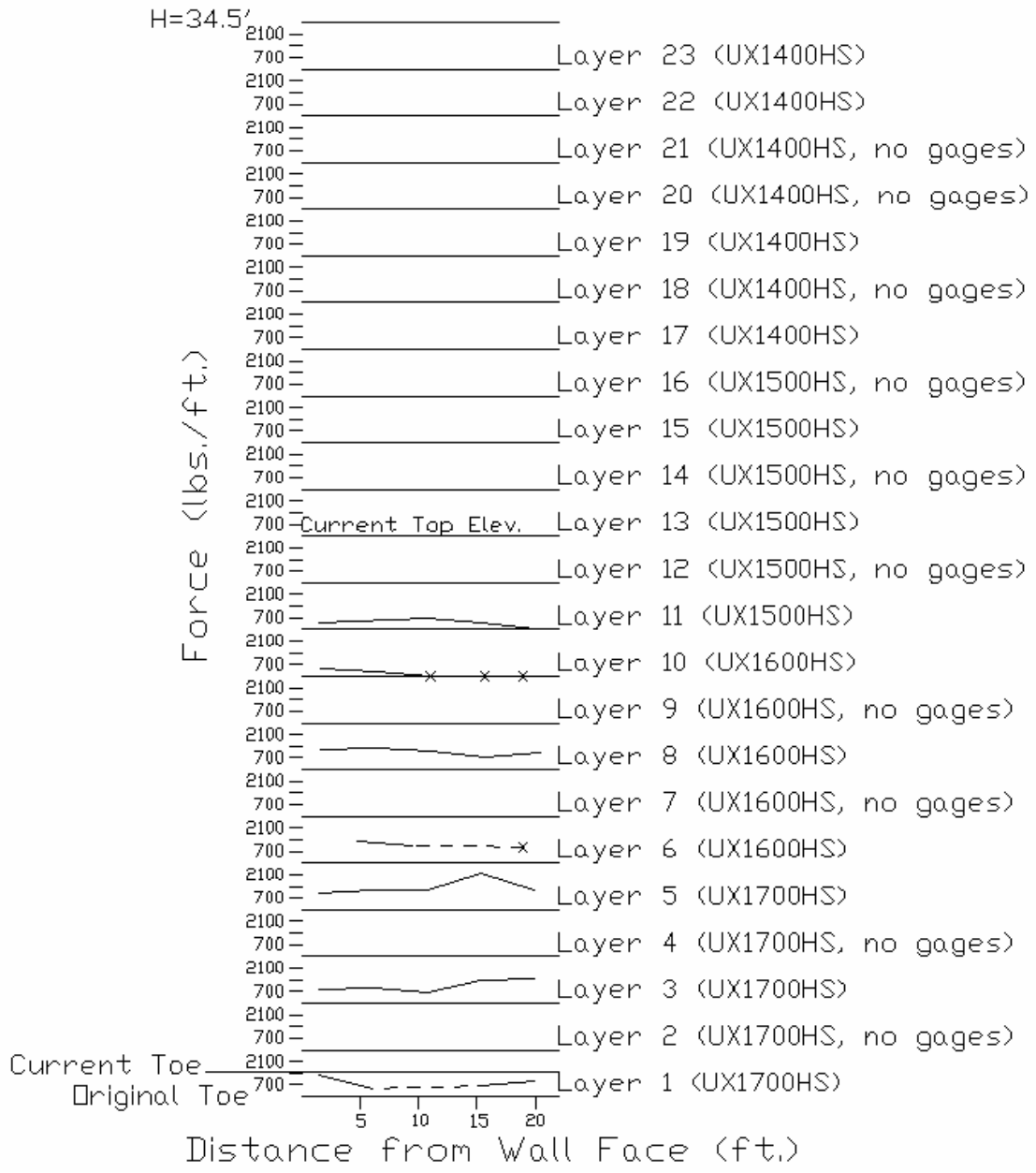

Figure 4.19 Forces Measured 7/24/06

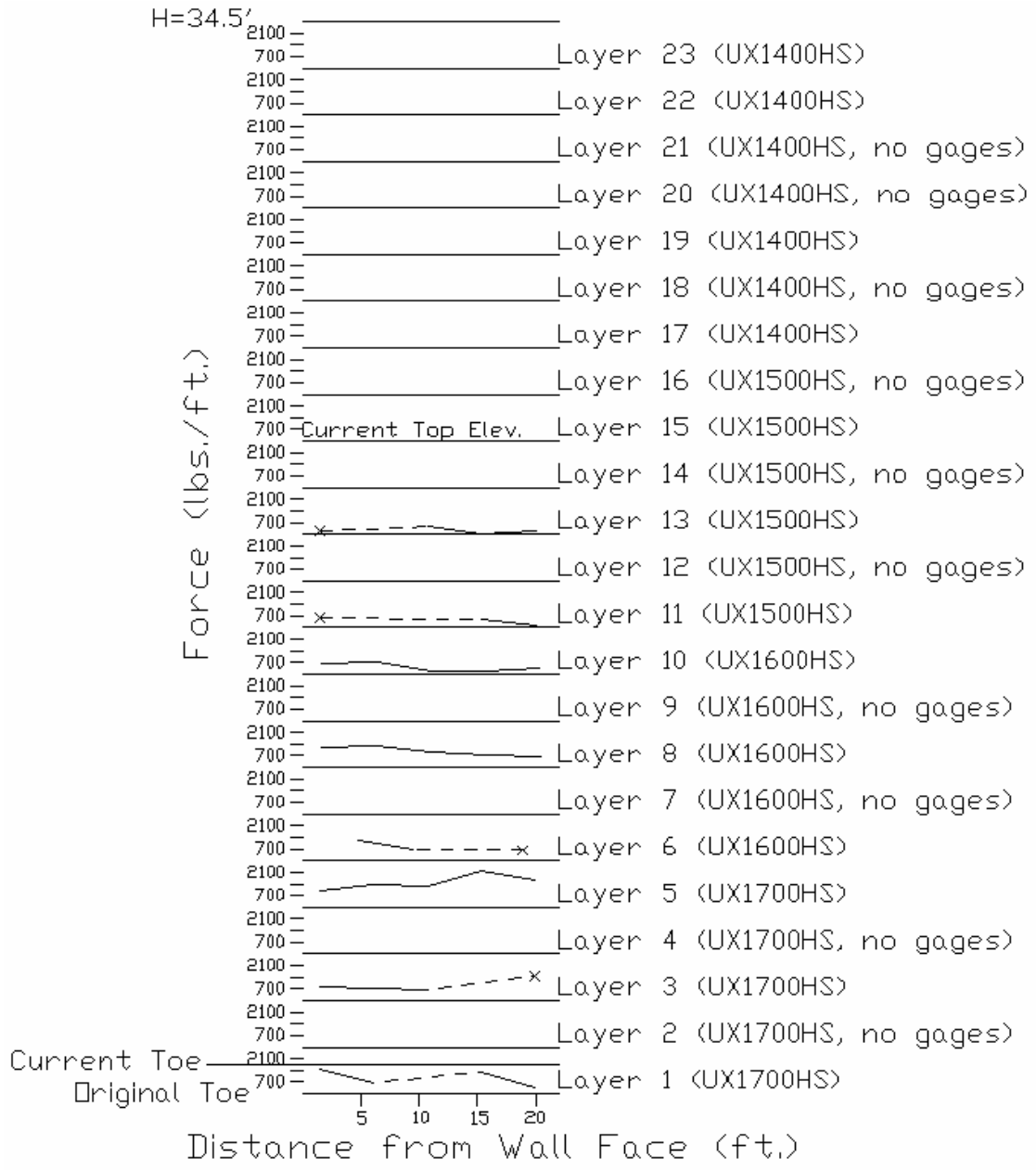

Figure 4.20 Forces Measured 8/11/06

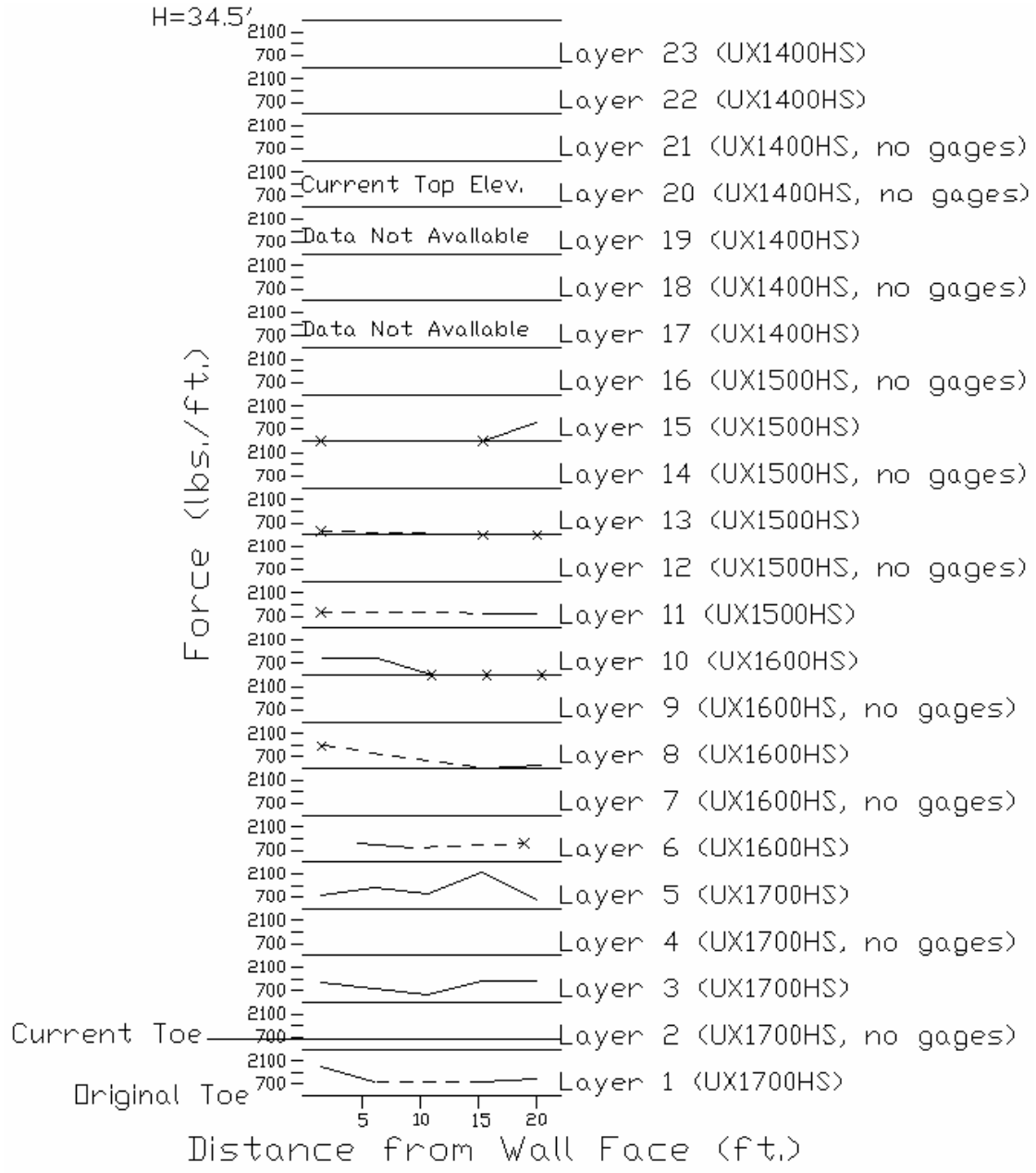

Figure 4.21 Forces Measured 10/5/06

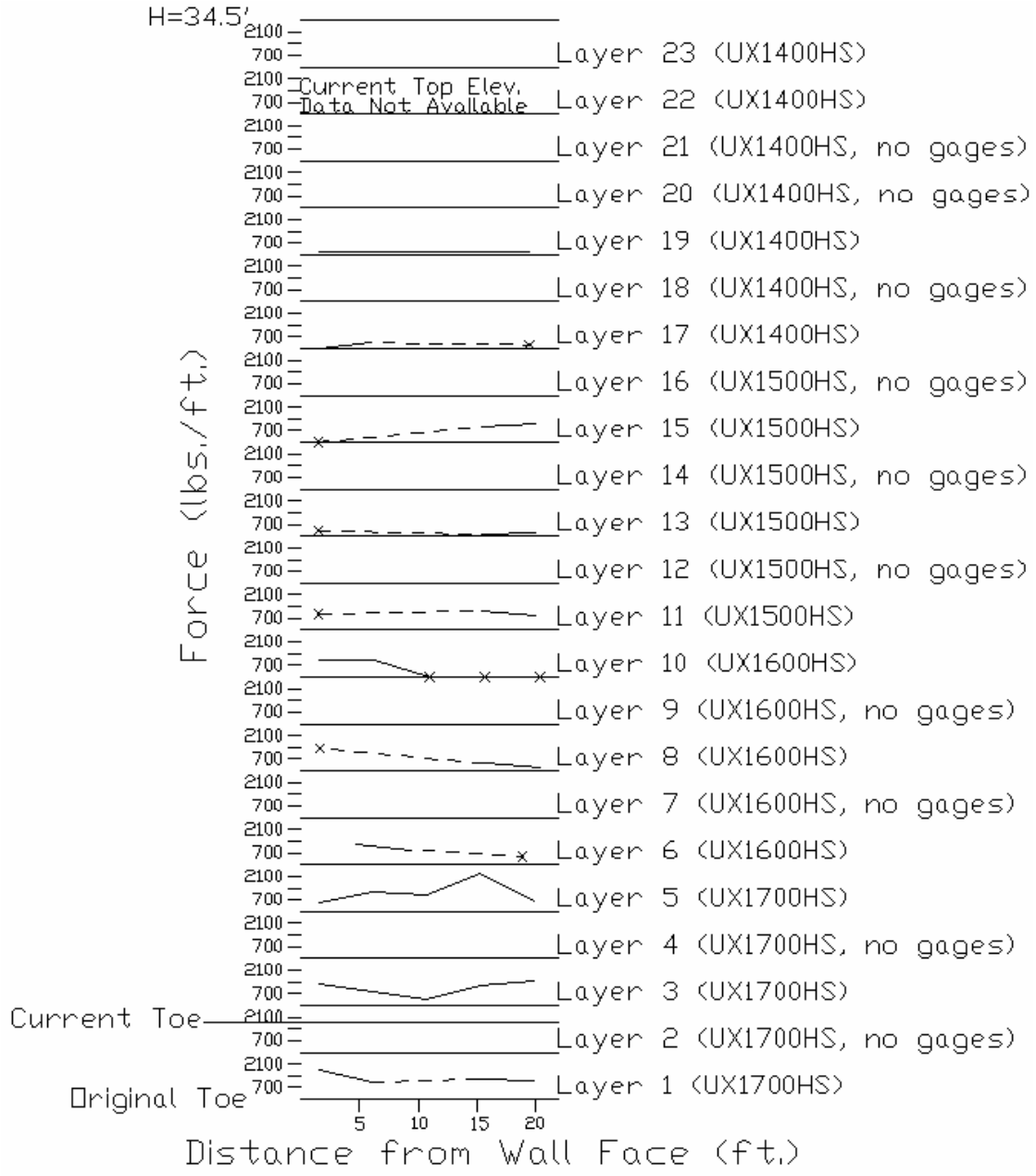

Figure 4.22 Forces Measured 11/9/06

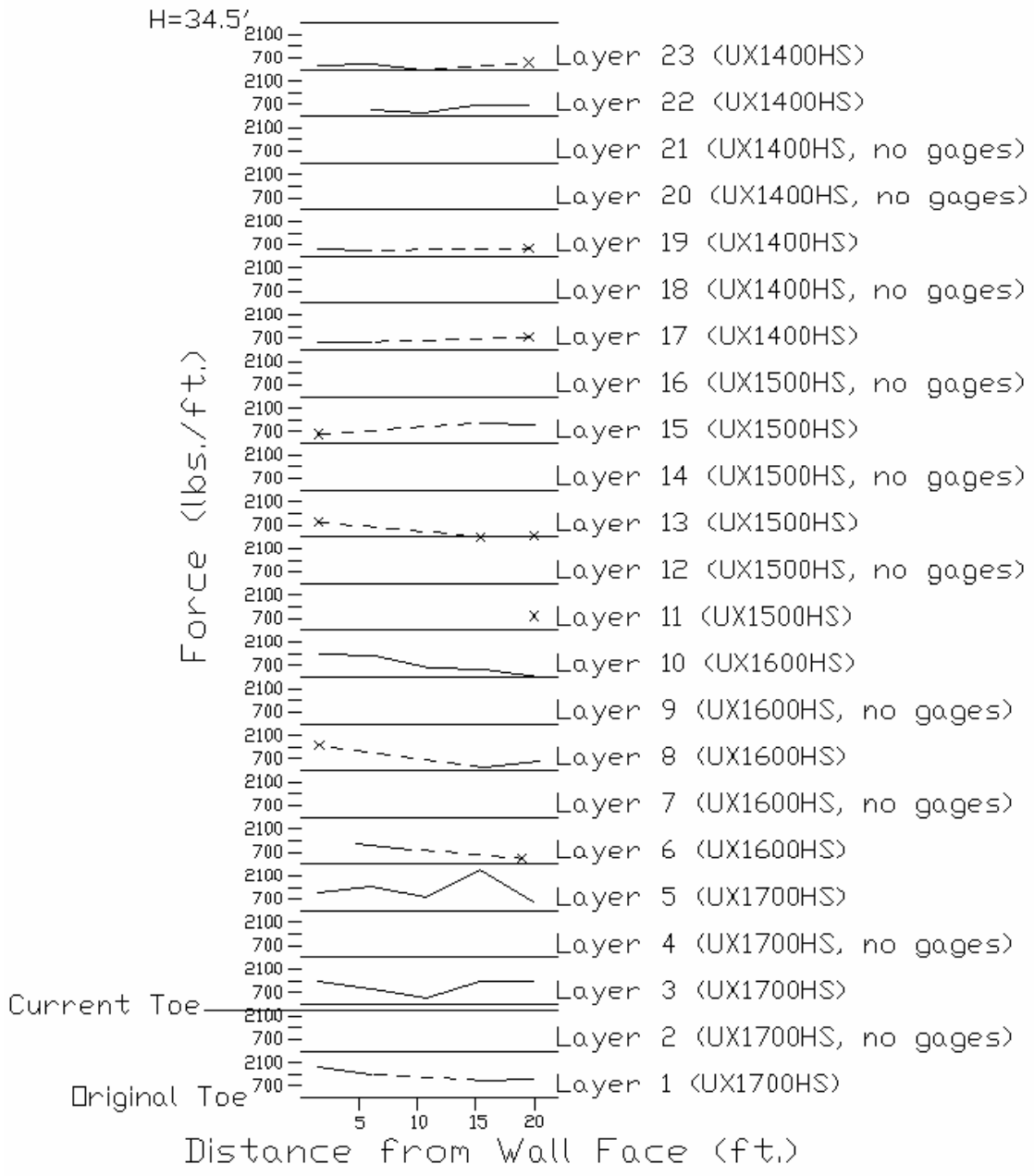

Figure 4.23 Forces Measured 12/5/06

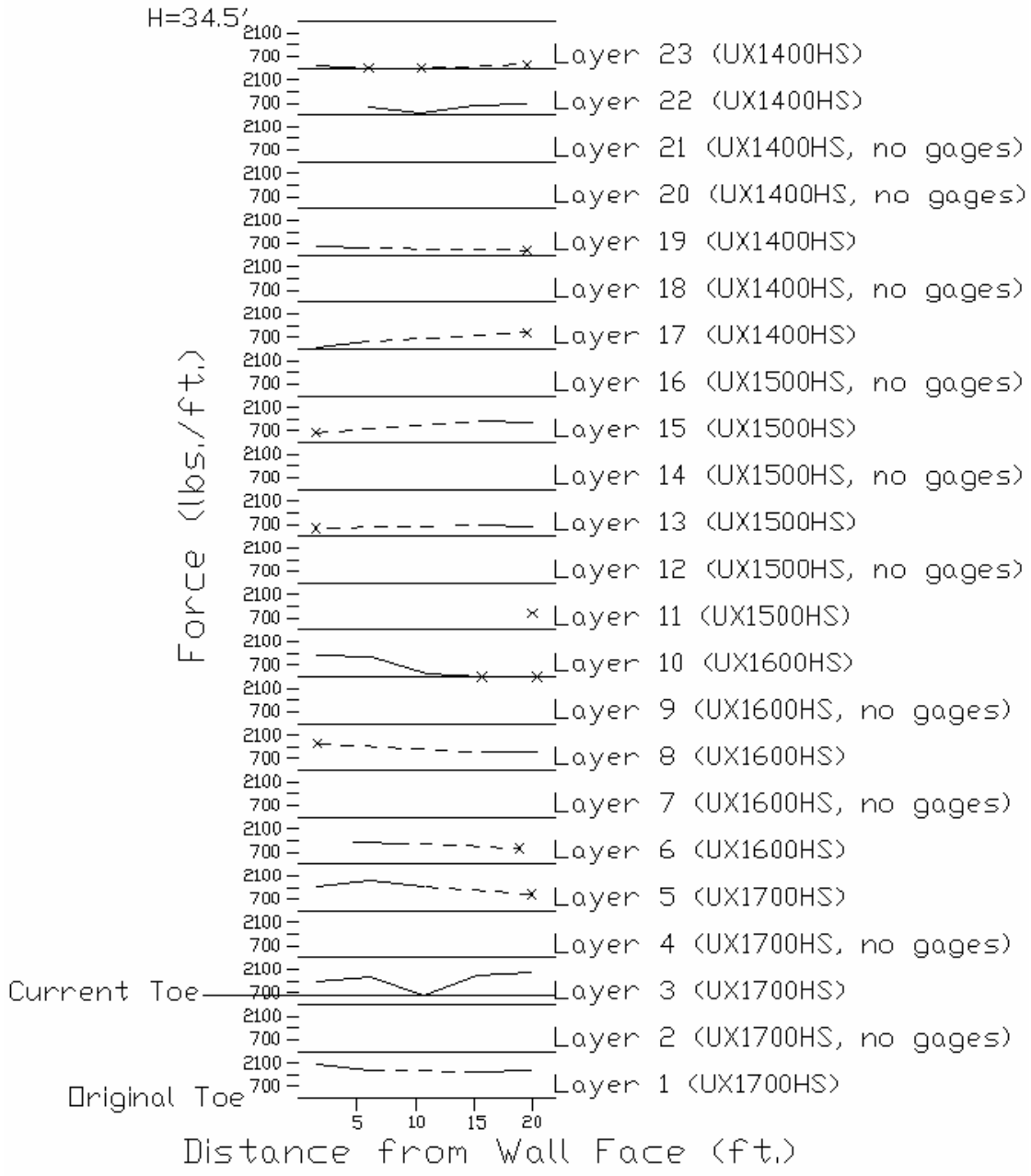

Figure 4.24 Forces Measured 1/12/07

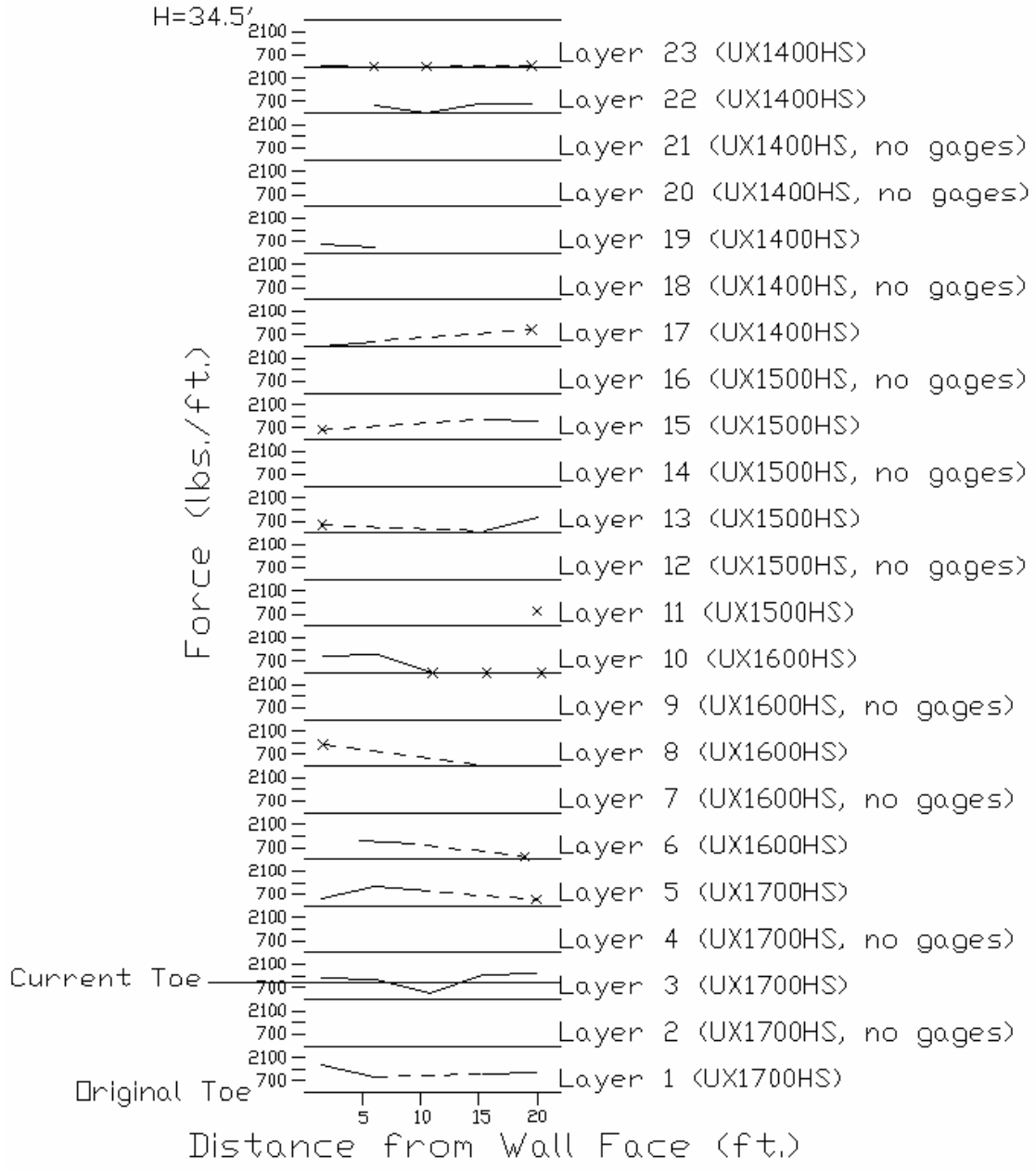

Figure 4.25 Forces Measured 2/12/07

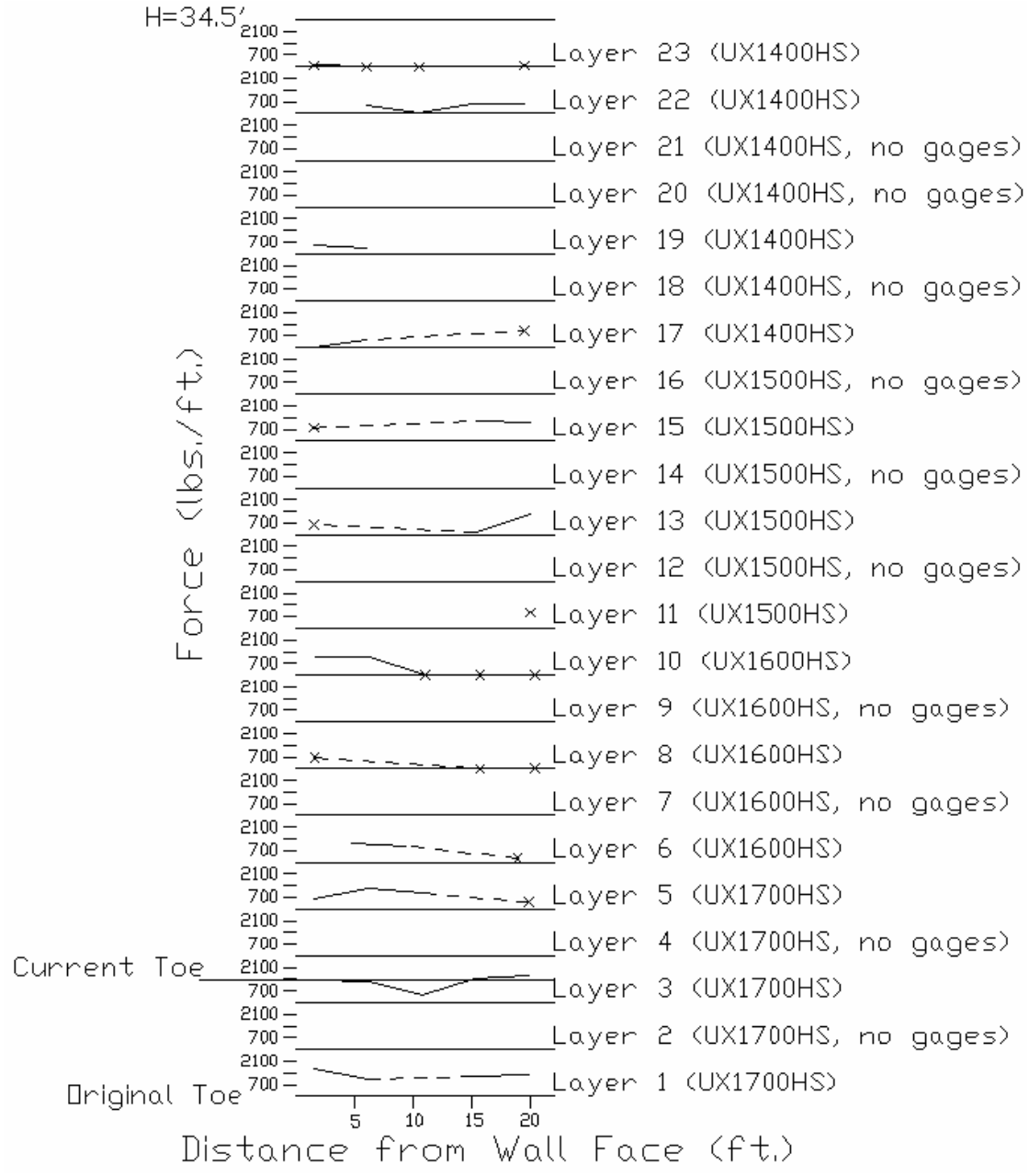

Figure 4.26 Forces Measured 3/12/07

4.2 Settlement Plates

Readings were taken from the settlement plates at least on a weekly basis by the Delaware Department of Transportation. The data was looked at to determine the status of the embankment to verify that construction could be continued. If excessive settlement occurred over a period between readings, construction was delayed temporarily. Figure 4.27 shows settlement plate data for station 289+00. Each date shown corresponds to a date during which an instrumented layer of geogrid was installed, up until November 28, 2006, with one exception. The measurement for September 7, 2006 is included though no instrumented layer of geogrid was installed on this date. This addition is to show the very high rate of settlement that occurred since the previous reading, taken on August 31, 2006. After November 28, 2006, the dates shown were chosen to illustrate the continued settlement. It should be noted that construction at this wall section was completed on December 1, 2006. After this date, no additional load was applied. Data for settlement plate 289-53R is not shown since the initial reading was not taken until more than 10 weeks after the initial readings were taken for the other three settlement plates. As a result, the settlement that occurred at this offset point over those 10 weeks is not represented in the readings, and therefore, the readings show an incorrectly low amount of settlement for this offset.

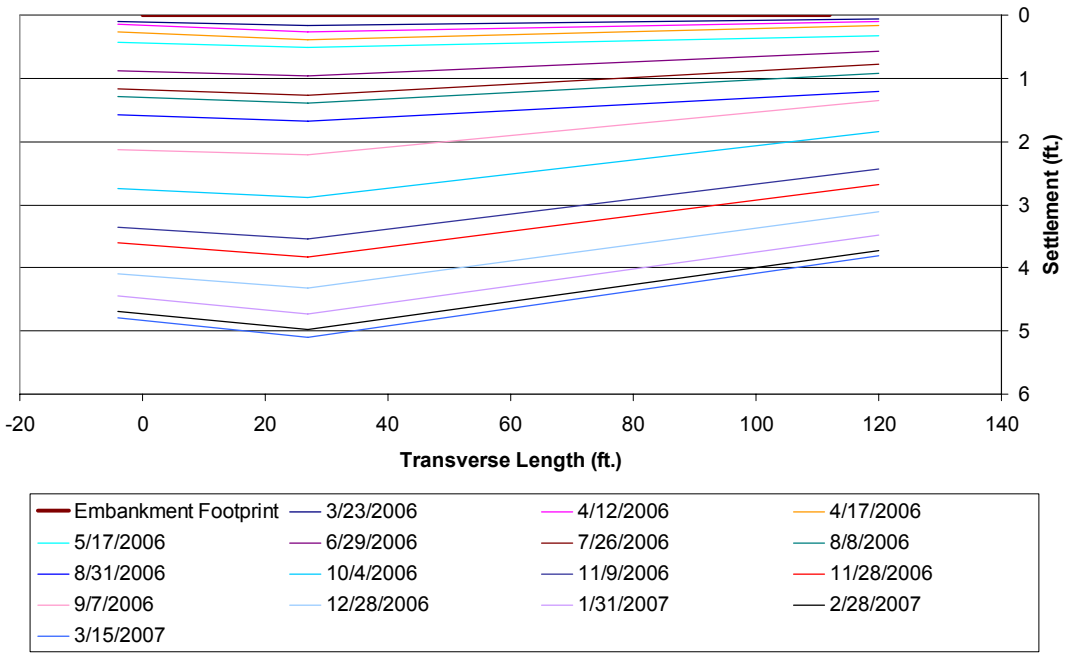

Figure 4.27 Settlement Profile for Station 289+00

As illustrated by Figure 4.27, the settlement increased as additional layers were added to the embankment. The large amount of settlement that occurred is not surprising, considering the large embankment and soft foundation soils. However, the settlement that has occurred is greater in magnitude, and has occurred faster than originally predicted by the designer. This will be discussed in Chapter 5.

4.3 Piezometers

The piezometer data was collected weekly by DelDOT. The following two figures show readings from the four piezometers located at different offsets at station 289+00. Figure 4.28 shows the change in head difference with time, as read from the piezometers. Figure 4.29 shows the change in pressure difference with time. These figures present the piezometer data for dates on which a layer of instrumented

geogrid was installed, through the installation of the last layer on November 28, 2006. As before, it should be noted that construction at station 289+00 was completed on December 1, 2006. Data from dates after this are shown to illustrate the continuing trend in the data.

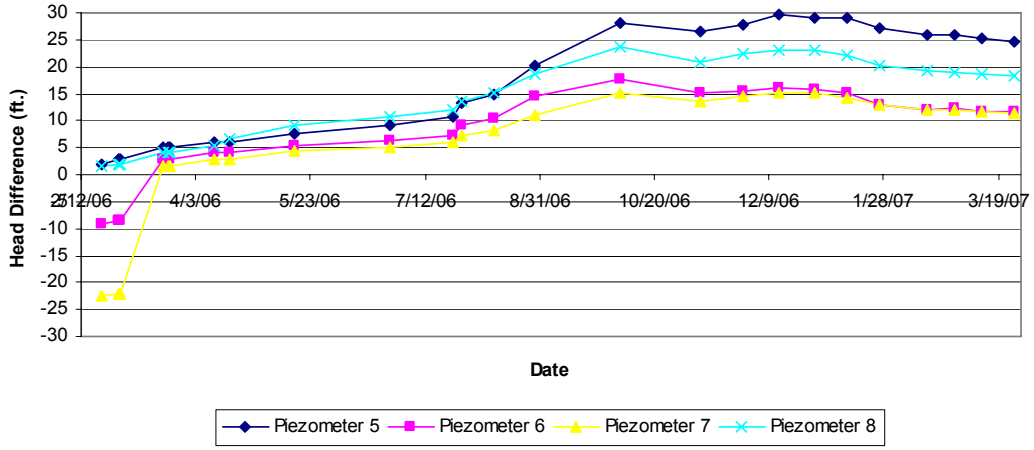

Figure 4.28 Piezometer Readings – Change in Head Difference with Time

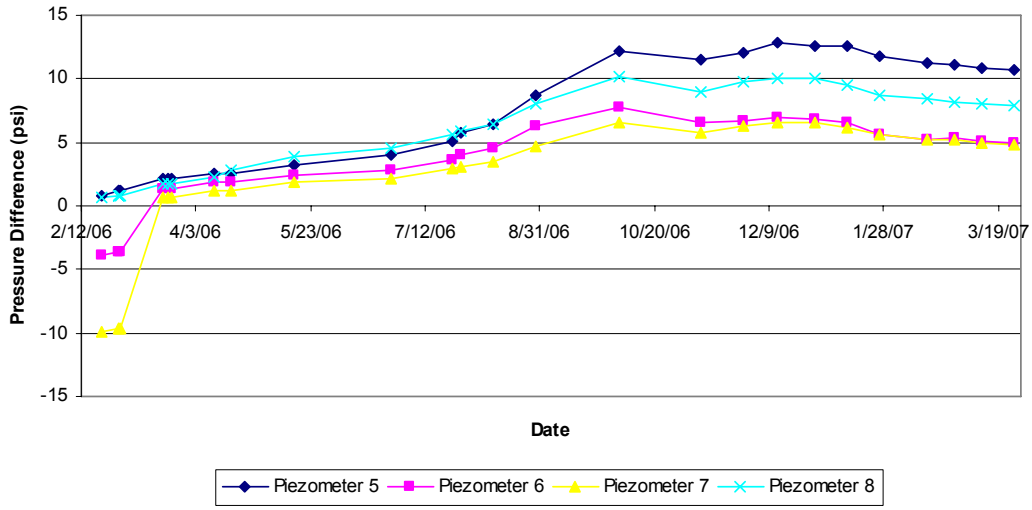

Figure 4.29 Piezometer Readings – Change in Pressure Difference with Time

It should be noted that the readings taken for piezometer 6 and piezometer 7 before March 24 appear to be erroneous readings. Otherwise, the trend shows that as additional layers were added to the embankment, the excess pore water pressure in the foundation soil increased. The higher readings are somewhat surprising since prefabricated vertical drains (PVDs) were installed, which should allow drainage. If proper drainage is permitted, excess pore water pressure should not accumulate. This may be an indication that the piezometer readings may not be entirely reliable in this application. The reading is taken at the tip of the piezometer, which is merely a single point in an enormous volume of soil. Thus, it is possible that the point reading is not representative of the surrounding area. On the other hand, the readings began to decrease in the second to third week of January. This indicates that since no additional load was being added after construction was completed at this location in the beginning of December, the pore water pressure has begun to dissipate at a

constant, yet slow rate. The relatively high excess pore water pressures and the slow dissipation could be an indication that the PVDs are not functioning properly. This will be further analyzed in Chapter 5.

4.4 Inclinometers

Readings of the installed inclinometers were taken by DelDOT on a weekly basis. These readings were monitored to ensure the stability of the embankment under construction. Data was downloaded from the field storage unit and then processed using a program provided by the manufacturer of the inclinometers. The data is expressed in graphs, as shown in Figures 4.30 through 4.40. Again, it should be noted that construction was completed at station 289+00 on December 1, 2006.

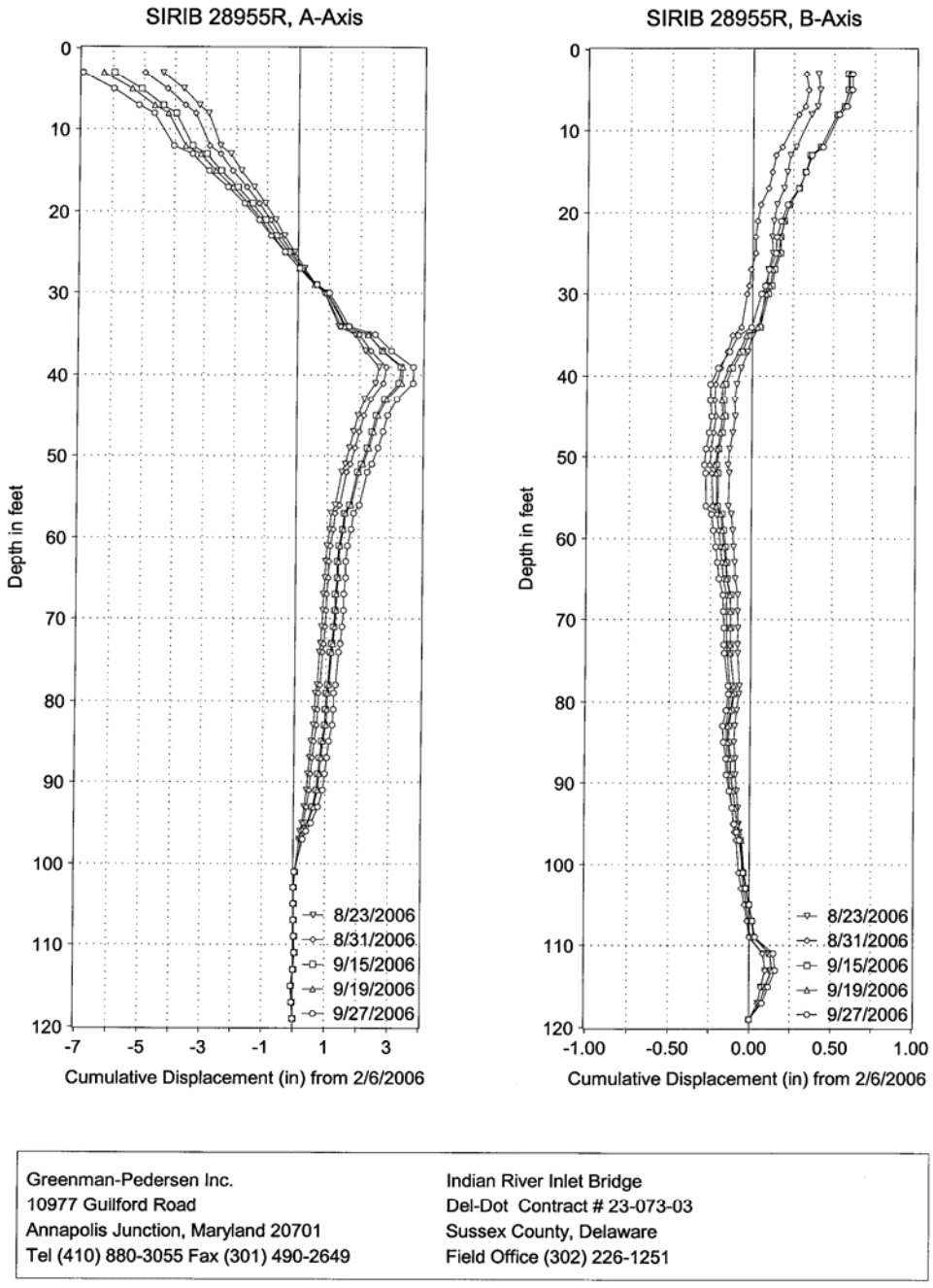

Figure 4.30 Inclinometer 289-55R Data: 8/23/06 – 9/27/06

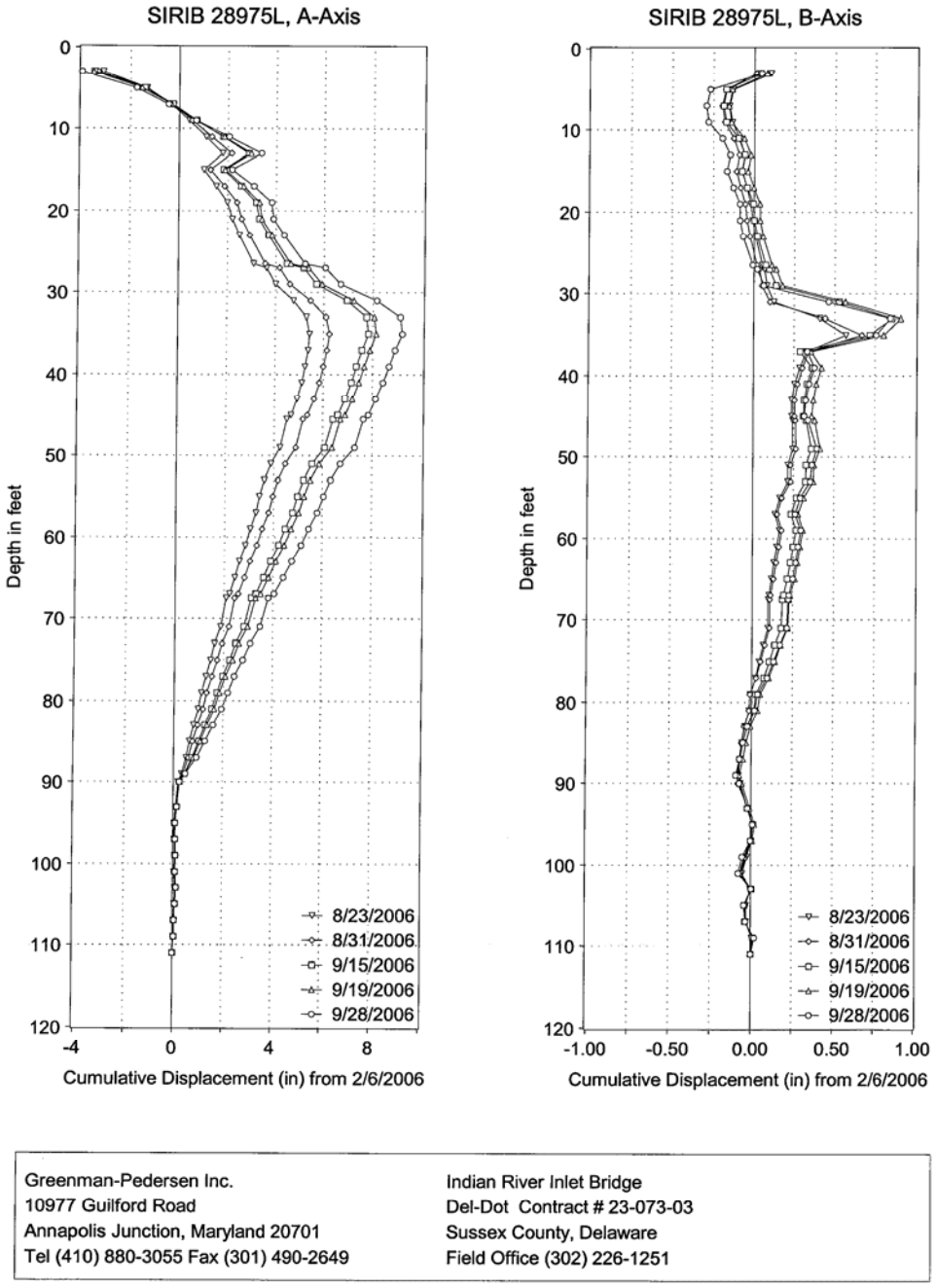

Figure 4.31 Inclinometer 289-75L Data: 8/23/06 – 9/28/06

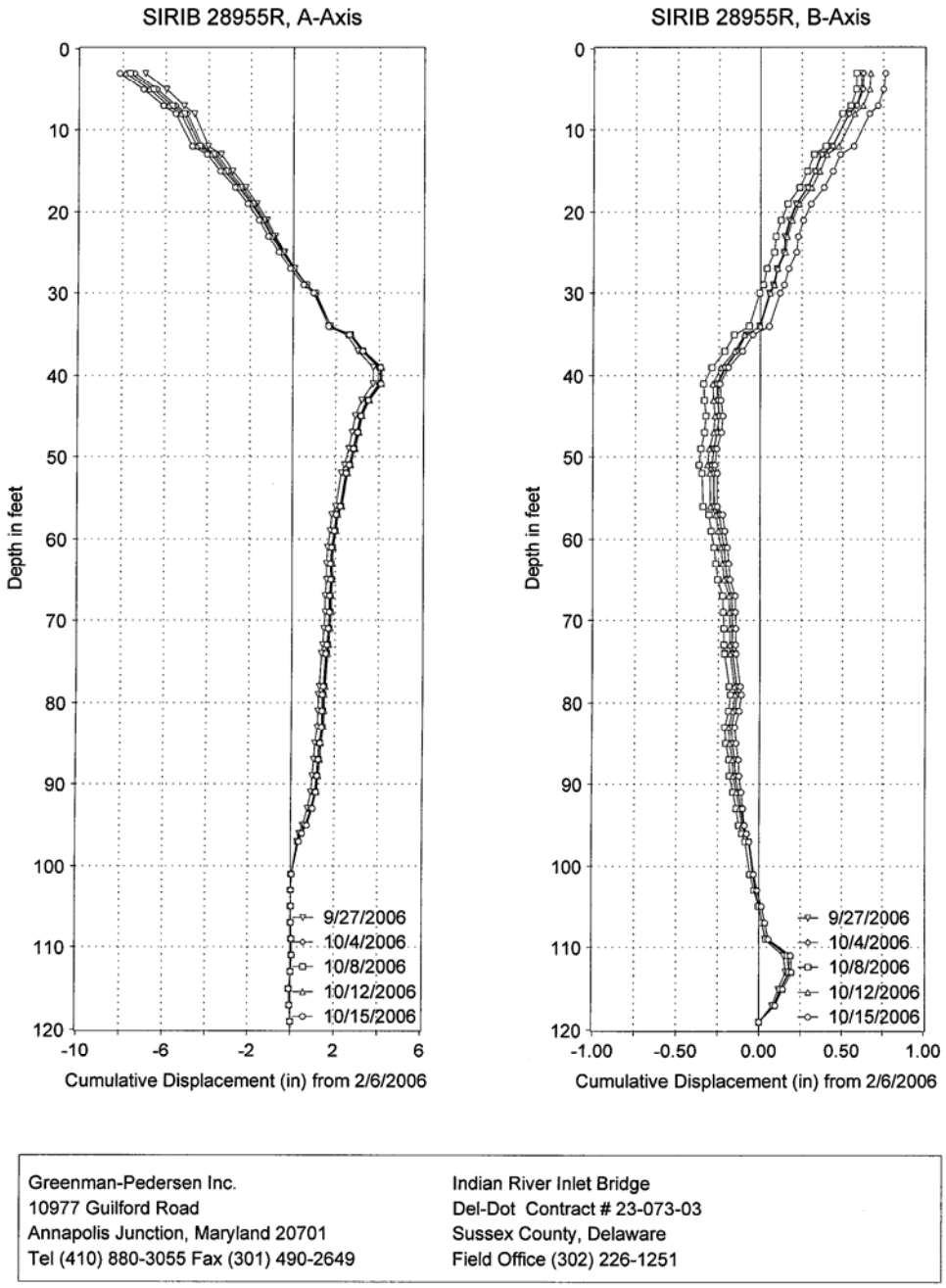

Figure 4.32 Inclinometer 289-55R Data: 9/27/06 – 10/15/06

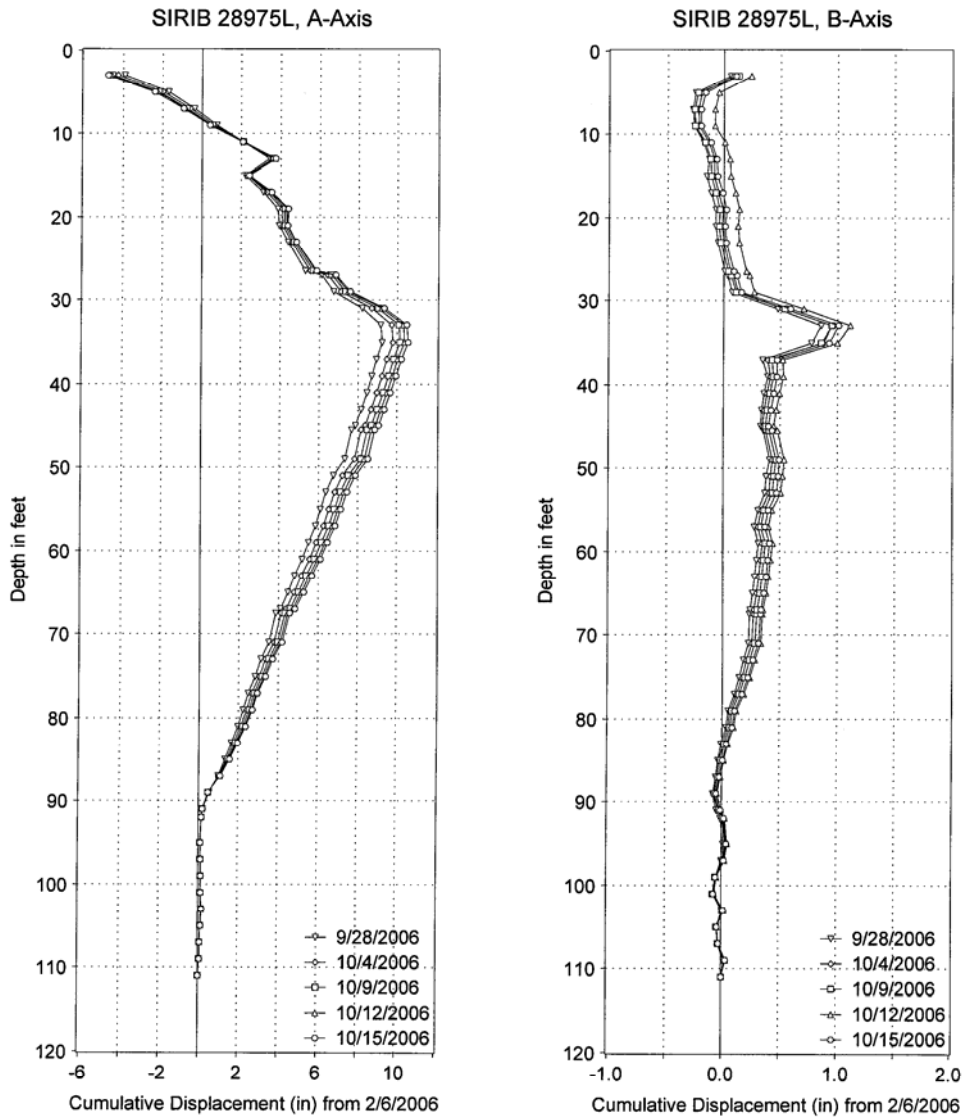

Figure 4.33 Inclinometer 289-75L Data: 9/28/06 – 10/15/06

As a result of large movements occurring in the end of September and beginning of October, inclinometer readings were taken at an interval of every three days in October, and into November, when movements became smaller. During the 10/16/06 reading, the probe could not pass below a depth of 20 feet in the casing at inclinometer 289-75L. The replacement inclinometer was completed on October 24, 2006, and labeled 289-75A.

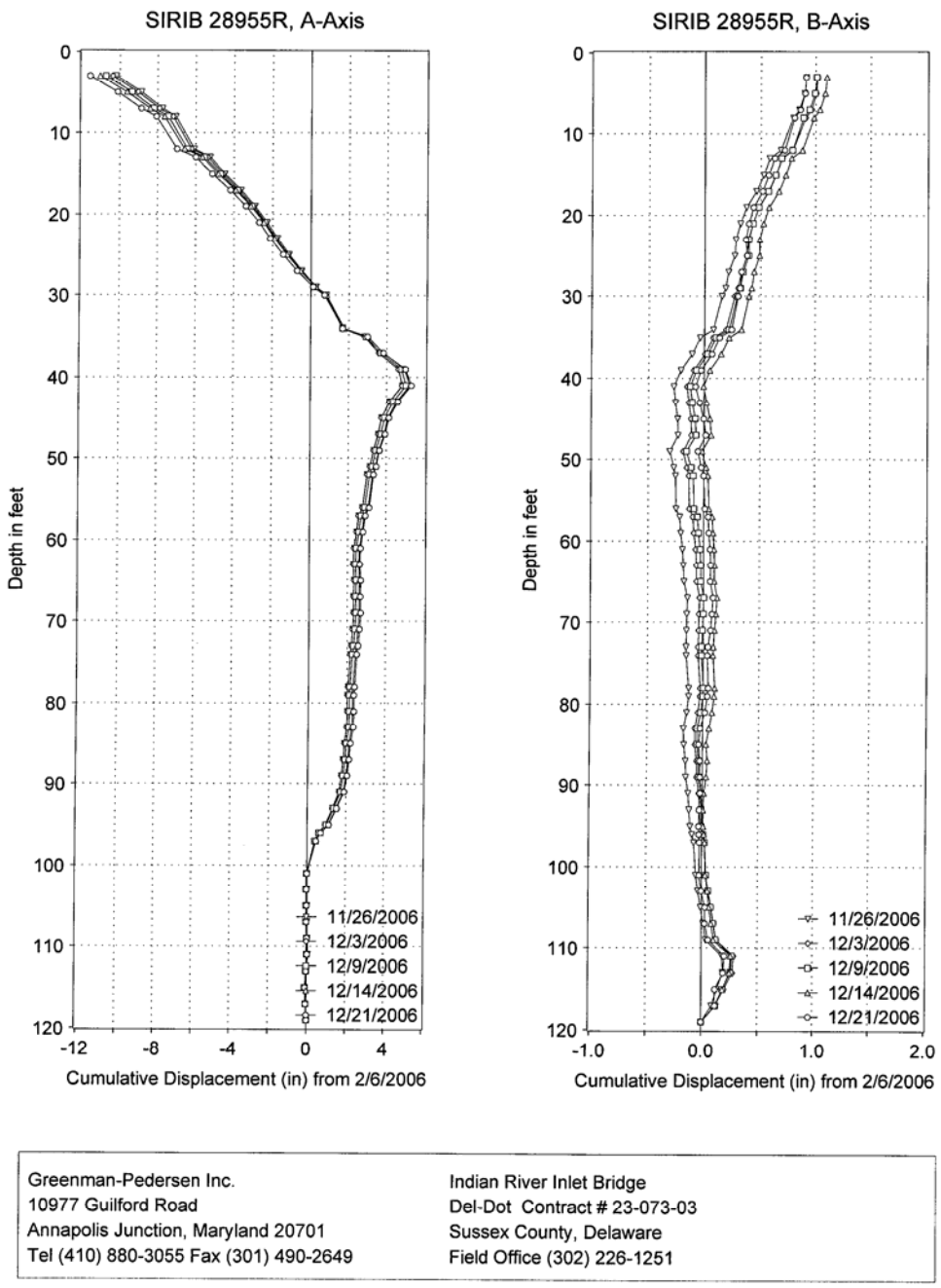

Figure 4.34 Inclinometer 289-55R Data: 11/26/06 – 12/21/06

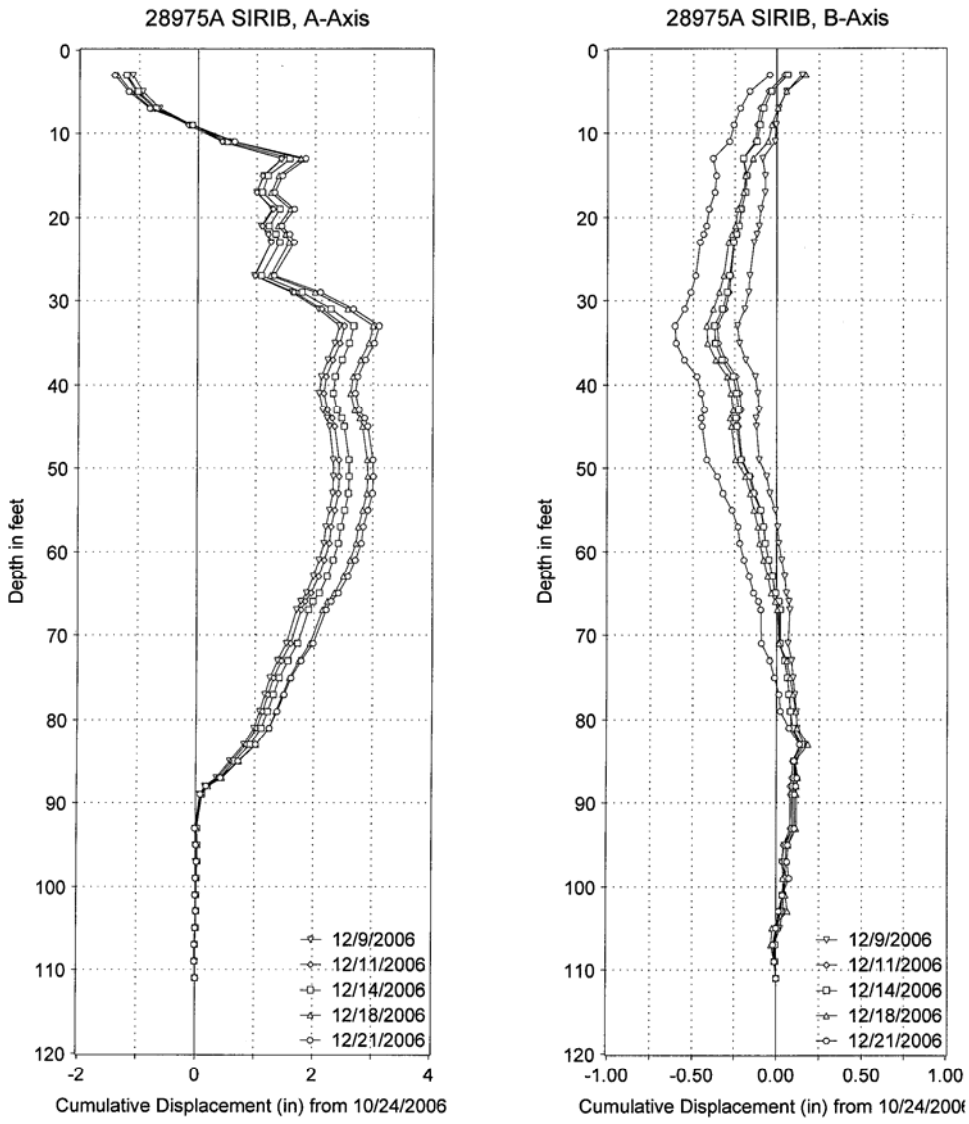

Figure 4.35 Inclinometer 289-75A Data: 12/9/06 – 12/21/06

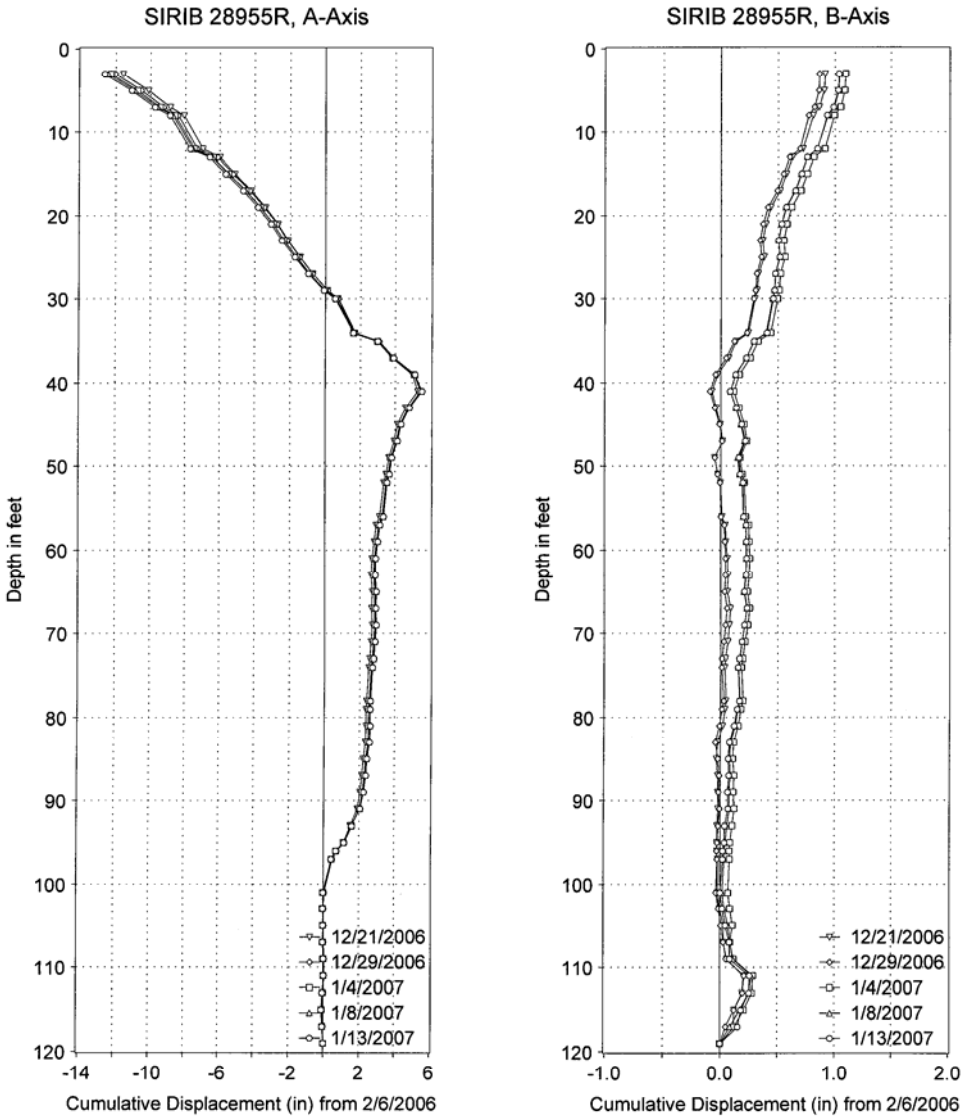

Figure 4.36 Inclinometer 289-55R Data: 12/21/06 – 1/13/07

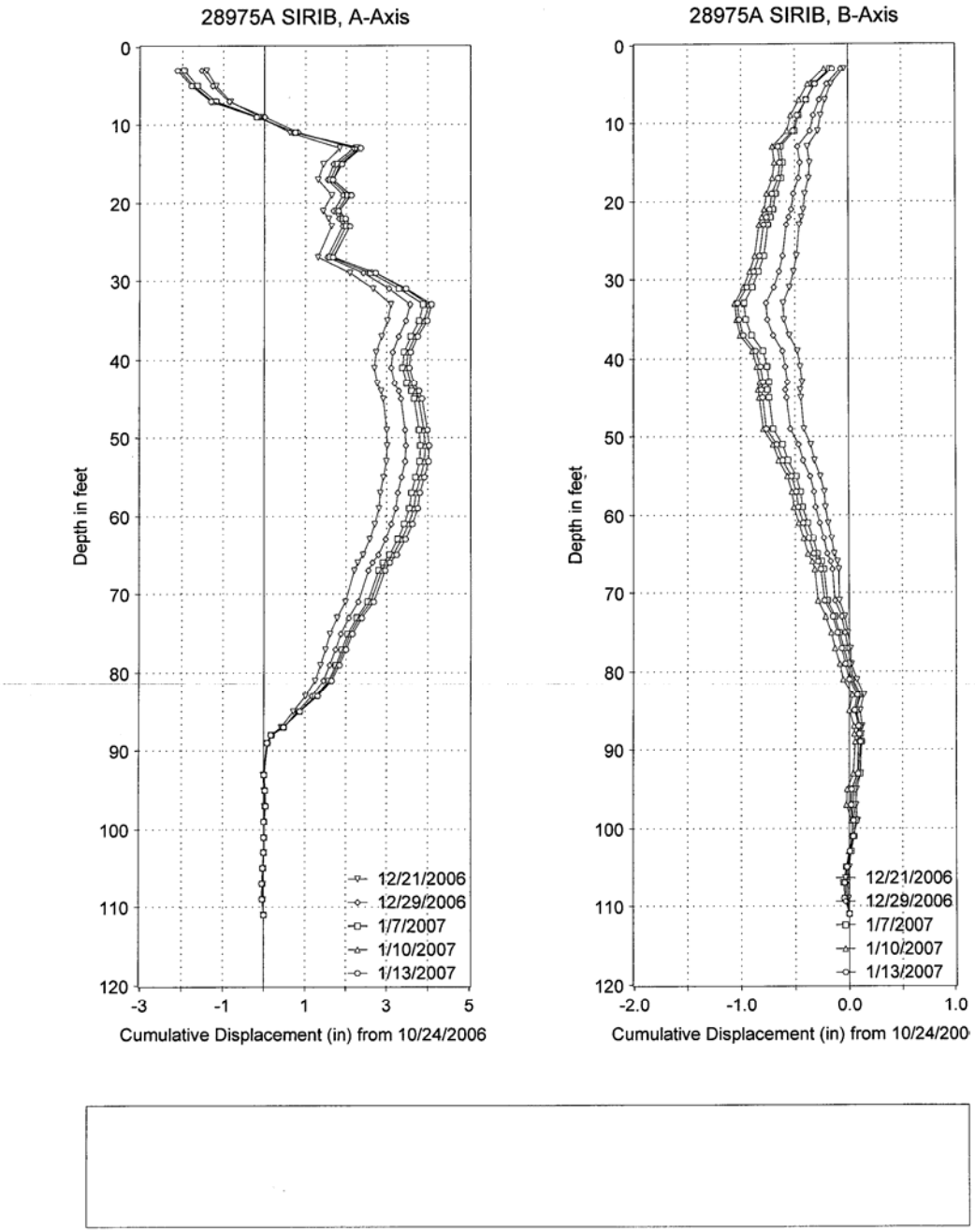

Figure 4.37 Inclinometer 289-75A Data: 12/21/06 – 1/13/07

After January 7, 2007, readings from inclinometer 289-55R became unreliable. Readings were no longer taken from this inclinometer, and a replacement was installed on January 29, 2007. This replacement inclinometer was labeled 289-55A.

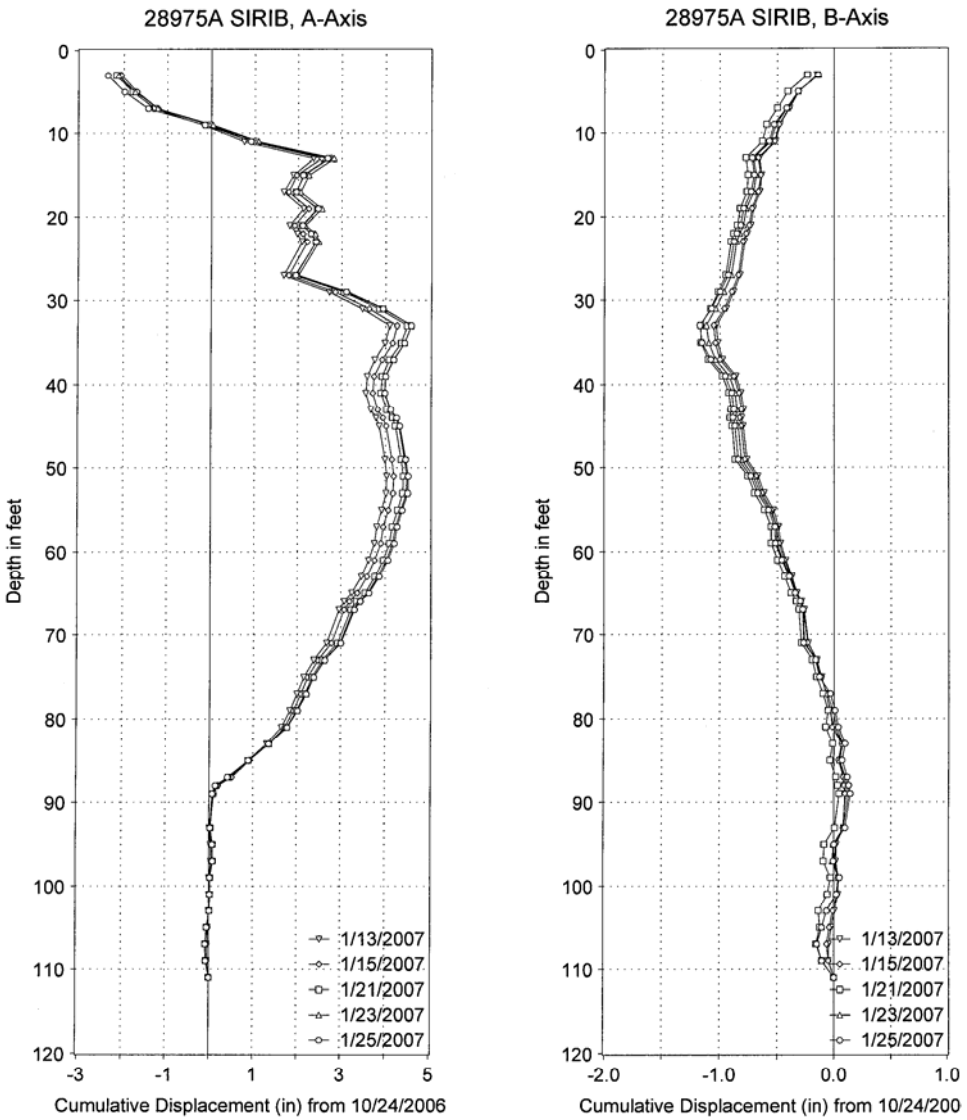

Figure 4.38 Inclinometer 289-75A Data: 1/13/07 – 1/25/07

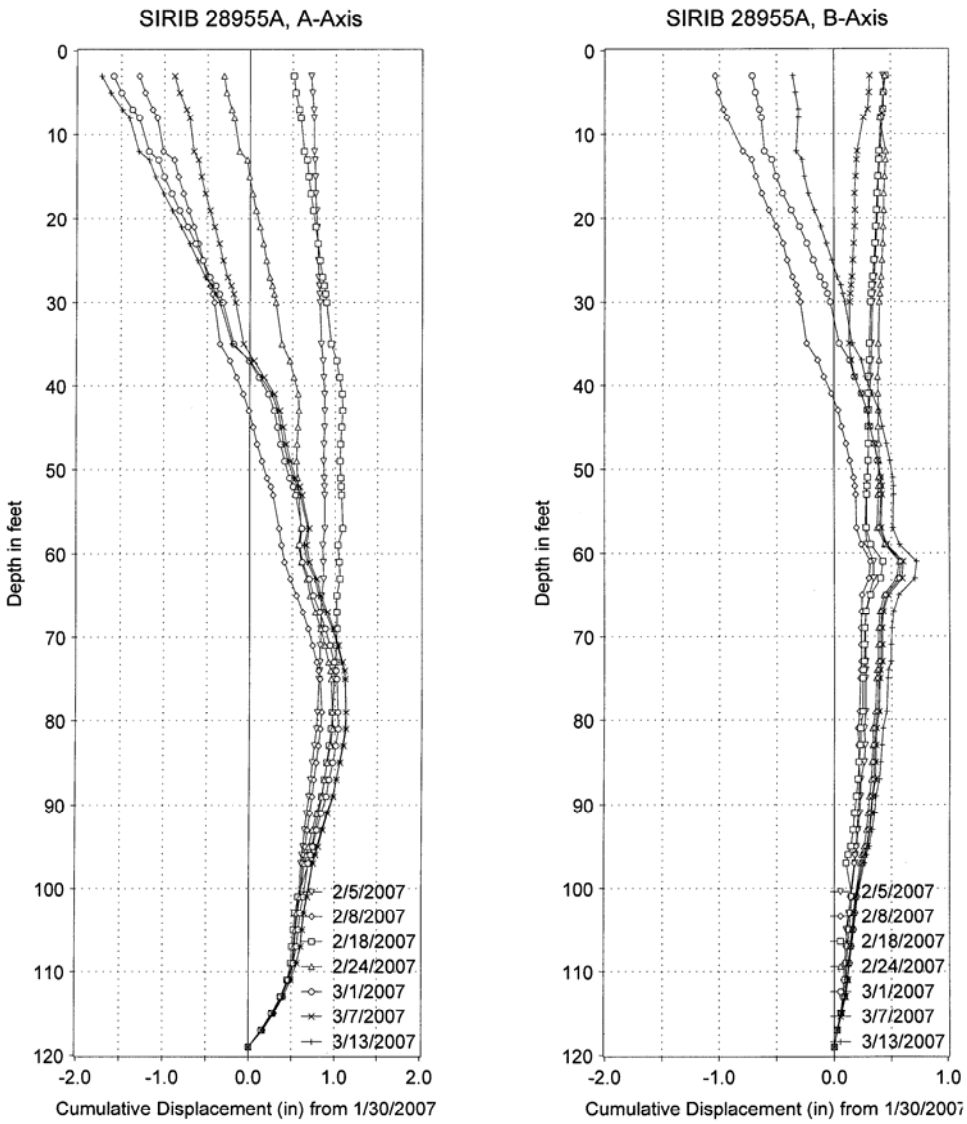

Figure 4.39 Inclinometer 289-55A Data: 2/5/07 – 3/13/07

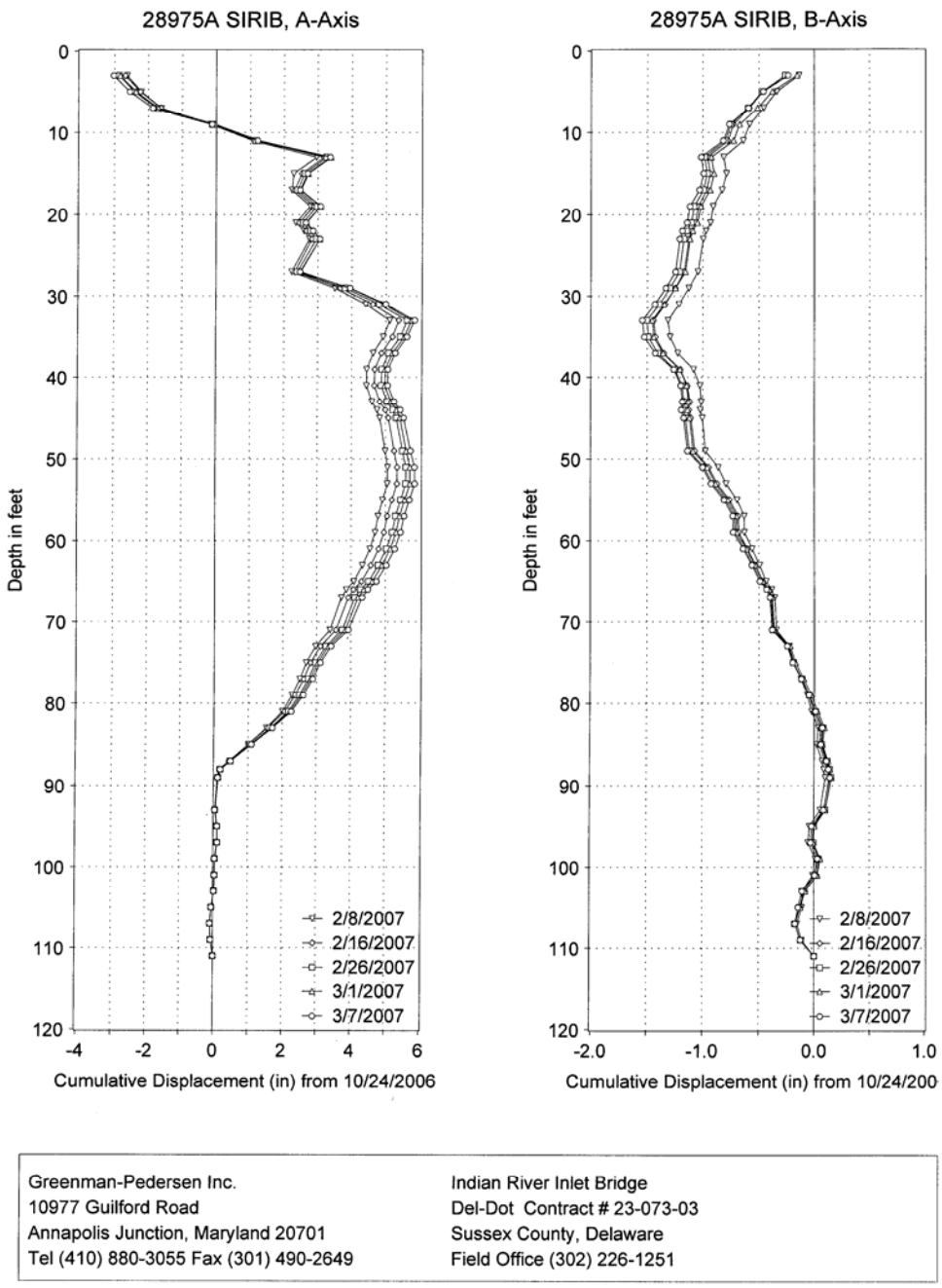

Figure 4.40 Inclinometer 289-75A Data: 2/8/07 – 3/7/07

As illustrated by the figures, very large horizontal movements exceeding one foot have occurred in the top 10 feet of the foundation soil. Significant horizontal movements have also occurred at greater depths, with movements as large as three inches occurring as deep as 70 feet below the ground surface.

To track the rate of movement occurring, the measured change in horizontal movement between measurements (Delta H) was divided by the time (T) between the measurements. This was also done for the measured change in vertical movement (Delta V). Both quantities were converted to inches per day and expressed graphically. Figures 4.41 and 4.42 show the rate of inclinometer movement, both horizontally and vertically, for both inclinometers located at station 289+00.

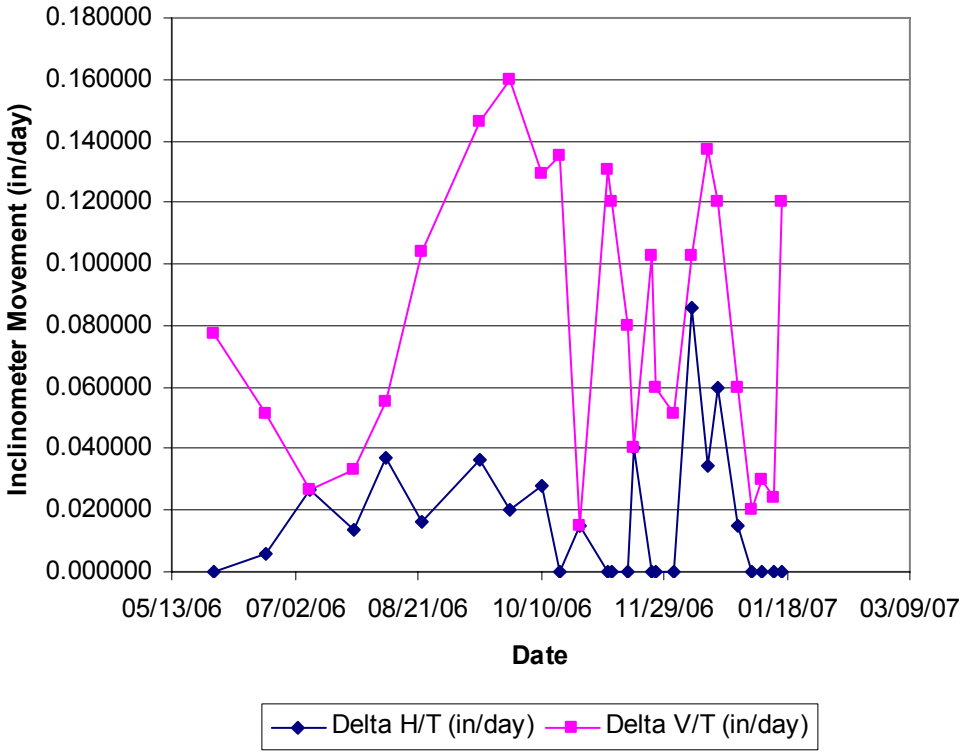

Figure 4.41 Movement Rate Plot for Inclinometer 289-55R

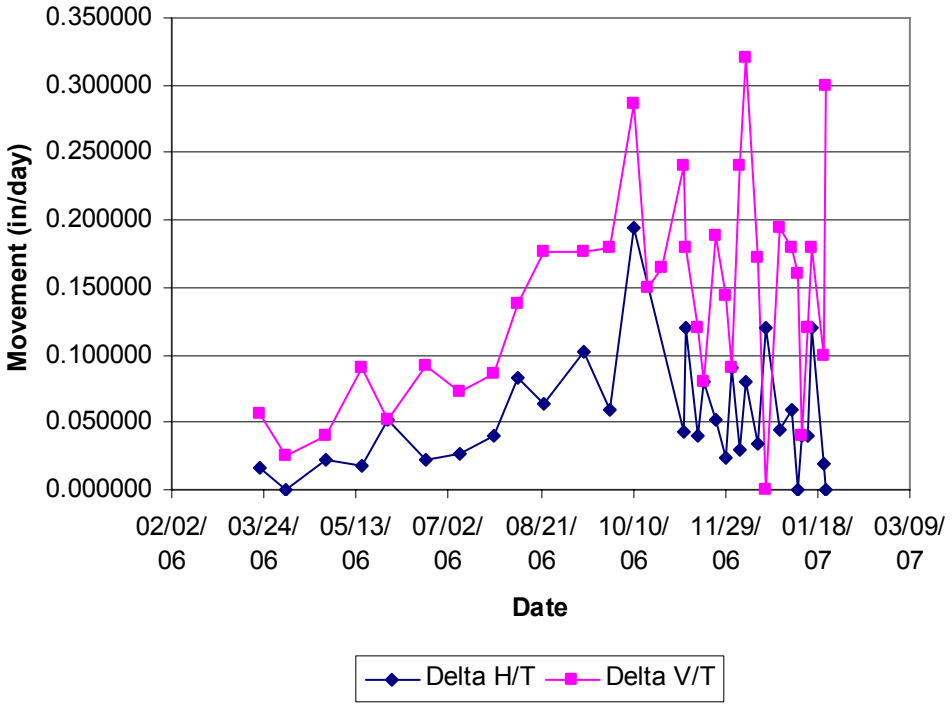

Figure 4.42 Movement Rate Plot for Inclinometers 289-75L and 289-75A

In general, the horizontal and vertical movement rates tend to increase as construction of the embankment continues. This is intuitive; as more load is added to the system, it is likely that the soil will respond, meaning more movement will begin to occur. When these movement rates begin to consistently decrease, it is likely that the system has become stable.

Chapter 5

INTERPRETATION OF DATA

5.1 Strain Gages

The strains in the geogrid, as well as the corresponding forces, are presented in Chapter 4. The changes in strain as a result of continued construction are evident. Little to no strain was measured during the first two months of construction, when the wall height was still relatively low, and minimal load was being applied, resulting in relatively minimal settlement. Figures 4.1 through 4.3 show the small strains that did develop. The first relatively significant strains were measured in May, when the wall height was around 15 feet. Figure 4.4 shows the strain distribution in May. In absolute terms, these measured strains were still small, less than one percent for the most part. The corresponding forces in the geogrid were generally less than 1,000 pounds per foot. However, it can be seen that a few areas of higher strain have begun to develop. The location of these higher strains is towards the back of the reinforcement, away from the face of the wall, and is most evident in geogrid layer 3 and layer 5.

The increase in strain and force measured in the geogrid in May appears to be a result of the settlement occurring. Recall that the top of the 60 foot thick clay layer is at a depth of about 30 feet below the base of the wall, so, a sand layer separates the wall from the consolidating clay layer. As can be seen in Figure 5.3, when the top elevation of the wall reached approximately elevation 15', the rate of

settlement began to increase drastically. It is probable that at this wall height, the stress influence reached the clay layer, resulting in substantial settlement.

Strains continued to increase slowly through June, July, and August, as construction proceeded. This trend is demonstrated by Figures 4.5 through 4.7. The locations of higher strain in layers 3 and 5, however, increased more drastically. By October and November, all of the strains continued to increase gradually. Many of the reinforcement layers developed strains in excess of one percent. In observing the more recently installed higher reinforcement layers, it can be seen that the pattern of higher strains developing away from the wall face is continuing. By construction completion in December, strains in excess of three percent were measured near the back of the reinforcement in layers 3, 5, 15, 17, and 22. The January 12, 2007 reading, illustrated by Figure 4.11, shows a slight overall increase in strain throughout the wall. High strains, exceeding three percent, developed near the rear of reinforcement layers 5 and 17. However, layer 5 was not instrumented with high elongation strain gages, and the high strain caused the gage near the rear of the layer to reach its capacity.

The large magnitude of relative settlement may be the reason that higher strains are developing near the back of the reinforcement. As the wall consolidates, it is likely that the sand backfill is settling more than the so-called coherent mass as defined by the reinforced soil. Thus, the sand backfill could be creating a down drag force at the boundary of the sand backfill and the reinforced soil zone. This phenomenon would induce stresses into the rear of the reinforced soil resulting in greater stress in the rear end of the reinforcement.

The February 12, 2007 reading shows a slight decrease in the strains and forces measured throughout the wall. This is seen in Figure 4.12. One possible explanation for the decrease in readings is the wall, and lower reinforcement layers, settling into the foundation soil. The instrumented portion of the wall has settled into the foundation soil approximately four feet at this point. This could subject lower reinforcement layers to passive resistance in the front. Hence, the lower levels will not carry as much load as if they were above grade. In addition, as the base of the wall continues to settle, the effective height of the wall also decreases. The decreased height could cause stresses in the upper layers of the wall to become less. The March 12, 2007 data, as shown in Figure 4.13, shows only a very slight increase in strains and forces, if any at all. The fact that there was an increase shows that the wall continues to undergo settlement. However, where there were increases, they were very small. This probably indicates that the system is beginning to stabilize.

It is recommendable to include a parameter in design to account for average strain in the reinforcement. Figure 5.1 shows an example settlement profile for an embankment constructed over soft foundation soil. Assume that Lo represents the length of the reinforcement, as installed. L is the length of the reinforcement after it has been strained from settlement. Then, d is the differential settlement between the two opposite ends of the reinforcement. The angle alpha is a measure of how much the reinforcement has rotated downward due to the settlement, assuming the front of the reinforcement is fixed at the face of the wall.

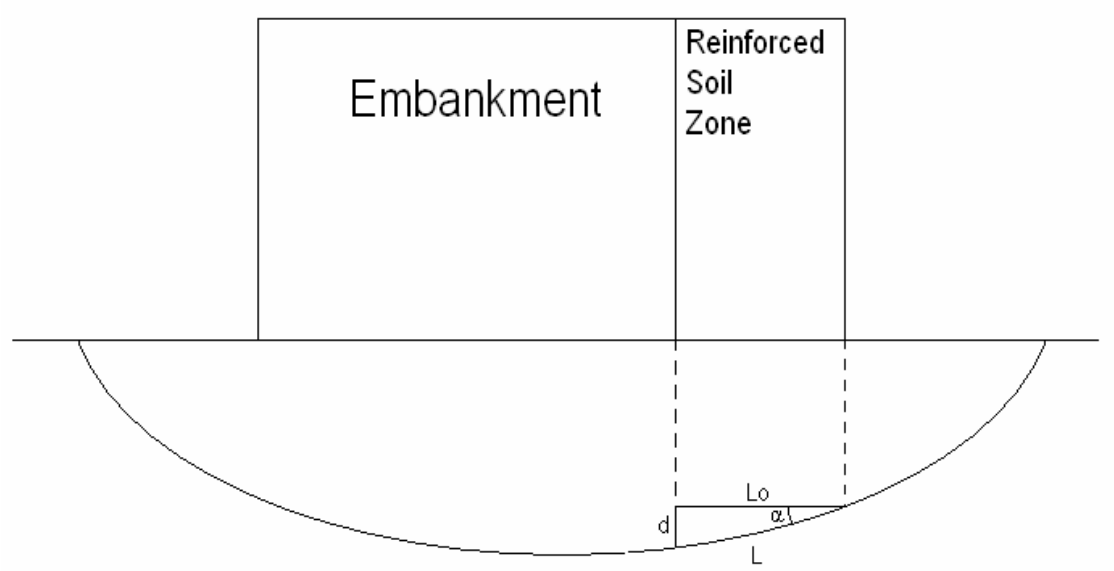

Figure 5.1 Schematic for Assessing Average Strain Due to Large Settlement

Average strain is defined in general by the following equation:

$\varepsilon = (L - Lo)/Lo$ (10)

where: ε = strain

L = length after elongation

Lo = original length

Figure 5.1 provides the following equation from the trigonometry of the schematic:

$L = Lo/\cos\alpha$ (11)

This assumes that L, the hypotenuse of the triangle shown, is about equal to the actual curved length of the reinforcement. Substituting Equation 11 into Equation 10 yields:

$\varepsilon = [(1/\cos\alpha) - 1]$ (12)

In examining this equation, it can be seen that strain becomes more significant as the angle, α, increases. When the angle is five degrees, the strain is about 0.4%. When

the angle is 10 degrees, the strain increases to over 1.5%. If the angle measures 15 degrees, the corresponding strain is over 3.5%. In the latter case, the differential settlement, d, would be equal to almost 27 percent of the original reinforcement length. Clearly, as large settlements occur, strain in the reinforcement becomes significant. Using the model developed in the computer program FoSSA® to predict ultimate settlement values, as discussed in Section 5.2, results in a differential settlement between the front and rear of the reinforcement equal to 1.47 feet. This yields an angle of 3.8 degrees. Then, substituting this angle measure into Equation 12, the average strain in the geogrid is 0.22%. This provides evidence that the large strains observed are likely a result of down drag force.

5.2 Settlement

As shown in Section 4.2, the magnitude of settlement has exceeded the original prediction of the designer. For station 289+00, the original predicted ultimate settlement was 45 inches at the center of the embankment (Joe Wallen, personal communication, June 26, 2006). The settlement of plate 289-35L exceeded this value first, as measured on November 24, 2006, slightly less than nine months after construction began. Using the measured settlement values in conjunction with the computer program FoSSA®, a model of the embankment was calibrated to produce modified predictions of settlement.

Using the FoSSA® software, a scale model of the embankment and foundation soils was constructed. The soil properties as provided by the designer (Joe Wallen, personal communication, October 16, 2006) were assigned appropriately. The properties used are shown in Table 5.1. A settlement profile was then generated for various increments corresponding with different wall heights during construction.

The generated values of settlement were then compared to measured data for the same wall height. Using the soil data provided by the designer resulted in predicted settlements less than the measured settlements. To produce settlements that match those measured in the field, the compression index of the clay layer was increased. The one-dimensional model for time-rate consolidation used the same coefficient of consolidation as used by the designer. Only the compression index was modified, and this was done for one time reading. This process was iterated until the altered compression index value yielded settlement predictions that matched the measured data for the one settlement reading. Thus, the calculated settlements for all other times are based on that adjusted compression index, and are considered predictions.

Table 5.1 Data Input into FoSSA® for Settlement Predictions

Layer Thickness (ft.)	Cc	e_0	Cv (ft^2/day)	PVD Pattern	Drainage
58	Calibrated	1.4	0.05	6' Triangular	Top and Bottom

The first value for the compression index that appeared to make the calculated data match the measured data is $C_c = 0.78$. This value was calculated to match the measured data from October 30, 2006, which are shown by the "Measured after 10 Layers" points in Figure 5.2. This figure illustrates the data calculated using $C_c = 0.78$ versus the measured data. The calculated curve labeled "Calculated after 444 Days" represents the projected settlement profile half a year after the completion of construction. Likewise, the curve labeled "Calculated after 626 Days" represents the projected settlement profile one year after construction completion.

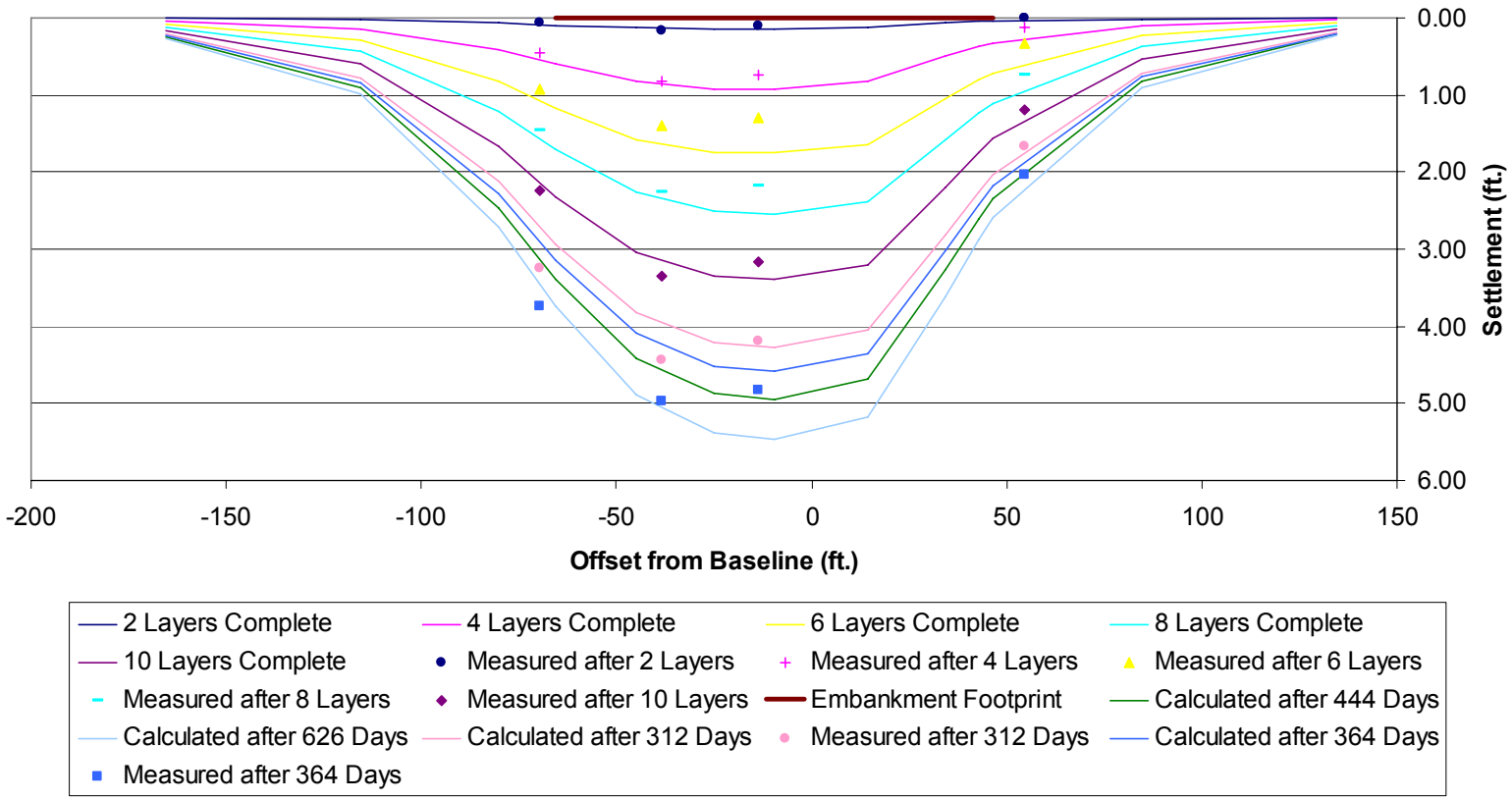

Figure 5.2 Settlement Profile Generated Using C_c = 0.78

As seen, the agreement between the calculated data and the field measured data is very good for the time period during which construction was continuing. However, the magnitude of the settlement measured after construction completion exceeds the predicted settlement magnitude. In order to account for this, the compression index was readjusted. Through trial and error, as previously described, an adjusted compression index of $C_c = 0.88$ was determined to provide the most accurate representation of the post-construction settlement magnitude. This value is significantly higher than the original value of $C_c = 0.5$ used by the designer. Figure 5.3 illustrates how the readjusted settlement profiles correspond to the measured settlement.

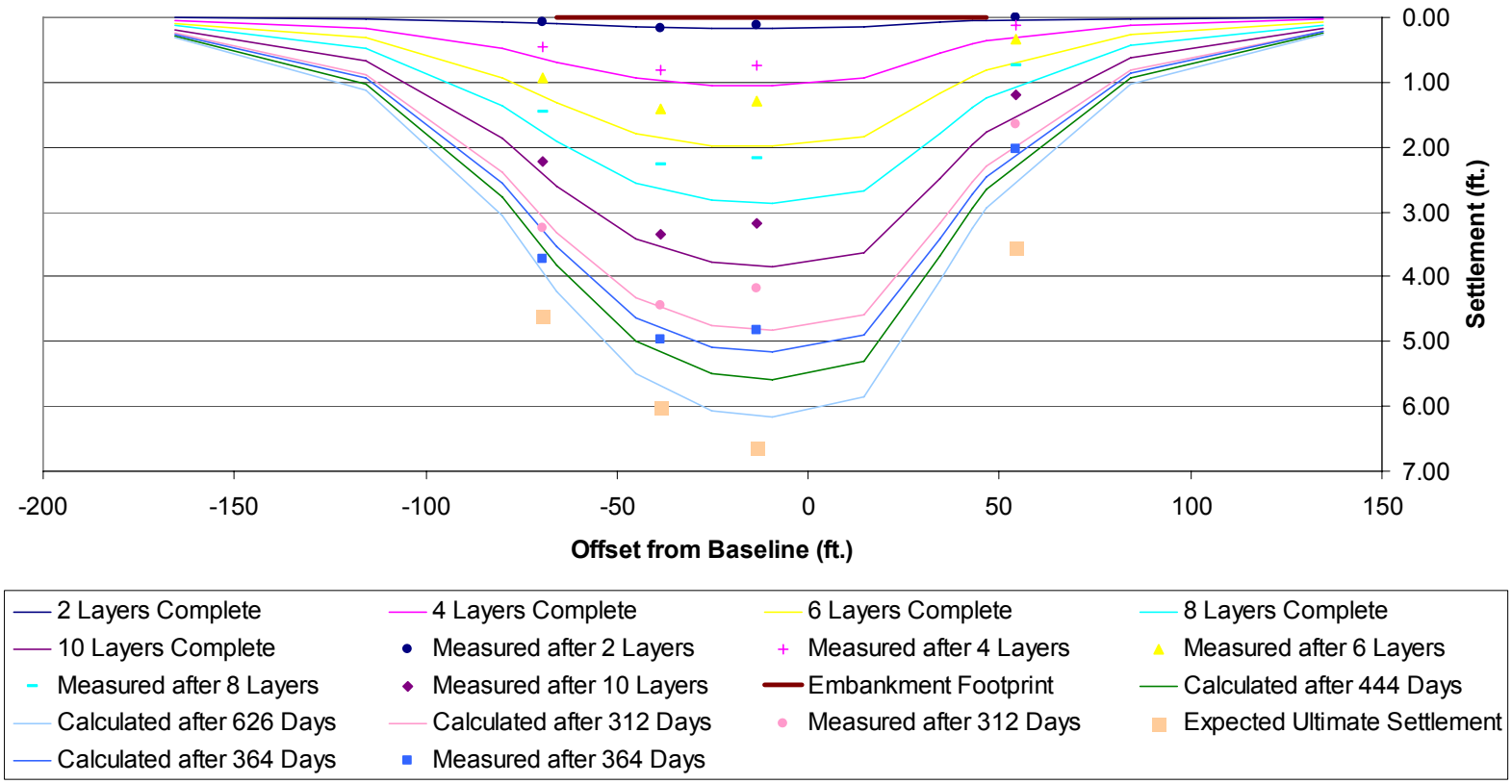

Figure 5.3 Settlement Profile Generated Using C_c = 0.88

The $C_c = 0.88$ settlement profiles do not correspond as well with field measurements of settlement during construction. However, this is logical. The settlement profile was generated using the computer program FoSSA®, as described previously. A staged construction method was used to accurately represent the embankment construction, so that the correct embankment height was used at each interval. However, for each interval, the current height of the embankment was applied instantaneously. Then, for calculation purposes, half of the actual elapsed time was used. This represents the average load applied by embankment construction because the entire load was used in the calculation, but only half the full time. In reality, the full time has elapsed, but the embankment was not at full height for that time. The two scenarios are approximately equal. Yet, this could explain why the predictions during construction exceed the actual measured data. Tables 5.2 through 5.5 contain some of the data used to generate Figure 5.2 and Figure 5.3. Each table provides data from a different settlement plate, as identified. Predicted values are shown for various times, and compared to data measured at each time increment.

Table 5.2 Predicted versus Measured Settlement at Plate 289-70L

Days	Layers	Predicted - Cc=.078 Sc(t) [ft]	Predicted - Cc=0.88 Sc(t) [ft]	Measured Sc(t) [ft]
22	2	0.06	0.07	0.07
106	4	0.42	0.47	0.46
161	6	0.82	0.92	0.93
197	8	1.21	1.36	1.46
244	10	1.66	1.87	2.23
312	Full Height	2.12	2.39	3.24
364	Full Height	2.27	2.57	3.73
444	Full Height	2.46	2.77	N/A
626	Full Height	2.71	3.06	N/A

Table 5.3 Predicted versus Measured Settlement at Plate 289-35L

Days	Layers	Predicted - Cc=.078 Sc(t) [ft]	Predicted - Cc=0.88 Sc(t) [ft]	Measured Sc(t) [ft]
22	2	0.13	0.15	0.16
106	4	0.83	0.94	0.82
161	6	1.58	1.78	1.4
197	8	2.26	2.55	2.27
244	10	3.04	3.43	3.34
312	Full Height	3.82	4.31	4.44
364	Full Height	4.10	4.62	4.98
444	Full Height	4.42	4.99	N/A
626	Full Height	4.88	5.51	N/A

Table 5.4 Predicted versus Measured Settlement at Plate 289-15L

Days	Layers	Predicted - Cc=.078 Sc(t) [ft]	Predicted - Cc=0.88 Sc(t) [ft]	Measured Sc(t) [ft]
22	2	0.14	0.16	0.11
106	4	0.92	1.04	0.74
161	6	1.76	1.98	1.30
197	8	2.51	2.83	2.17
244	10	3.36	3.79	3.17
312	Full Height	4.21	4.75	4.19
364	Full Height	4.52	5.10	4.83
444	Full Height	4.88	5.50	N/A
626	Full Height	5.38	6.07	N/A

Table 5.5 Predicted versus Measured Settlement at Plate 289-53R

Days	Layers	Predicted - Cc=.078 Sc(t) [ft]	Predicted - Cc=0.88 Sc(t) [ft]	Measured Sc(t) [ft]
22	2	0.04	0.05	no data
106	4	0.36	0.41	0.13
161	6	0.80	0.90	0.33
197	8	1.24	1.40	0.74
244	10	1.74	1.97	1.2
312	Full Height	2.25	2.54	1.66
364	Full Height	2.42	2.73	2.04
444	Full Height	2.61	2.94	N/A
626	Full Height	2.88	3.25	N/A

Figure 5.4 represents another view of the settlement at station 289+00. This figure shows the settlement measured by settlement plate 289-35L, which is the settlement plate that has undergone the greatest amount of settlement at station 289+00. This curve is compared to a curve generated using the values of settlement predicted using $C_c = 0.88$. The predicted curve extends for a duration of 1,000 days. The point at which the average consolidation (Uave.) reaches 90 percent is also marked. The average consolidation, by definition, is the settlement at a given time divided by the ultimate settlement. The progression of construction is represented by vertical lines, labeled by elevation. This elevation is the top level of the wall at that point during construction. Table 5.6 corresponds to Figure 5.4 and shows a few selected values of the measured data versus the predicted data.

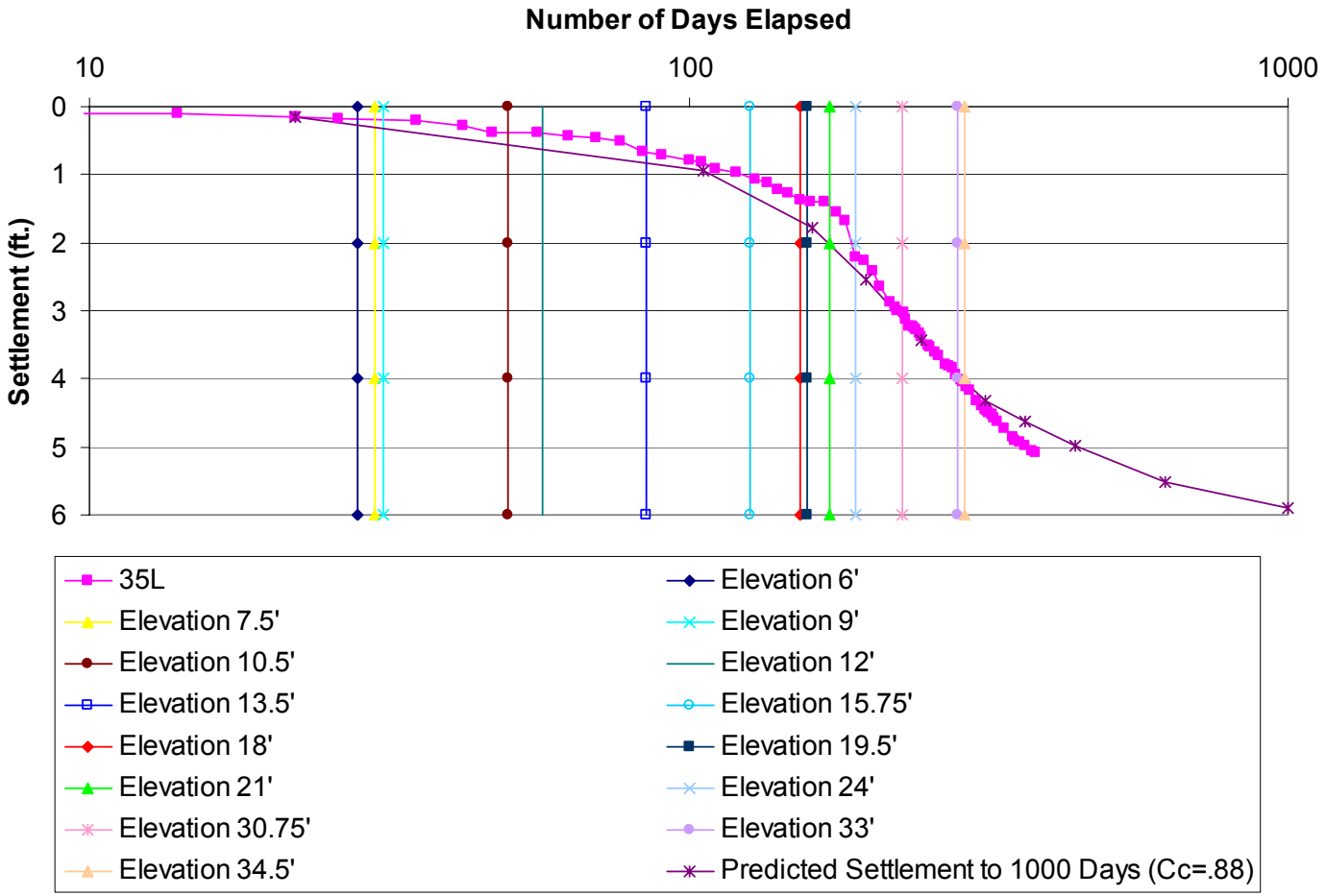

Figure 5.4 Settlement at Plate 289-35L

Table 5.6 Measured versus Predicted Data Values at Plate 289-35L

Days Elapsed	Layers	Sc(predicted) [ft]	Sc(measured) [ft]
22	2	0.15	0.16
106	4	0.94	0.82
161	6	1.78	1.4
197	8	2.55	2.27
244	10	3.43	3.34
312	Full Height	4.31	4.44
364	Full Height	4.62	4.98
444	Full Height	4.99	N/A
626	Full Height	5.51	N/A
1000	Full Height	5.89	N/A

Examining the data measured by settlement plate 35L, it can be observed that the rate of settlement increased substantially after the wall height reached about 15 feet in May. It is likely that the settlement rate increased at this time because the level of stress induced into the clay layer became significant as a result of this load. After this, the settlement rate increased somewhat, then remained more or less constant until the beginning of March, when it appears as though the rate is beginning to decrease slightly. This is indicated by the curve of measured values tending to become more horizontal. The predicted settlement curve matches the measured curve with good accuracy. In addition, the predicted curve shows a decrease in the settlement rate around approximately the same time. If future settlement

measurements continue to make the curve more horizontal, this will reveal whether the prediction is accurate.

5.3 Pore Water Pressure

As shown in Section 4.3, piezometric readings indicate relatively high excess pore water pressure in the foundation soil. In addition, dissipation of the pore water pressure appears to be slow. The highest pore water pressure occurs in the foundation soil immediately after load is applied. This occurs because water is not compressible, and as a result, the load application causes pressure to build up. Thus, the entire load is initially supported by the water in the soil. Since the construction process is not instantaneous, there is not an exact point in time that can be pinpointed to represent the maximum pore water pressure. In general, however, the end of construction represents this time. At this point, the entire load has been applied to the foundation soil. So, the initial pore water pressure can be assumed to occur at the end of construction. After this point, pore water pressure begins to dissipate as consolidation occurs.

However, this may not occur as described when prefabricated vertical drains are installed. Since PVDs significantly shorten the drainage path, the dissipation of excess pore water pressure is much quicker, and may be nearly as fast as the rate at which it generates. In this case, there will be little to no buildup of excess pore water pressure by the end of construction. The high excess pore water pressure described in Section 4.3 implies that the PVDs may not be functioning properly, at least in the vicinity of the piezometers.

A useful way to monitor the pore water pressure dissipation is by graphing the ratio of the current excess pore water pressure to the theoretical initial pore water

pressure versus time. The theoretical initial pore water pressure can be calculated as the stress due to the applied load at the tip of the piezometer. The calculation was performed to determine the theoretical initial pore water pressure at the same depth and transverse location at which the piezometers are installed. A different value was calculated for each respective embankment height as it increased during construction. The current pore water pressure is read from the piezometers. When the ratio is one, it means that no pore water dissipation or consolidation has taken place, and the water in the soil is carrying the entire applied load. Figure 5.5 shows how the ratio of the initial to current pore water pressure increased as construction progressed, until the beginning of October. At this point, 30.75 feet of the 34.5 feet final height had been constructed, but deformations in the wall resulted in construction being temporarily stopped. This allowed for the excess pore water pressure to dissipate somewhat until the final few feet of the wall were constructed, with the final layer completed by December 1. Table 5.7 shows some of the numerical data from Figure 5.5. In the table, $d(\sigma z)$ is the stress increase due to the applied load, and $pwp/d(\sigma z)$ is the ratio of excess pore water pressure to the theoretical initial pore water pressure.

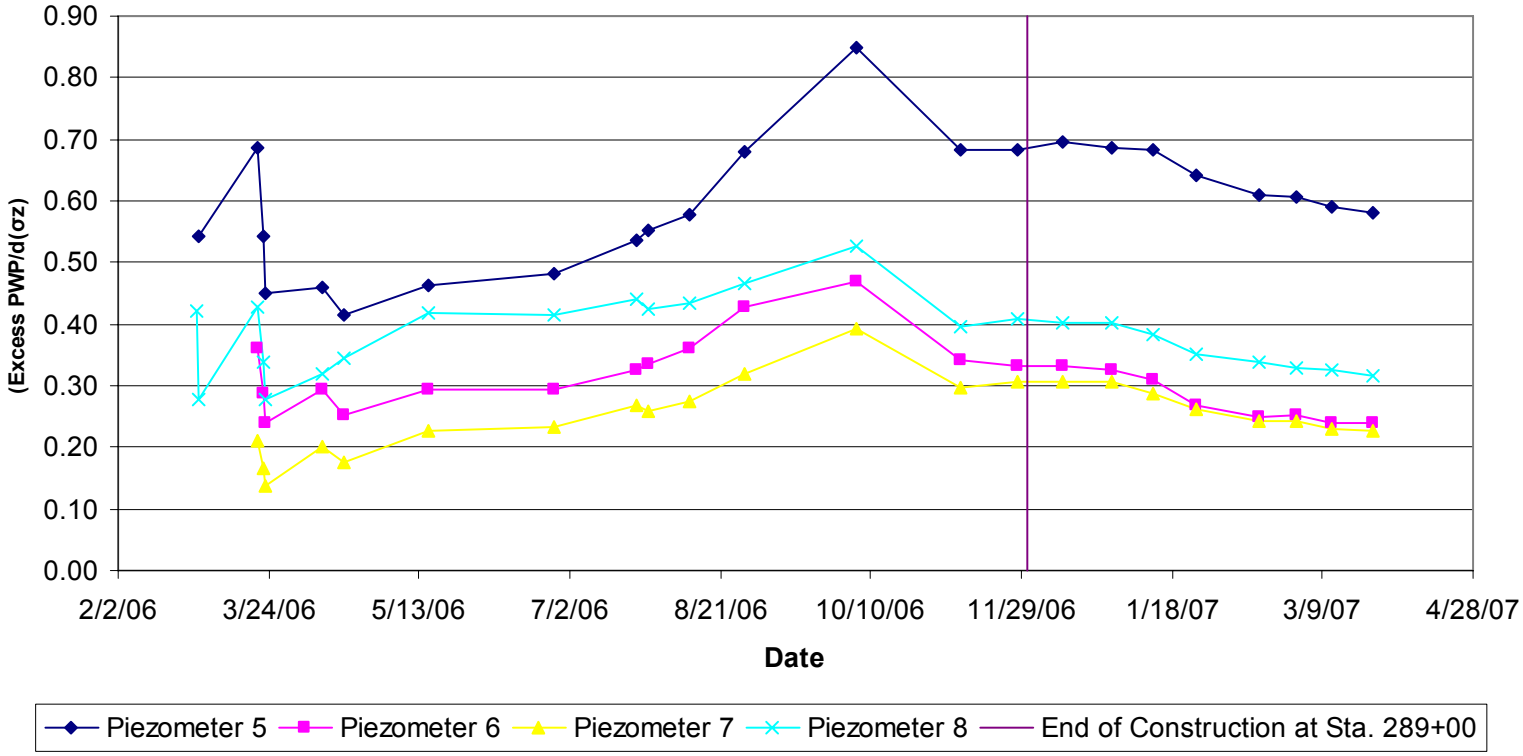

Figure 5.5 Ratio of Current to Initial Pore Water Pressure versus Time

Table 5.7 Ratio of Current to Initial Pore Water Pressure Values and Corresponding Times

Date	Piezometer							
	5		6		7		8	
	d(σz) (psi)	pwp/d(σz)	d(σz) (psi)	pwp/d(σz)	d(σz) (psi)	pwp/d(σz)	d(σz) (psi)	pwp/d(σz)
3/23/06	4.64	0.45	5.40	0.24	5.14	0.14	6.09	0.28
4/11/06	5.44	0.46	6.32	0.29	6.08	0.20	7.18	0.32
4/18/06	6.25	0.41	7.24	0.25	7.04	0.17	8.28	0.34
5/16/06	7.07	0.46	8.17	0.29	7.99	0.23	9.38	0.42
6/27/06	8.28	0.48	9.56	0.30	9.43	0.23	11.04	0.42
7/24/06	9.50	0.54	10.94	0.32	10.86	0.27	12.69	0.44
7/28/06	10.31	0.55	11.87	0.33	11.82	0.26	13.80	0.43
8/11/06	11.12	0.58	12.79	0.36	12.78	0.27	14.90	0.43
8/29/06	12.74	0.68	14.64	0.43	14.69	0.32	17.11	0.47
10/5/06	14.37	0.85	16.49	0.47	16.60	0.39	19.31	0.53
11/9/06	16.80	0.68	19.26	0.34	19.47	0.30	22.62	0.40
11/28/06	17.61	0.68	20.18	0.33	20.43	0.30	23.73	0.41
12/13/06	18.41	0.70	21.09	0.33	21.40	0.31	24.85	0.40
12/29/06	18.41	0.68	21.09	0.32	21.40	0.31	24.85	0.40
1/12/07	18.41	0.68	21.09	0.31	21.40	0.29	24.85	0.38
1/26/07	18.41	0.64	21.09	0.27	21.40	0.26	24.85	0.35
2/16/07	18.41	0.61	21.09	0.25	21.40	0.24	24.85	0.34
2/28/07	18.41	0.61	21.09	0.25	21.40	0.24	24.85	0.33
3/12/07	18.41	0.59	21.09	0.24	21.40	0.23	24.85	0.32

After construction completion, there was a slight increase in the pore water pressure, probably due to the last layer of the wall being added after the temporary pause in construction. After this brief increase in pore water pressure, it begins to dissipate as the system starts to stabilize. As illustrated, this is occurring at a slow rate. The piezometers are installed within a zone in which prefabricated vertical drains are also installed. However, the theoretical initial pore water pressure values

used in Figure 5.5 correspond to a situation where no PVDs exist. Therefore, it would be expected that the PVDs would have a significantly greater influence on the rate of excess pore water pressure dissipation. This is again an indication that at least some of the PVDs may not be functioning properly. The trend, however, in agreement with the large observed settlement magnitude. The substantial pore water pressure in the soil renders the soil weaker than assumed in design. In addition, it appears that the consolidation time is longer than predicted by the designer.

It should be pointed out that piezometric readings alone are not very reliable, as the exact soil conditions at the tip of the piezometer are not fully known. For example, there could be a thin seam of sand at the piezometer tip that was not identified by soil boring. However, combined with settlement plate measurements, piezometric readings can be very reliable. That is, if the measured trends mutually support each other, the value of the measured excess pore water pressure can provide insight into effective stress, thus implying the gain in shear strength due to consolidation. In the present case, the measured trends are in agreement. For that reason, the indication that the PVDs in the vicinity of the piezometers are not functioning properly is strong.

5.4 Stability Analysis

In order to assess the global stability of the newly constructed embankment, an analysis was conducted using the computer program ReSSA®. The embankment was modeled using this software. Next, the foundation soils were depicted. The properties of the foundation soils were acquired from the designer (Joe Wallen, personal communication, October 16, 2006). The design assumed initial undrained shear strength of 450 pounds per square foot (psf) for the top of the clay

layer, with the strength increasing linearly with depth. In order to accurately represent the increase of strength with depth in the clay layer, the FoSSA® software was again used. The software uses the following equation to calculate the undrained shear strength of a soil layer:

$$S_u/\sigma_{Vc} = S \bullet (OCR)^m \qquad (9)$$

where: S_u = undrained shear strength

σ_{Vc} = effective vertical stress

S, m = empirical parameters

OCR = over consolidation ratio

For the normally consolidated clay being analyzed, OCR = 1 and m = 1. The effective vertical stress is calculated by the program, and thus, the undrained shear strength is determined as a function of depth (or effective stress). Therefore, adjusting S results in different undrained shear strengths with depth. A value for S was chosen, and the analysis was run, assuming embankment construction occurred instantaneously. This is a conservative assumption, as it will result in the greatest pore water pressure buildup, and therefore the least stability. A similar assumption was used by the designer, as it is customary in practice. The analysis provided the initial undrained shear strength at various depth intervals through the clay layer. The value for S was readjusted, and the analysis was rerun until an initial undrained shear strength equal to 450 psf was produced for the top of the clay layer. Table 5.8 shows the initial undrained shear strengths calculated for various depth intervals through the clay layer.

Table 5.8 Initial Undrained Shear Strength of the Clay Layer

Depth [ft]	Su [lb/ft²]
-29	451
-34.91	497
-40.48	540
-46.39	586
-52.29	631
-57.87	674
-63.78	720
-69.68	766
-75.59	811
-81.17	854
-87	900

Now that the increase in undrained shear strength through the clay layer has been determined, the information was entered into the ReSSA® software. The clay layer was divided into ten sublayers, each approximately six feet thick. A representative strength was then assigned to each sublayer. The soil profile, including the clay sublayers, is shown in Figure 5.6. In the figure, each soil layer and sublayer is numbered to correspond with Table 5.9. This table lists each layer and the properties that were assigned to it.

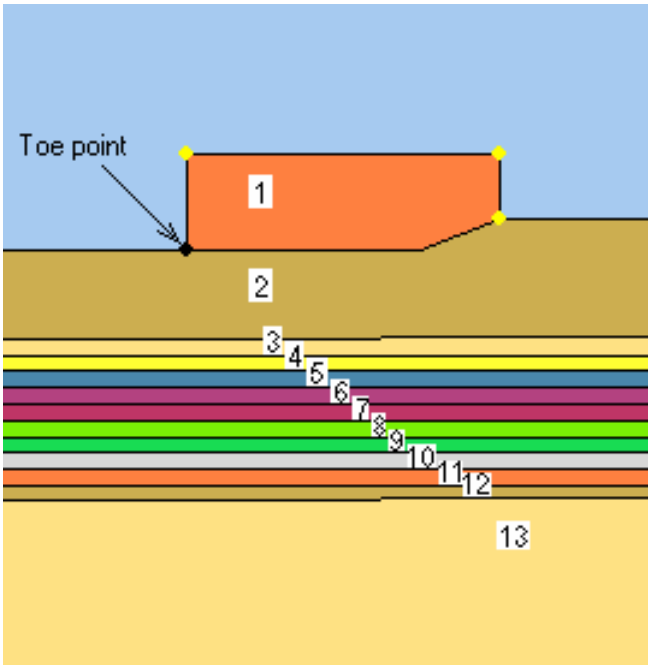

Figure 5.6 Soil Section Used in ReSSA®

Table 5.9 Soil Properties Used in ReSSA®

Soil Layer	Description	γ (pcf)	Φ (deg.)	c (psf)
1	Embankment Fill	125	32	0
2	Sand	120	32	0
3	Clay	100	0	451
4	Clay	100	0	496.3
5	Clay	100	0	539.8
6	Clay	100	0	585.5
7	Clay	100	0	631.1
8	Clay	100	0	674.3
9	Clay	100	0	720
10	Clay	100	0	765.7
11	Clay	100	0	811.3
12	Clay	100	0	854.5
13	Sand	130	34	0

The analysis was then run to determine the factor of safety against failure of the embankment. Two different failure modes were checked. The first was the rotational failure mode, which is analyzed by the program using the Bishop analysis. A minimum factor of safety equal to 1.35 was found. Figure 5.7 shows the critical circle as a thin white line, as well as the respective safety map.

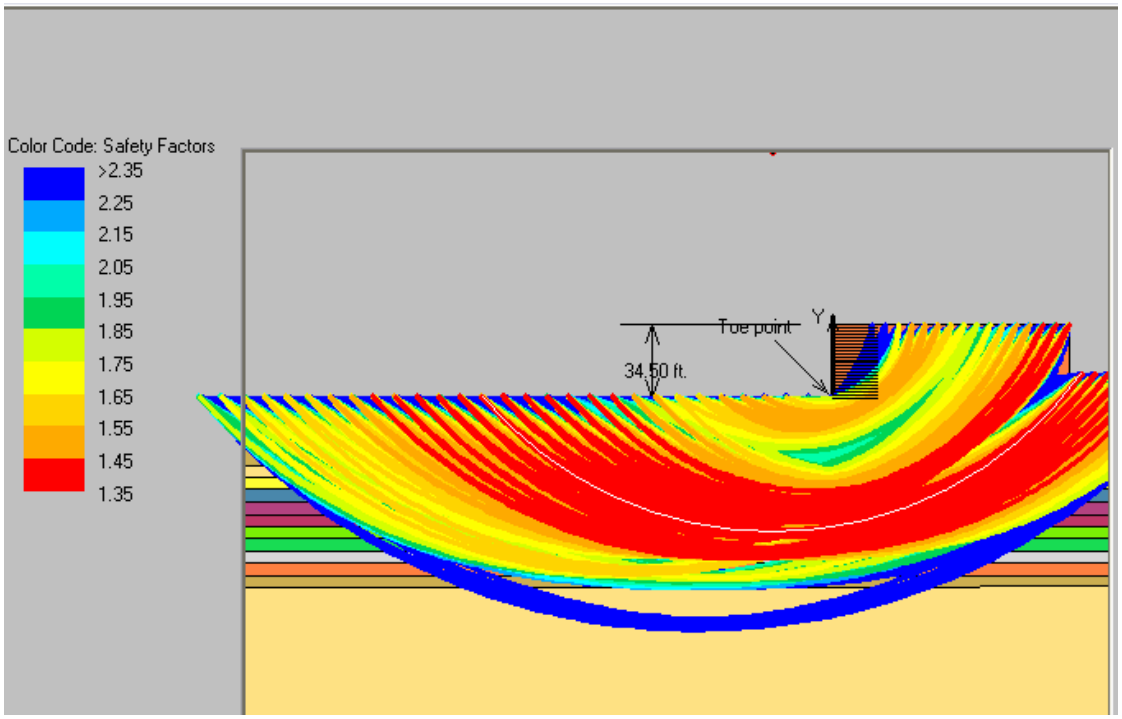

Figure 5.7 Factor of Safety against Rotational Failure

The second mode of failure checked is the three-part wedge mode. In this case, the Spencer method of analysis was used. The three-part wedge analysis yields a minimum factor of safety of 1.18. Figure 5.7 shows the critical wedge, as well as the safety map.

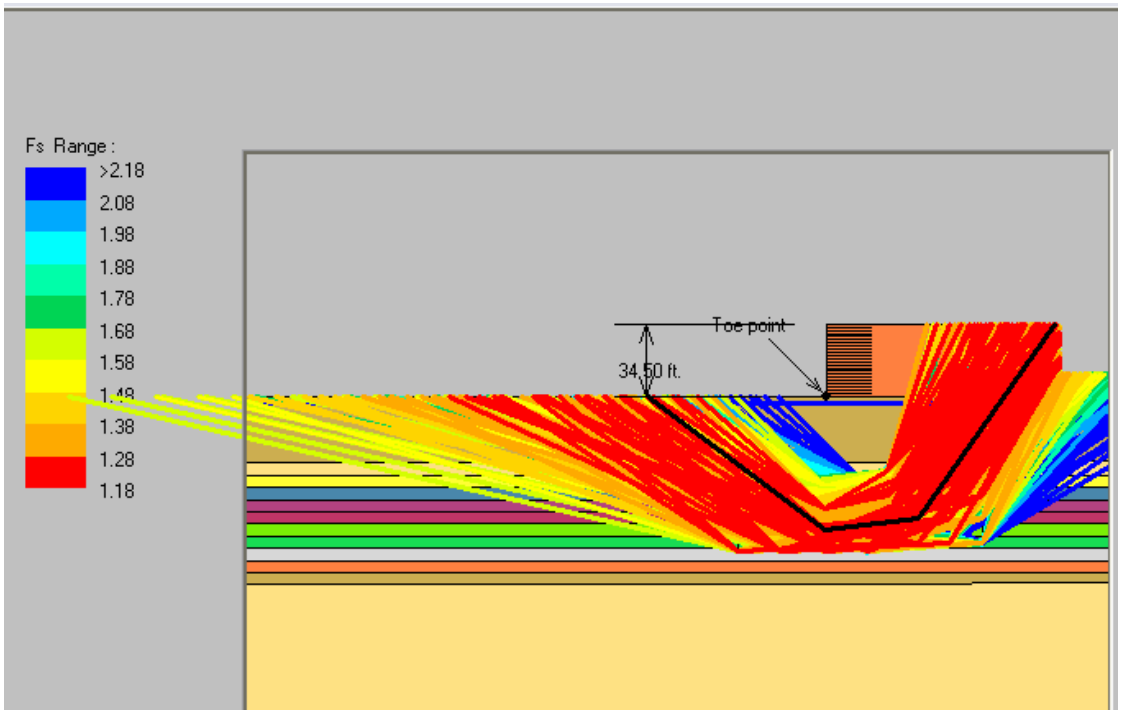

Figure 5.8 Factor of Safety for Three-Part Wedge Failure Mode

One observation is that the minimum factor of safety for the three-part wedge is considerably smaller than the minimum factor of safety determined using the Bishop analysis. One reason for this could be that a circle cannot capture the impact of a thin, weak horizontal sublayer of soil. The shear strength plays a role in dictating the failure mechanism, thus affecting the calculated factor of safety. The three-part wedge is better able to locate a horizontal plane with low shear strength, along which failure is most likely. Another observation to be made is that both mechanisms indicate that potential deep seated failure does not extend through the reinforced zone.

The low factors of safety produced by the two analyses should not be surprising considering the inclinometer data shown in Section 4.4. The first sizable horizontal movements were observed at both inclinometers installed at station 289+00

during September. Figure 5.5 shows that the highest levels of excess pore water pressure also occurred at this time. Figure 4.30 shows horizontal movements close to three inches, while Figure 4.31 shows horizontal movements around nine inches. The maximum horizontal movements occurred between the depths of 35 to 40 feet. This depth range coincides with the top 10 feet of the clay layer, as the top of the clay layer is about 29 feet deep.

Figure 4.34 shows cumulative horizontal movements measured by inclinometer 289-55R of five inches in December, again at a depth of 40 feet. Figure 4.35 shows cumulative horizontal movements measured by inclinometer 289-75A, which replaced inclinometer 289-75L, as described in Section 4.4. The measured movement is about three inches, but this must be added to the movement of nine inches that was measured by the previous inclinometer. Thus, over a foot of horizontal movement occurred at depths between 35 and 55 feet through December. Figures 4.36 and 4.37 show that the horizontal movement continued to increase by about an inch through January. Finally, Figure 4.40 shows measurements taken in the beginning of March that are nearly six inches at depths between 35 and 55 feet. Again, this is an additional six inches added to the nine inches measured by the previous inclinometer, totaling fifteen inches.

The clay layer extends from 29 feet below the ground surface to a depth of 89 feet. It appears that major horizontal movements are occurring at depths between 35 and 55 feet, near the middle of the clay layer. The safety maps shown in Figures 5.7 and 5.8 show that the lowest factor of safety exists near the middle of the clay layer. In addition, the critical slip surface in both figures is at a depth of about 60 feet. This reinforces the prediction of the stability analyses performed.

Given that the analyses were performed for the initial condition before any excess pore water pressure dissipation occurred, the factor of safety will increase with time. When consolidation is complete, the pore water pressure will return to the hydrostatic level, which will increase the effective stress. The shear strength will therefore increase linearly with depth. It should be noted that this is only true after consolidation is complete. The designer assumed that the undrained shear strength increases linearly with depth during consolidation. However, while consolidation is taking place, undrained shear strength does not increase linearly with depth, as the excess pore water pressure is not linear with depth. The only times that the pore water pressure and effective stress increase linearly with depth are before consolidation begins, and after consolidation is complete, when hydrostatic conditions exist.

An analysis can be done to determine the factor of safety after consolidation is complete. At this point, the shear strength at the top of the clay layer will be equal to the effective stress, which can be quickly calculated, and is 1,858 pounds per square foot. Using FoSSA® in the same manner as before, the increase in shear strength with depth can be found. The results are shown in Table 5.10.

Table 5.10 Shear Strengths of the Clay Layer after Consolidation

Depth [ft]	Su [lb/ft²]
-29.00	1858
-34.91	1947
-40.48	2029
-46.39	2115
-52.29	2199
-57.87	2278
-63.78	2360
-69.68	2440
-75.59	2520
-81.17	2595
-87.00	2673

Now, these values can be entered into ReSSA®, and a stability analysis can be conducted. As before, two failure modes were checked. The Bishop method was first used to check the rotational mode of failure. This analysis yielded a minimum factor of safety of 1.46. Figure 5.9 shows the critical circle as a thin white line, as well as the safety map.

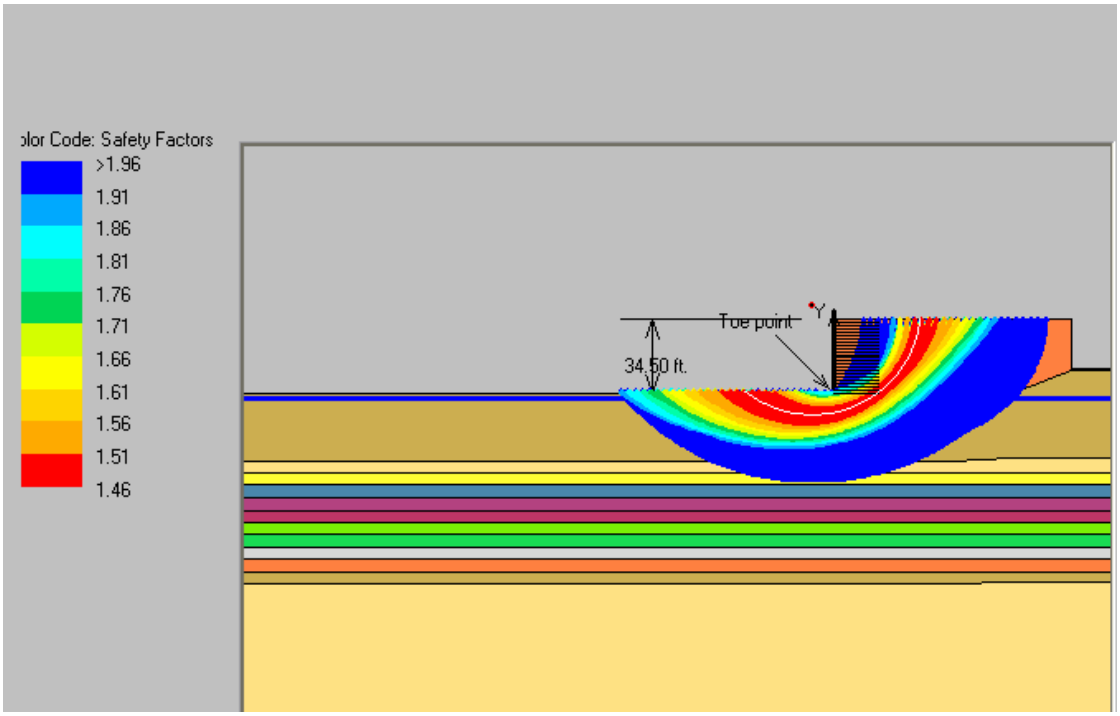

Figure 5.9 Post-Consolidation Factor of Safety against Rotational Failure

Next, the three-part wedge mode of failure is checked using the Spencer method. This analysis reveals a minimum factor of safety of 1.33. Figure 5.10 shows the critical wedge and the safety map.

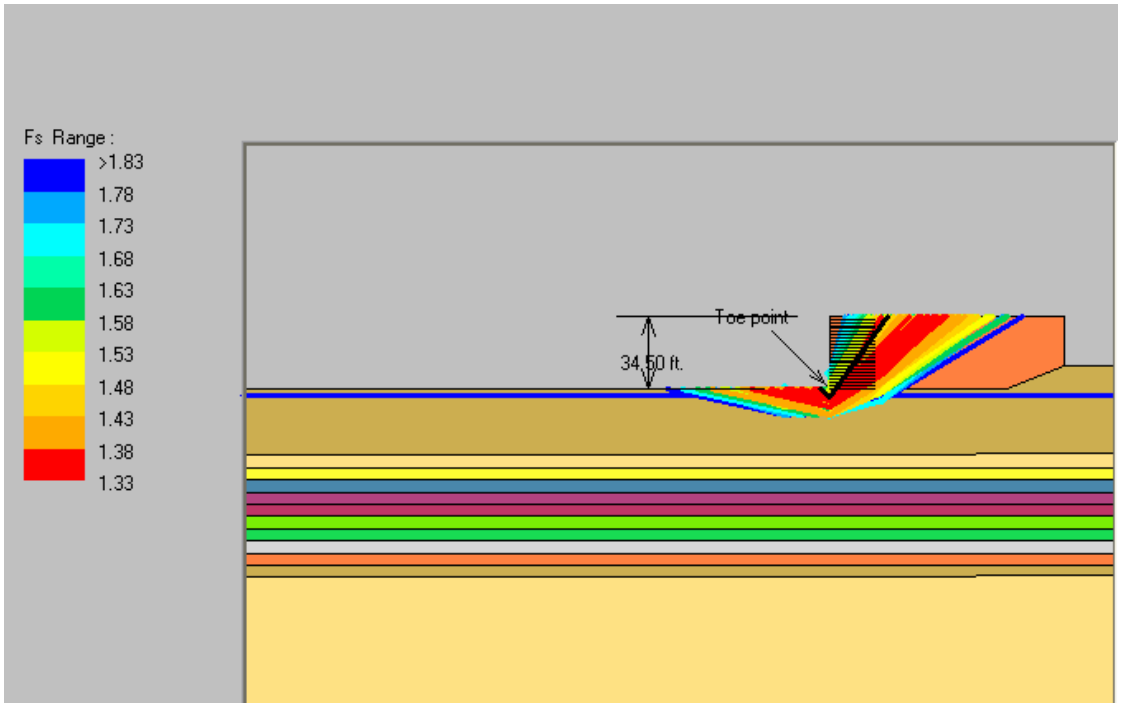

Figure 5.10 Post-Consolidation Factor of Safety for Three-Part Wedge Failure Mode

As expected, after consolidation is complete, the factor of safety increases. In each analysis, the critical surface no longer extends through the clay layer, as the clay has gained strength. The critical surface now exists much closer to the base of the embankment. Both analyses produce a factor of safety greater than 1.3, which is the factor of safety necessary to ensure adequate global stability. Hence, after consolidation is complete, the embankment should be stable.

5.5 Summary of Interpretations

The data collected from the strain gages, settlement plates, piezometers, and inclinometers at station 289+00 appear to be in agreement. Increases in strain and

force in the geogrid reinforcement measured by the installed strain gages coincide with increased settlement, as measured by the settlement plates at station. High values measured from the strain gages indicate that the large magnitude of settlement occurring is exerting a down drag force on the rear of the geogrid reinforcement, inducing high strains. The settlement rate escalated quickly in May, when it appears that the stress induced by construction of the embankment reached the clay layer. Accordingly, during May the first significant values of strain were measured in the geogrid.

It appears that an accurate prediction of settlement can be made by altering the compression index. Adjusting the compression index from the original value of $C_c = 0.5$, provided by the designer, to $C_c = 0.88$ produces settlement predictions that match measured settlements relatively well. Using the adjusted compression index, the predicted ultimate settlement at station 289+00 is about 80 inches. Taking February 28, 2006, the day that the first layer of fill was placed, as the starting point, 90 percent consolidation will occur in approximately 584 days, and 95 percent consolidation will occur in about 766 days.

The large amount of settlement occurring is in agreement with the piezometer data. The highest excess pore water pressure readings were taken at the end of September and the beginning of October. Afterwards, dissipation of the excess pore water pressure has occurred at a very slow rate. The high pore water pressure buildup and the slow rate of dissipation are indicators that the prefabricated vertical drains are not functioning properly. As a result, the soil is rendered weaker than assumed in design, thus explaining the unanticipated large magnitude of settlement.

The inclinometers have shown large horizontal movements, particularly at depths between 35 and 55 feet. This depth coincides with the top half of the clay layer. The stability analyses conducted for the condition at which the highest level of excess pore water pressure exists indicate that the factor of safety against global failure is the lowest near the middle of the clay layer. Thus, the stability analyses appear to be a reasonable predictor of what is occurring. The analyses also explain the magnitude of the horizontal movements that have occurred in the clay layer. Horizontal movement exceeding one foot should not be unexpected, when considering the low factor of safety determined through analysis. The Bishop analysis yielded a minimum factor of safety of 1.35, but the Spencer analysis produced a minimum factor of safety of 1.18.

Stability analyses were also conducted for the time at which consolidation is complete, when the pore water pressure has returned to the hydrostatic level. As expected, these analyses reveal an increase in the factor of safety. The Bishop analysis produced a minimum factor of safety of 1.46. The minimum factor of safety generated using the Spencer analysis was 1.33. Therefore, the embankment should stabilize as pore water dissipation continues.

Chapter 6

CONCLUSIONS AND RECOMMENDATIONS

The purpose of this thesis was to explore the effects of large settlement on the geogrid reinforcement of a mechanically stabilized earth wall. Current design practices for MSE walls assume a competent foundation. In this project, a deep, soft clay layer caused the constructed MSE wall to settle large amounts. The effect of this settlement on the geogrid reinforcement in the wall was monitored using strain gages.

6.1 Conclusions

Strain gages were attached to high density polyethylene geogrid panels using a specialized technique. Thirteen geogrid panels were instrumented with strain gages and installed into the MSE wall at station 289+00, at vertical intervals from elevation 0' to 33'. Strain gages were also installed on geogrid samples, which were used for calibration testing in the laboratory at the University of Delaware. Calibration testing was used to develop two relationships. First, equations were curve-fitted to relate the resistance measured in ohms from the strain gages to the percentage of strain in the geogrid. Second, equations were curve-fitted that relate the percentage of strain in the geogrid to the force in pounds per foot in the geogrid. Resistance measurements could then be taken from the gages in the field and subsequently converted to strain and force. Measurements were taken regularly throughout construction of the wall. Measured data was also available from

settlement plates, piezometers, and inclinometers installed at the same station as the strain gages.

Analyzing the data collected from the various instruments installed at station 289+00 has been valuable in determining how the soft foundation soil is responding to the embankment load, as well as how the embankment is behaving, having been constructed on a poor foundation. The settlement plates, piezometers, and inclinometers are helpful in assessing how the foundation soil is responding to the embankment load. The strain gages attached to the geogrid reinforcement give an indication of how the wall and embankment are behaving while settlement is occurring.

The settlement plate data shows that settlements have far exceeded the original predictions of the designer. Through analysis using the computer program FoSSA®, a model of the embankment was calibrated to produce modified predictions of settlement that more closely match the settlement measured in the field. This was accomplished by adjusting the compression index from the value used by the designer, $C_c = 0.5$, to $C_c = 0.88$. The ultimate settlement predicted by the designer at station 289+00 is 45 inches. Using the adjusted compression index, the ultimate settlement at this station is expected to be about 80 inches.

The data from the piezometers at station 289+00 is consistent with the observed settlement. The excess pore water pressure was greatest near the end of construction, as is generally expected. However, after the peak pore water pressure value was reached, dissipation of excess pore water pressure is occurring at a slow, but steady rate. This coincides with the fact that settlement is continuing at a constant rate.

Stability analyses conducted reveal that the factor of safety against deep seated failure of the embankment at the end of construction was between 1.18 and 1.35 for the condition assuming instantaneous embankment construction and no excess pore water pressure dissipation. The low factor of safety is in agreement with the large horizontal movement measured by the inclinometers. In addition, the depth at which the predicted critical failure planes and surrounding areas with a low factor of safety according to the safety maps are located correspond to the depth at which the largest horizontal movements have been measured by the inclinometers. Stability analyses conducted for the post-consolidation condition show an increase in the factor of safety to an acceptable level.

The strain gage data is particularly important. There is little known regarding the behavior of a mechanically stabilized earth wall that is constructed on poor foundation soil. In general, design for MSE walls assumes a competent foundation. Thus, monitoring the strain in the geogrid reinforcement is important in order to determine the effect of large settlement on the structure.

Data collected from the strain gages in this research project gives an indication of how the reinforcement is responding to the settlement of the structure. Strains higher than are typical for MSE walls have been observed over the entire length of the reinforcement. It appears that the highest strains in the geogrid are occurring near the back of the reinforcement, away from the face of the wall. This is most likely due to the sand backfill settling at a faster rate than the reinforced soil. As a result, the backfill is exerting a down drag force on the rear boundary of the reinforced soil mass. This down drag force subjects the geogrid reinforcement to stress that is not typically considered in design.

6.2 Recommendations for Further Research

The best way to complete this research is to continue to collect and analyze data from all of the instrumentation installed at station 289+00. At the time of the writing of this thesis, the embankment continues to undergo significant settlement. Excess pore water pressure levels remain high, and are dissipating slowly, indicating the settlement will continue for some time. Even after settlement is nearly complete, it will still prove useful to continue monitoring the strain gages. This will reveal long-term effects such as creep of the geogrid reinforcement. There is not much knowledge concerning the behavior of geogrid reinforced mechanically stabilized earth walls constructed over poor foundation soils. Hence, there is a great deal of knowledge to be gained from this research.

REFERENCES

Bay, James, Loren Anderson, Aaron Budge, and Mark Goodsell. (2003). Instrumentation and Installation Scheme of a Mechanically Stabilized Earth Wall on I-15 with Results of Wall and Foundation Behavior. Utah State University, Logan, UT.

Slope Indicator. (2006a). Digitilt Inclinometer Probe. Mukilteo, WA: Durham Geo Slope Indicator.

Slope Indicator. (2006b). Vibrating Wire Piezometer. Mukilteo, WA: Durham Geo Slope Indicator.

Soong, T.-Y. and Koerner, R. M. (1998). Laboratory Study of HDPE Geomembrane Waves. Proceedings 6 ICG (pp.301-306). Atlanta: IFAI.

Won, M-S. and Y-S Kim. (2006). Application of strain gauges to measure nonwoven geotextile deformation in reinforced soil wall. In J. Kuwano and J. Koseki (Eds.), Proceedings of the 8th International Conference on Geosynthetics (pp. 945-948). Rotterdam: Millpress.

Delaware Center for Transportation
University of Delaware
Newark, Delaware 19716